Yttrium Silicate Ceramics Dispersed with SiC Particles for Self-healing Environmental Barrier Coating Applied to Si Based Ceramic Composites

(Si 基セラミック複合材料に向けた自己治癒耐環境遮蔽コーティングのための SiC 粒子分散イットリウムシリケートセラミックス)

VU DINH HUY

Research Supervisor

Professor NANKO MAKOTO

Nagaoka University of Technology

Graduate School of Engineering

June 2020

Abstract

Aim of the present dissertation is to develop the self-healing function of ceramic-based composites for environmental barrier coatings which were applied to protect Si-based ceramics and their composites from hot steam corrosion. Silicon-based ceramics, including silicon nitride and silicon carbide as well as their ceramic matrix composites such as SiC fiber-reinforced SiC composites (SiC_f/SiC), are used as high-temperature structural components for hot-section in gas turbine engines. These materials present an excellent high-temperature oxidation resistance under dry and clean air due to formation of a protective silica layer. However, in water vapor generated during combustion process in gas turbine engines, these ceramics were susceptible to hot corrosion and recession. The protective silica layer reacts with water vapor to form gaseous oxidation products such as $Si(OH)_4$. In order to extend lifetime of these materials, application of environmental barrier coatings (EBCs) to protect them from water vapor corrosion is needed.

Recent studies on EBCs showed that rare-earth (RE) silicates (RE_2SiO_5 and $RE_2Si_2O_7$) are potential materials for the EBCs due to their phase stability and low CTE close to those of silicon-based ceramic substrates. However, application of these ceramics must face a challenge on their brittle property. In actual applications, further cracking can be induced by foreign object damage, mechanical fatigue or thermal shock. In case of crack formation in the EBCs, the substrates will be no longer protected from the corrosive environment due to penetration of oxygen and water vapor. Under these circumstances crack-healing abilities are essentially necessary for the EBCs to increase their lifetime and reliability.

The self-healing function of SiC/Y_2SiO_5, $SiC/Y_2Si_2O_7$ and SiC/Y_2SiO_5-$Y_2Si_2O_7$ composites are investigated and discussed in this dissertation to develop self-healing EBC materials applied for Si-based ceramic composite substrates. Investigation of the self-healing function for each composite is carried out and discussed via surface crack-disappearance by thermal oxidation, self-healing-induced strength recovery and oxidation resistance. Effect of SiC volume fraction on self-healing performance and oxidation resistance of SiC/Y_2SiO_5-$Y_2Si_2O_7$ composites is investigated as well. In order to discuss the self-healing mechanism of the composites, evaluation of the diffusion coefficient of Y^{3+} and O^{2-} ions in the Y_2SiO_5 matrix is conducted. The diffusion couple experiments are conducted to determine the diffusion coefficient of Y^{3+} ion. The oxygen diffusivity in Y_2SiO_5 matrix is evaluated via oxidation kinetics of SiC/Y_2SiO_5 composites.

SiC/Y_2SiO_5-$Y_2Si_2O_7$ composites exhibit a considerable self-healing performance at high temperature caused by the oxidation of SiC dispersoid. The self-healing ability and oxidation resistance of the composites are proportional to SiC volume fraction. The formation of oxidation product layer and the volume expansion are responsible for closure of the surface cracks. The diffusivity of Y ion in Y_2SiO_5, which is not been yet reported in literature, is exhibited.

List of contents

List of tables

List of figures

Chapter I

Introduction

1.1 Evolution of the gas turbine operating temperature

Gas turbine engines have become important, widespread and reliable devices in the field of power generation, transportation and other applications. It has profoundly affected society since its initial development during the Second World War. It has enabled the cost of long distance travel to be dramatically reduced while also making it more reliable and reducing transit time. It is also used extensively worldwide for the efficient generation of electricity. In spite of many years of development, overall efficiency of gas turbine engines remains far from thermodynamic limit for hydrocarbon combustion. All of the applications of gas turbine can be advanced by continued improvements to their fuel efficiency and power output.

Demand for more powerful and higher fuel efficiency of gas turbine engines will require a significant increase in the turbine inlet temperature [1-3]. Over the past 50 years the increase in the turbine inlet temperature have been achieved due to advances in nickel-base superalloys, air-cooling technologies and thermal barrier coatings (TBCs), as shown in Figure 1.1 [1, 2, 4, 5, 6]. The operating temperatures of engines are now approaching the melting point of nickel-base superalloys. Further increases in the gas turbine inlet temperature are not possible without the implementation of advanced TBCs with very low thermal conductivity that reduce the alloy surface temperature by insulating it from the hot gas. However, this strategy is approaching its limitation because: coating sintering leads to a loss of compliance and increased thermal conductivity [7-10], the bond coat oxidation rate increases rapidly with

temperatures [7, 11, 12], and calcium-magnesium-aluminum-silicate (CMAS) melting and infiltration cause premature coating failure [13, 14].

All of the considerations listed above are strong incentive for development of advanced materials systems with enhanced thermal capability. Based on the very high working temperature desired, ceramics and their composites systems are the most viable to replace nickel-base superalloys. The ceramic matrix composites (CMCs) possess requisite toughness and damage tolerance with the added benefit of considerably reduced density (technical ceramics are generally 30-50 % of the density of nickel-based superalloys) and the ability to operate at higher temperatures (~1400°C) without the need for cooling air [2, 3].

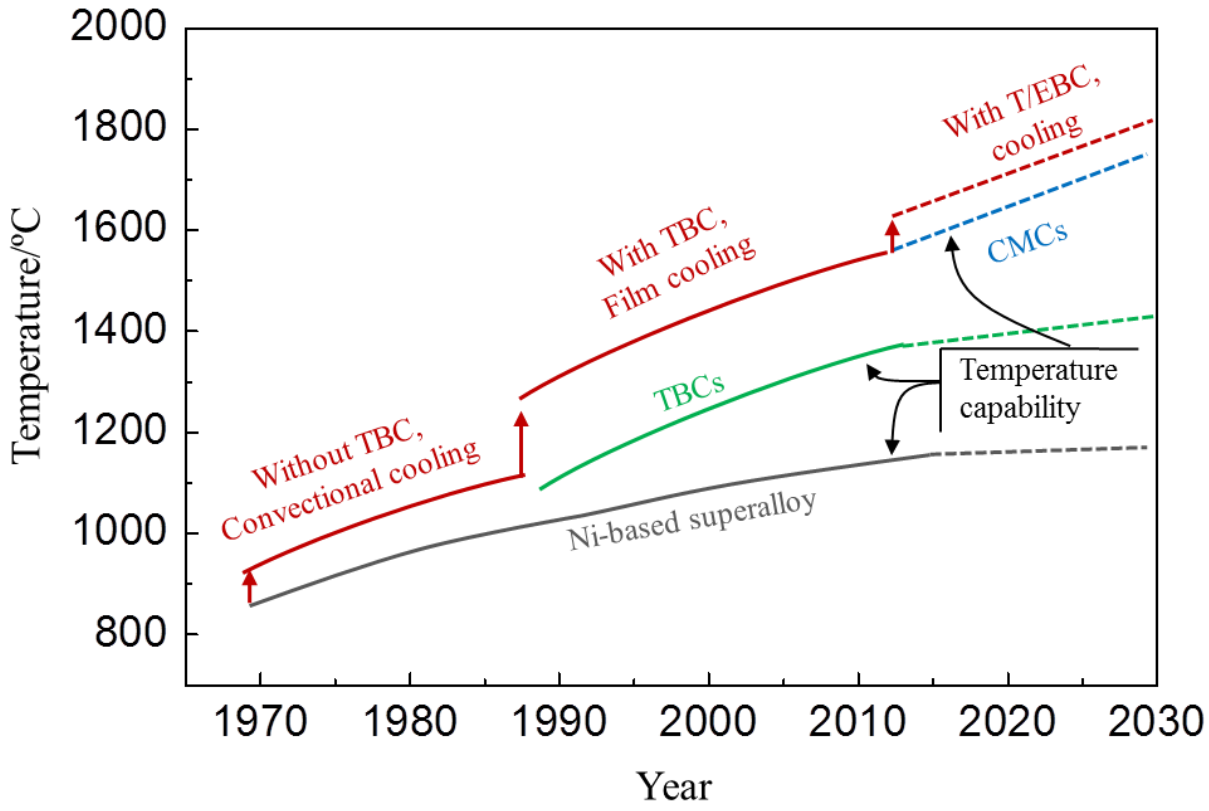

Figure 1.1 Evolution of turbine inlet gas temperature with the implementation of turbine blade materials, cooling concepts, coatings and CMCs [2]

1.2 Silicon carbide ceramic matrix composites

Because of the high temperature mechanical capabilities and physical properties, ceramic materials are considered as an attractive option to replace nickel-base superalloys for use in turbine engine hot-section. However, due to the brittle nature of ceramic failure, even tough monolithic ceramics such as Si_3N_4 have insufficient fracture toughness for critical gas turbine applications, some type of reinforcement phase is required in order to increase material toughness and mechanical durability. This requirement has led to the development and implementation of fiber-reinforced ceramic matrix composites. Among many CMC systems being studied, silicon carbide (SiC) fiber-reinforced SiC matrix composites (SiC_f/SiC) were identified as the leading candidate for turbine engine core structures [15].

A SiC_f/SiC CMC is composed of woven SiC fibers (such as Hi-Nicalon S and Sylramic fibers [16-19]) that are coated with a thin boron nitride (BN) interphase (< 1 μm) which is embedded in a Si/SiC matrix. The BN interphase is typically applied by chemical vapor deposition (CVD) or chemical vapor infiltration (CVI) from a gaseous precursor. Its main function is to arrest and/or deflect micro-cracks in the matrix that form under load thereby protecting the SiC fibers from early failure and allowing for fibers pullout during crack propagation [2, 17, 20, 21, 22]. The Si/SiC matrix is incorporated into the CMC by one or more of the following processing routes [3, 17, 21, 22]. The first route involves CVI where SiC is infiltrated into the fiber preform from a gaseous precursor. This process yields fully dense SiC and a composite with 10-15 % residual porosity. The second route involves infiltrating particle slurries into fiber preform via immersion or pressure assisted routes followed by sintering. The third route use a polymer impregnation and pyrolysis (PIP) process to infiltrate a polymer precursor of the matrix into the fiber preform that will form SiC upon

pyrolysis. This process results in composite with higher 10 % porosity. The fourth route uses melt-infiltration. The fiber preform is consolidated with carbon and infiltrated with liquid Si where the liquid Si reacts with carbon to form SiC and residual Si. This route yields a SiC_f/SiC CMC with low residual porosity.

One typical advantages of Si-based ceramics is their excellent high temperature oxidation resistance in dry air due to the formation of a solid, slow growing, protective silica scale (SiO_2), as equation (1.1) [23-26].

$$SiC + \frac{3}{2}O_2(g) = SiO_2 + CO(g) \quad (1.1)$$

However, in the presence of hot combustion gases containing high velocity, high pressure water vapor at high temperature, the protective SiO_2 scale grown on SiC reacts with water vapor to form a gaseous silicon hydroxides ($Si(OH)_4$) via equations (1.2) and (1.3) [25-30].

$$SiC + 3H_2O(g) = SiO_2 + 3H_2(g) + CO(g) \quad (1.2)$$

$$SiO_2 + H_2O(g) = Si(OH)_4(g) \quad (1.3)$$

The growth of the protective SiO_2 scale exhibits parabolic oxidation kinetics whereas the volatilization of SiO_2 exhibits linear kinetics [23-30]. Since these reactions occur simultaneously the oxidation and volatilization behavior of SiC is described by paralinear kinetics. SiC recession rate significantly greater than 1 μm/h has been observed in the 1300-1350°C range [28]. This can severely impair the lifetime and performance of SiC components due to shape change, which would cause them unfit for turbine engine application. Consequently, the SiC_f/SiC CMCs must be protected by environmental barrier coatings (EBCs) to prevent water vapor corrosion during operational lifetimes of thousands of hours.

The design of EBC systems has been focused on providing both thermal and

environmental protection. The desired qualities for an EBC is: (1) environmental stability and low oxygen permeability, (2) low coefficient of thermal expansion (CTE) which is close to that of SiC to prevent cracking via thermal stress mismatch, (3) high-temperature chemical and phase stability, and (4) low thermal conductivity for increasing thermal protection and reducing cooling air requirements [31].

1.3 Development trend of environmental barrier coatings

1.3.1 First generation environmental barrier coatings

Early CMC coating development focused mainly on protecting silicon based ceramics from corrosion by molten salts. The first EBCs were proposed in the 1990's and consisted of a mullite ($3Al_2O_3$•$2SiO_2$) coating applied directly to the SiC substrate [32] because of its close CTE match with SiC. However, a major drawback to these mullite coatings was the formation of surface cracks that allowed corrosive species to penetrate deep into the coating to the substrate. In process of conventional plasma sprayed mulltie, considerable amount of amorphous mullite phase was appeared due to the rapid cooling of molten mullite during its solidification on a cold substrate. The crystallization of the amorphous phase under thermal cycling, which accompanies a volumetric change, was identified as the primary cause of the coating cracking [32]. Subsequently, a modified plasma spray process was developed that eliminated the amorphous mullite form the coating. However, one issue was later determined that the recession in high velocity combustion environments due to the volatilization of the silica by presence of water vapor. In order to overcome the recession of mullite, a water vapor resistant coat was added on top of the mullite coating. Consequently, the first generation EBC was developed by using YSZ (ZrO_2-8 mass% Y_2O_3) as an overlay of the mullite coating [33, 34].

Thermal cycling tests in water vapor revealed that the coating quickly cracked and delaminated at either the YSZ-mullite or the mullite-SiC interfaces. The rapid failure was attributed to the CTE mismatch between YSZ, mullite and the substrate [33, 35, 36]. One additional drawback of such coating with mulltie applied directly to the substrate was the formation of a porous, low viscosity SiO_2 scale at the mullite-SiC interface [31]. This was linked to both chemical contamination of the SiO_2 scale and the bubbling of gaseous species through the scale. This leads to poor adhesion and premature spallation of the coating at the mullite- SiC interface [34, 37]. Improving adherence of the coating was determined to be critical priority for enhanced durability.

1.3.2 Second generation EBCs

Several alkaline earth and rare earth silicates were identified with well-matched CTEs that exhibited little weight change during high temperature, high water vapor pressure environmental exposure, as shown in Table 1.1. Barium strontium aluminum silicate (BSAS) was applied to replace the YSZ top coat because it has a low silica activity and CTE that is well matched with the substrates. Adding BSAS second phase in the mullite coating also significantly reduced the tensile stress, resulting in far superior crack resistance compared to the unmodified mullite coating [38]. Another innovation in second generation EBCs was the development of a Si bond coat which further enhanced the EBC performance by providing significantly improved adherence. These EBCs were proved for thousands of hours at 1250°C on the SiC/SiC CMC combustor liners of three Solar Turbines Centaur 50s gas turbine engines [38]. However, BSAS reacts with thermally grown silica, which was formed on Si bond coat by oxidation, to generate a low melting glass (~1300°C) that causes EBC degradation and premature failure at temperatures above 1300°C [39]. Besides, a projection based

on a silica volatility model in conjunction with BSAS volatility data form high steam low velocity environments indicates a BSAS recession of approximately 70 μm after 1000 h at 1400°C, 6 atm in total pressure, and 24 m/s gas velocity [39]. Actual gas turbines operate at significantly higher pressure and gas velocities, increasing the projected recession to much higher levels. This finding indicated that the need for EBC topcoats to have reasonably matched CTE, low volatility, and high temperature phase stability over extended durations.

Table 1.1 Thermal expansion coefficient of EBC materials, adapted from Lee [40]

Material	CTE (10^{-6} K^{-1})	Melting Point (°C)	Application
Y_2SiO_5	5-6	1980	Top coat
Yb_2SiO_5	3.5-4.5, 7-8[93]	1950	
Er_2SiO_5	5-7, 7-8[93]	1980	
$Lu_2Si_2O_7$	3.8	unknown	
$Yb_2Si_2O_7$	4-6	1850	
$Y_2Si_2O_7$	3.9	1775	
BSAS (monoclinic)	4-5	1300	
BSAS (hexagonal)	7-8	1300	
Mullite	5-6	1800	Intermediate coat
Al_2O_3	6.0-8.4	2072	
Si	3.5-4.5	1414	Bond coat
SiC, SiC/SiC	4.5-5.5	2545	Substrate
Si_3N_4	3-4	1875	

Some rare earth silicates have been identified as promising candidates due to their low CTE, phase stability and low silica activity. Yttrium (Y), ytterbium (Yb) and lutetium (Lu) silicates exhibit some of the low volatilities in steam. The CTE of these and other candidate materials are summarized in Table 1.1. Rare earth monosilicates (RE_2SiO_5; RE = rare earth element) are significantly less volatility than BSAS in water vapor, while the volatilities of rare earth disilicates ($RE_2Si_2O_7$) are similar to that of BSAS [40]. Like BSAS, the RE-silicates are reportedly unstable as single layer coatings applied to SiC substrates, and a tri-layer RE-silicates/mullite/silicon coating approach same to the BSAS top coat EBC has been proposed [40].

The tri-layer RE-silicates based coatings have lifetimes of several hundred hours during steam-cycling at 1380°C in 90 % H_2O-balance O_2 [40, 41]. One potential disadvantage of rare earth silicate coatings compared to BSAS coating is their susceptibility to through-thickness cracking. In case of SiC/SiC substrate, the cracks propagate from the top coat and stop within the intermediate coat or at the interface of the intermediate coat/Si bond coat. In contrast to the same EBC on Si_3N_4 substrate, cracks typically penetrate through the Si bond coat all the way to the interface of Si/Si_3N_4. Some cracks branch laterally within the Si bond coat [40]. In both of substrates, the penetration of oxygen along the cracks will cause the oxidation which accelerate the degradation of the Si bond coat as well as the substrate. The degradation of the Si bond coat will eliminate the adherence of the EBCs as well. These may affect the long-term durability and protection of the RE-silicate based coatings under frequent thermal cycling.

In order to maintain the durability and protection of rare earth silicate EBCs under thermal cycles, the crack propagation have to be stopped when it appears within the top coat. The idea to solve this problem is introduce self-healing function to the top

coat. The top coat introducing self-healing function will be anticipated to serve longer time and more reliable with the ability of healing by itself. With respect to this proposal, the rare earth silicate ceramic must have the self-healing function as well.

1.4 Self-healing function of ceramics based composites

Structural ceramic materials are known as one of the prime candidates used for manufacturing of high temperature apparatus because of excellent heat resistance, mechanical strength and wear resistance [42]. But their ductility and fracture toughness are fairly lower than the metallic materials due to the sensitivity to flaws. Several investigators have found that the strength of the structural ceramics can be increased by heating them. Heat treatment of the ceramic materials containing cracks can result in complete or partial recovery of the strength of the materials. This phenomenon is generally called "self-healing". The self-healing function in the structural ceramics was firstly reported in 1970's [43]. The monolithic alumina was heated up 1700 or 1900°C in order to obtain its strength recovery. Although its bending test results show less effective on strength recovery. The self-healing mechanism at that moment was the re-sintering process where cracks seem to heal via the disappearance of void space between adjacent grains. Due to the complex requirements as well as less effectiveness, this approach has limited work attributed to it today.

The self-healing in ceramics has been rapidly developed since 1992 when the self-healing function in silicon nitride ceramics was reported by Choi et al. [44]. The Si_3N_4 ceramic containing 10 % MgO additives was oxidized at high temperature to generated $MgSiO_3$ and accompanied with N_2 gas. The oxidation kinetics of the ceramic was controlled by the diffusion of Mg^{2+} ion through the grain boundary to the

surface. The outward diffusion of Mg^{2+} caused the formation of an oxidation product layer which is responsible for healing of surface cracks and recovering of the strength. Lately in 1995, Chu et al. reported the self-healing function in SiC/mullite composites [45]. At high temperature, the SiC phase was oxidized in to SiO_2 which accompanies a volume expansion. The volume expansion cause the closure of surface cracks as well as reduction of stress concentration on crack tips which consequently involved strength recovery. The self-healing mechanism of the SiC/mullite ceramic matrix composites is revealed in Figure 1.2. Following the idea, research on crack-healing function of SiC/Al_2O_3 composites had been conducted by Ando et al. [46]. Although Al_2O_3 matrix possesses a self-healing ability induced by re-sintering, the self-healing function of the composites comes from the volume expansion generated by oxidation of SiC into SiO_2. The crack-disappearance also resulted in the strength recovery of the composites.

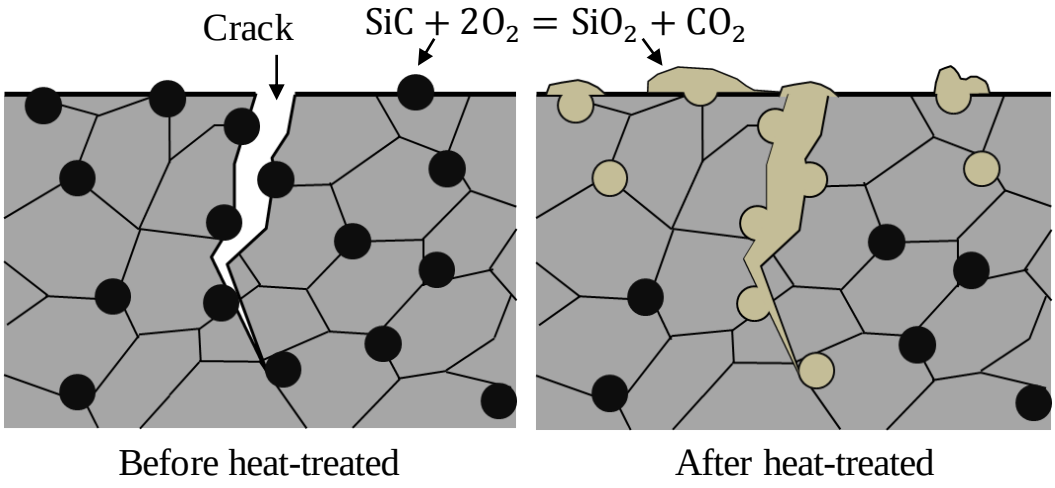

Figure 1.2 Schematic illustrates the self-healing mechanism of SiC/mullite matrix composites

Self-healing function at high temperature has been also reported lately for ceramic-based composites dispersed with metallic dispersoids as Ni/Al_2O_3 [47], Co/Al_2O_3 [48], and Ni/mullite [49]. Unlike the volume expansion induced

crack-healing of SiC/ceramic composites, the diffusion of metallic ions acts as the major role in crack-healing performance of metal/ceramic composites. With the diffusion mechanism, self-healing of metal/ceramics composites is expected to perform repeatedly. Figure 1.3 shows the oxidation mechanism which induced surface crack disappearance of the composites. The oxidation of metallic phase induces the diffusion of metallic cations and oxygen anions which cause the formation of surface layer and oxidized zone. The formation of the surface layer is responsible for self-healing function whereas the development of the oxidized zone is representative for oxidation resistance of the composites. The developments of the surface layer and oxidized zone are varied, depending on characteristics of matrix materials and dispersoids.

Since above studies were reported, the self-healing function of ceramic-based composites has been considered as a promising solution for high-temperature applications of structural ceramics. Self-healing function in ceramics, therefore, could be an excellent approach to improve lifetime and reliability of the EBC layers which play a major role in protection of the SiC/SiC CMC substrate at high temperature in combustion environments.

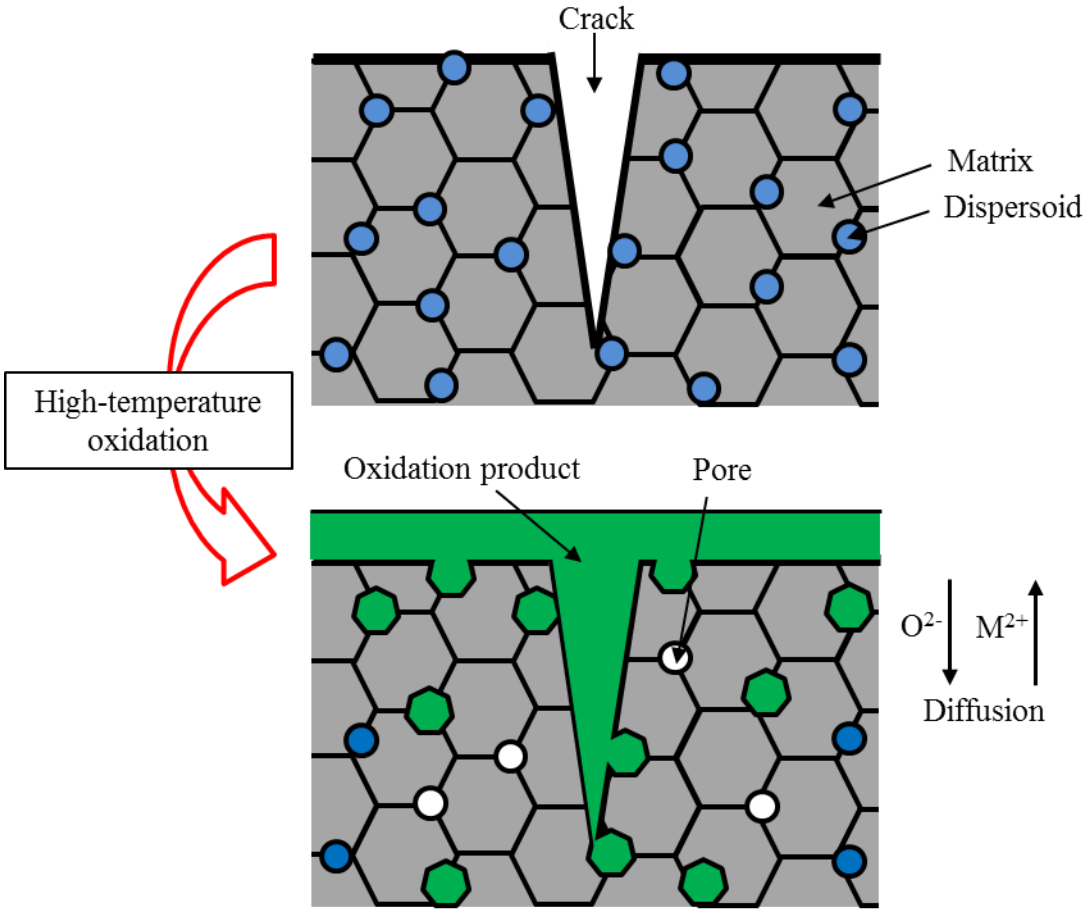

Figure 1.3 Schematic describe the self-healing mechanism of metal/ceramic composites

1.5 Self-healing EBC materials applied for SiC_f/SiC CMC substrate

As mention in above sections, cracks formation in the EBC layers decreased their lifetime and reliability. The cracks formation was caused by mismatch stress between the topcoat, the immediate coat and the substrate when they work under multiple thermal cycles, where the heating and cooling are repeated. In order to extend lifetime of the EBCs, we have proposed self-healing CMCs as potential candidates for EBC materials. SiC/yttrium silicate composites, material candidates of this study, are selected as examples. For a few recent years, some other researches on self-healing EBCs have been also conducted. The crack-healing function of $Y_2Si_2O_7$/BSAS coating

dispersed with $TiSi_2$ was investigated by Chen et al. [50]. The mixture powder including $Y_2Si_2O_7$, BSAS and $TiSi_2$ powders was prepared by ball milling with ethanol to obtain the slurry. Then, the slurry was uniformly applied on all sides of C/SiC bar. The $TiSi_2$-dispersed $Y_2Si_2O_7$/BSAS coating on C/SiC CMC substrate was obtained by heat treatment the sample at 1470°C under argon. The coating samples with and without $TiSi_2$ dispersion were corroded at 1250°C under an atmosphere of 50 % H_2O-50 % O_2. As the results, the $TiSi_2$-dispersed $Y_2Si_2O_7$/BSAS coated on C/SiC has better durability than the $Y_2Si_2O_7$/BSAS coated C/SiC. This result was explained by self-healing of through-thickness cracks in the dispersed coatings which were generated by the mismatched CTE between carbon fibers and the SiC matrix. The cracks in the dispersed coating were much wider than those in the non-dispersed coating because of large mismatch CTE between the $TiSi_2$ dispersoid and $Y_2Si_2O_7$/BSAS. The cracks in the dispersed coating were completely closed by the oxidation of $TiSi_2$ under water vapor corrosion. The filling oxidation products, including SiO_2 and TiO_2, in the through-thickness cracks became denser with prolonged corrosion time. This fact indicated that this is a mass transport process. The closure of the cracks may block the penetration of water vapor into the C/SiC substrate along the cracks, thus improving the durability of the dispersed coating.

Crack-healing ability of SiC/$Yb_2Si_2O_7$-Yb_2SiO_5 composites, which were considered as promising EBC materials, was reported by Nguyen and his co-workers [51, 52]. Bulk samples of the composites dispersed with various volume fractions of SiC particles were fabricated by hot pressing at 1550°C, 30 MPa for 1 h, in argon atmosphere. The as-cracked samples were made by introducing the Vickers indentations on polished surface of as-sintered samples. The cracked samples were annealed at 1250°C for 2 h in air and argon. The crack-healing behavior of the

composites was investigated by evaluation of crack-disappearance and strength recovery. As the results, in the $Yb_2Si_2O_7$-Yb_2SiO_5 composites dispersed with 20 % SiC particles, the surface cracks were almost fully healed after annealing at 1250°C for 2 h in air. Strength of as-cracked samples was reduced by 30~50 %, compared to that of as-sintered samples. However, after annealing in air, the strength of all composites was recovered obviously. The healing of surface cracks reduced stress concentration at crack tips leading to the recovery of the strength. The cracks were healed by volume expansion of newly formed $Yb_2Si_2O_7$ phase. The formation of the $Yb_2Si_2O_7$ phase was considered as the reaction of Yb_2SiO_5 matrix and SiO_2 product which was generated by oxidation of SiC dispersoid.

1.6 Material candidates of the present dissertation

Three matrix materials, including yttrium monosilicate (Y_2SiO_5), yttrium disilicate ($Y_2Si_2O_7$) and mixing Y_2SiO_5-$Y_2Si_2O_7$ matrix, are described in this dissertation. The Y_2O_3-SiO_2 (Figure. 1.4) system was chosen over other rare earths since yttrium silicates satisfy most of the criteria a material candidate must have for an EBC layer. There have been limited experimental determinations of the thermochemical stability of yttrium silicates in high temperature water vapor. However, these data indicate that yttrium silicates possess sufficient stability for use as a water vapor resistant coating material for SiC/SiC CMC substrate [40, 53, 54, 55].

While Y_2SiO_5 exhibits excellent thermochemical stability in high temperature water vapor, it has a large CTE mismatch with SiC whereas $Y_2Si_2O_7$ possesses a good match to SiC (Table 1.2). Although $Y_2Si_2O_7$ has four polymorphs (triclinic-α, monoclinic-β and γ, orthorhombic-δ) [56-58], the volume change that accompanies most polymorphic transformation is expected to be small since the density of each

polymorph is similar (α= 4.30, β= 4.03, γ= 4.04, δ= 4.11 g/cm^3) [58]. However, the difference in CTE between α, δ polymorphs and β, γ polymorphs may lead to crack formation under multiple thermal cycles (Table 1.2) [59]. Similarly, Y_2SiO_5 possesses two polymorphs (X1 and X2) with differences in their CTE (Table 1.2) [60]. There is controversy over the temperatures associated with the polymorphic transformations in $Y_2Si_2O_7$ and Y_2SiO_5. Therefore, the temperatures reported in Table 1.2 represent the widely accepted polymorphic transformation temperatures [56, 61-65]. The melting temperatures of $Y_2Si_2O_7$ and Y_2SiO_5 reported in Table 1.2 are those which have been observed experimentally [57, 58, 66].

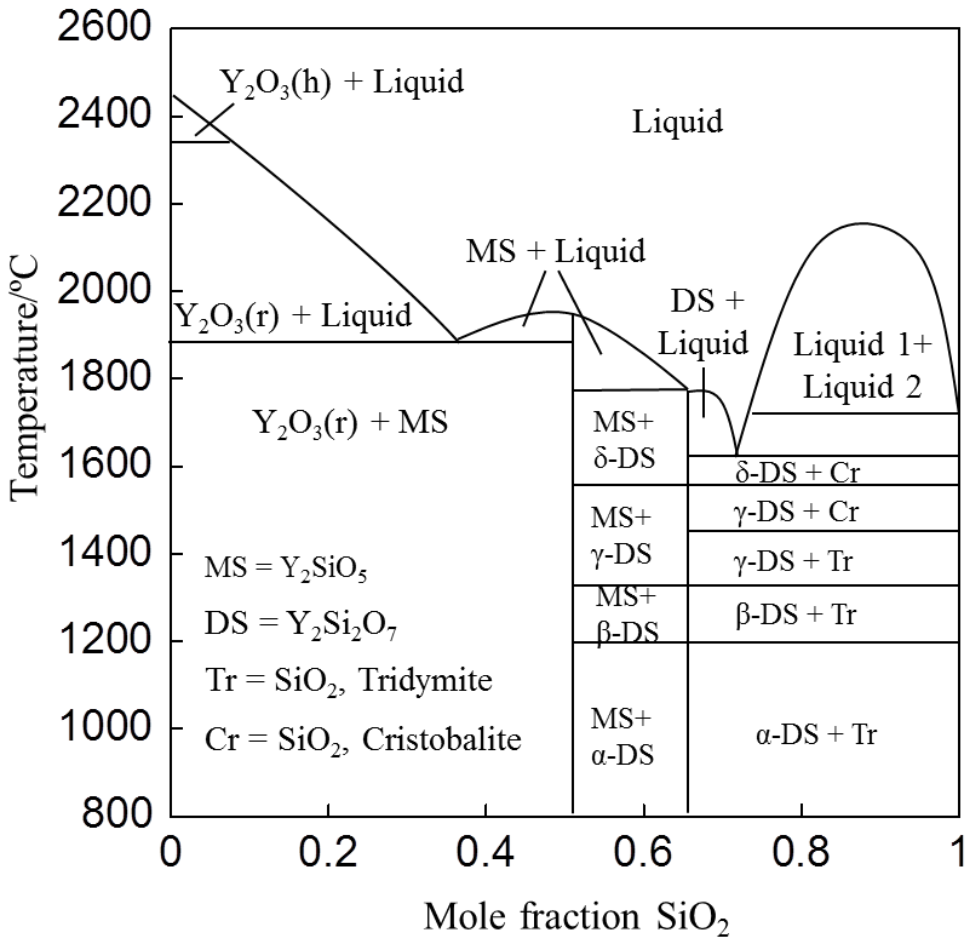

Figure 1.4 Y_2O_3-SiO_2 system phase diagram [56]

Table 1.2 Coefficient of thermal expansion (CTE) and melt/transformation temperature for $Y_2Si_2O_7$, Y_2SiO_5 and Y_2O_3

Material	Crystal structure/ Polymorph	CTE (10^{-6} K^{-1})	Melt/Transformation Temperature (°C)
$Y_2Si_2O_7$	Triclinic, α	8.0[59]	1225[57, 58]
	Monoclinic, β	4.1[59]	1445[57, 58]
	Monoclinic, γ	3.9[59]	1535[57, 58]
	Orthorhombic, δ	8.1[59]	1775[57, 58, 66]
Y_2SiO_5	Monoclinic, X1	8.7[60]	1190[57, 58]
	Monoclinic, X2	7.8[60]	1980[66]
Y_2O_3	Cubic, Hexagonal	8.2-9.5	2410

1.7 Scope of the present dissertation

The purpose of this dissertation is to develop the self-healing function for SiC particles dispersed rare earth silicate-based composites which are SiC/Y_2SiO_5, SiC/$Y_2Si_2O_7$ and SiC/Y_2SiO_5-$Y_2Si_2O_7$ composites. Self-healing function of the composites is evaluated through the surface crack-disappearance, self-healing induced strength recovery at room temperature and oxidation resistance. The surface crack-disappearance is estimated by the fraction of surface crack length before and after annealing in the air. The crack-healing effectiveness on strength recovery at room temperature is conducted by room temperature bending tests. Oxidation resistance of the composites is investigated through the growth of oxidized zone by heat treatment in the air. Effects of SiC volume fraction on self-healing performance and oxidation resistance of the mixing Y_2SiO_5-$Y_2Si_2O_7$ matrix composites is investigated by

following the above procedures. The self-healing mechanism of the composites is discussed as well. In order to discuss the self-healing mechanism, evaluation of the diffusion coefficients of Y and O ions in the matrices are conducted through diffusion couple experiments.

To achieve the objectives outlined above, the major topics are presented and discussed as following:

1. Chapter 2: Self-healing function of Y_2SiO_5 matrix composites dispersed with SiC particles.
2. Chapter 3: Self-healing function of $Y_2Si_2O_7$ matrix composites dispersed with SiC particles.
3. Chapter 4: Self-healing function of Y_2SiO_5-$Y_2Si_2O_7$ matrix composites dispersed with SiC particles. Effect of SiC volume fractions on self-healing of the composites is investigated as well.
4. Chapter 5: Diffusivity of ions in yttrium monosilicate.
5. Chapter 6: General conclusions.

Chapter II

Self-healing Function of SiC/Y_2SiO_5 Matrix Composites

2.1 Background

As the mention in previous section, yttrium monosilicate (Y_2SiO_5) possesses two monoclinic crystal structures named X1-Y_2SiO_5 low temperature phase and X2-Y_2SiO_5 high temperature phase. Single-phase X2-Y_2SiO_5 (hereafter written as Y_2SiO_5 for brevity) was the most thoroughly studied of the rare earth monosilicate because the X2-polymorph was successfully synthesized and stable at high temperatures. The mechanical and thermal properties of Y_2SiO_5 ceramic have been evaluated by Sun et al. [69, 70]. The results indicated that Y_2SiO_5 ceramic is very competitive candidate material for EBCs. Practically, Y_2SiO_5 coating on SiC-based ceramics can improve the high-temperature oxidation of the substrate efficiently [65, 71]. However, appearance of through-thickness cracks in the coating affected lifetime and protection of the coating [40]. From the above reasons, the self-healing function of Y_2SiO_5 ceramic matrix composites dispersed with SiC particles would be suitable for self-healing EBC applications.

In this chapter, the investigation of self-healing function for 5 vol% SiC/Y_2SiO_5 is conducted. The seal-healing ability is estimated through the fraction of surface crack-disappearance before and after heat treatment at 1100 to 1300°C for 1 to 24 h in air. The effectiveness of crack-healing function on their strength recovery is examined by three-point bending tests conducted for as-sintered, as-cracked and as-healed samples. To clarify the self-healing mechanism and oxidation resistance of the composites, oxidation tests are carried out at 1200 to 1400°C for 1 to 48 h in air. Some

basic information on mechanical properties of the SiC/Y_2SiO_5 composites such as hardness and fracture toughness are provided as well.

2.2 Experimental procedure

The single-phase Y_2SiO_5 powder was synthesized by using solid-state reaction method from raw powder mixture including Y_2O_3 (Nippon Yttrium Co., Ltd, 99.9 % purity, d= 1.1 μm) and SiO_2 powder (Nacalai Tesque, Inc., 99 % purity). The mixture in a molar ratio 1:1 consisting of Y_2O_3 and SiO_2 powder was ball-milled in a plastic bottle with ethanol and alumina balls for 24 h. After drying and manual crashing, the mixture was annealed at 1400°C for 20 h in air. The received powder was phase-identified by using X-ray diffraction (XRD). Figure 2.1 shows XRD pattern of the powder fabricated by the above procedure. Only single-phase Y_2SiO_5 is detected and it corresponds to standard pattern of Y_2SiO_5 (ICDD Card, No. 36-1476).

Samples preparation of 5 % SiC/Y_2SiO_5 composites was conducted as the following procedure. A slurry mixture consisting of 5 vol% SiC (Ibiden Co., Ltd, 99.9 % purity, 0.32 μm mean particle size), Y_2SiO_5 powder and ethanol was ball-milled for 24 h in a plastic bottle with alumina balls (5 mm in diameter). The ceramic slurry was dried at 100°C for 10 h in air and milled manually by using an alumina mortar to eliminate the agglomeration of the particles. Bulk specimens of the composites were fabricated by pulsed electric current sintering (PECS) with a graphite die in vacuum at 1600 °C under 70 MPa in uniaxial pressure for 5 min holding time. The density of the as-sintered sample was measured by the Archimedean method with toluene. The relative density (R.D.) of all the specimens fabricated by this procedure reached at least 99 % of the theoretical value of the composites. The bulk samples were then ground by a grinding wheel with diamond grains of 30 μm and polished

with diamond particles slurry (2 μm). Figure 2.2 shows polished surface of the as-sintered sample observed by the scanning electron microscope (SEM). SiC particles, which could be observed as black dots, were homogeneously dispersed in Y_2SiO_5.

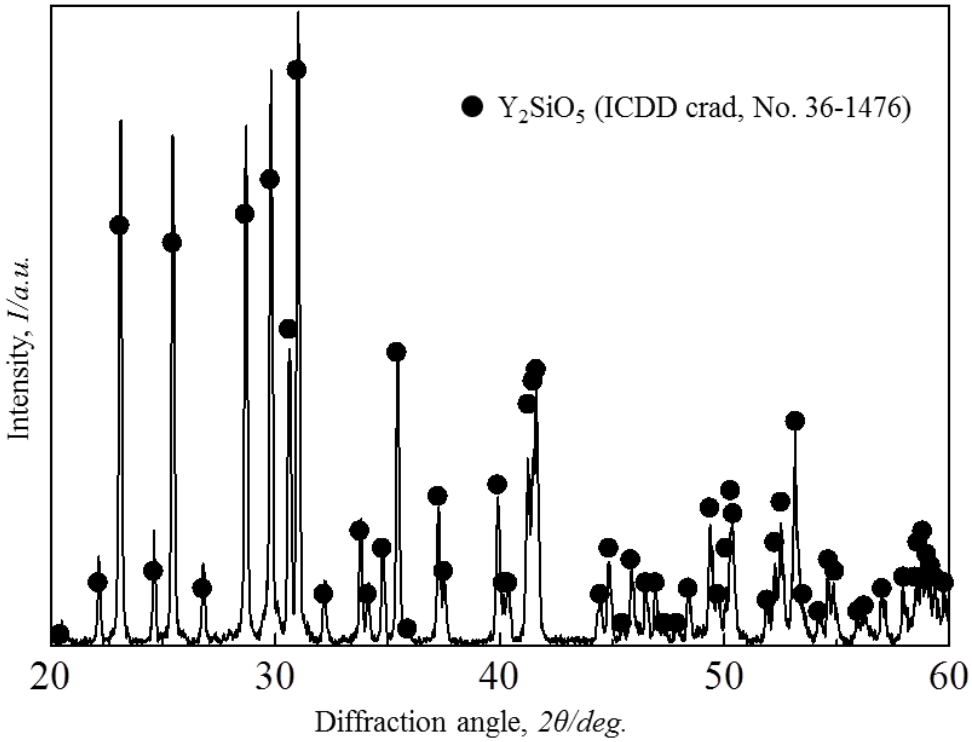

Figure 2.1 XRD pattern of obtained X_2-Y_2SiO_5 powder

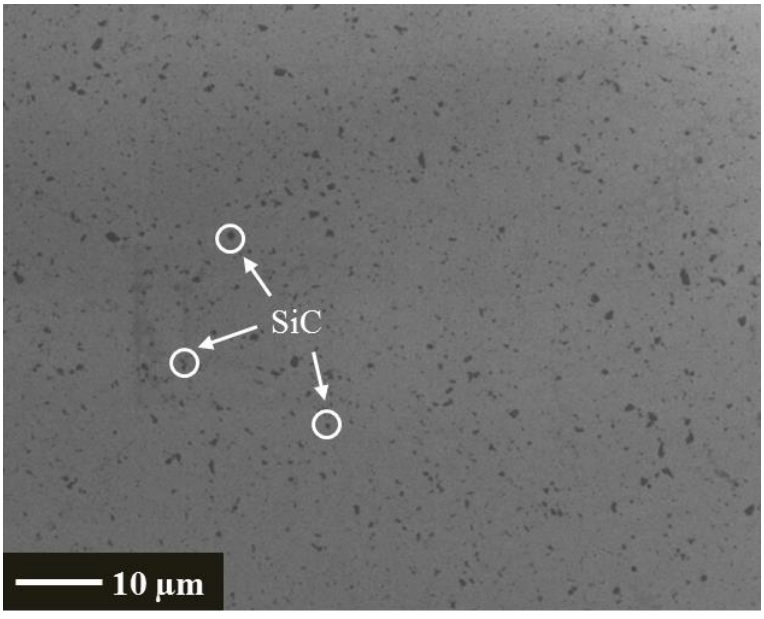

Figure 2.2 SEM image of the polished surface of as-sintered sample

The effectiveness of crack-healing was investigated by using specimens with introduced cracks on polished surface. Three Vickers indentations at a load of 20 N for 10 s were introduced to prepare 12 cracks on the sample surface. Semi-circular cracks with 200 μm in length and 100 μm in depth were made, as shown in Figure 2.3. The samples with introduced surface cracks were heat treated at temperatures ranging from 1100 to 1300°C for from 1 to 24 h in air. Surface crack disappearance was observed by SEM. The fraction of surface crack-disappearance was evaluated by basing on amount of surface crack length remaining after heat treatment as Maruoka et al. mentioned previously [67]. The oxidized samples were also analyzed by using X-ray diffraction (XRD) for phase identification on the sample surface.

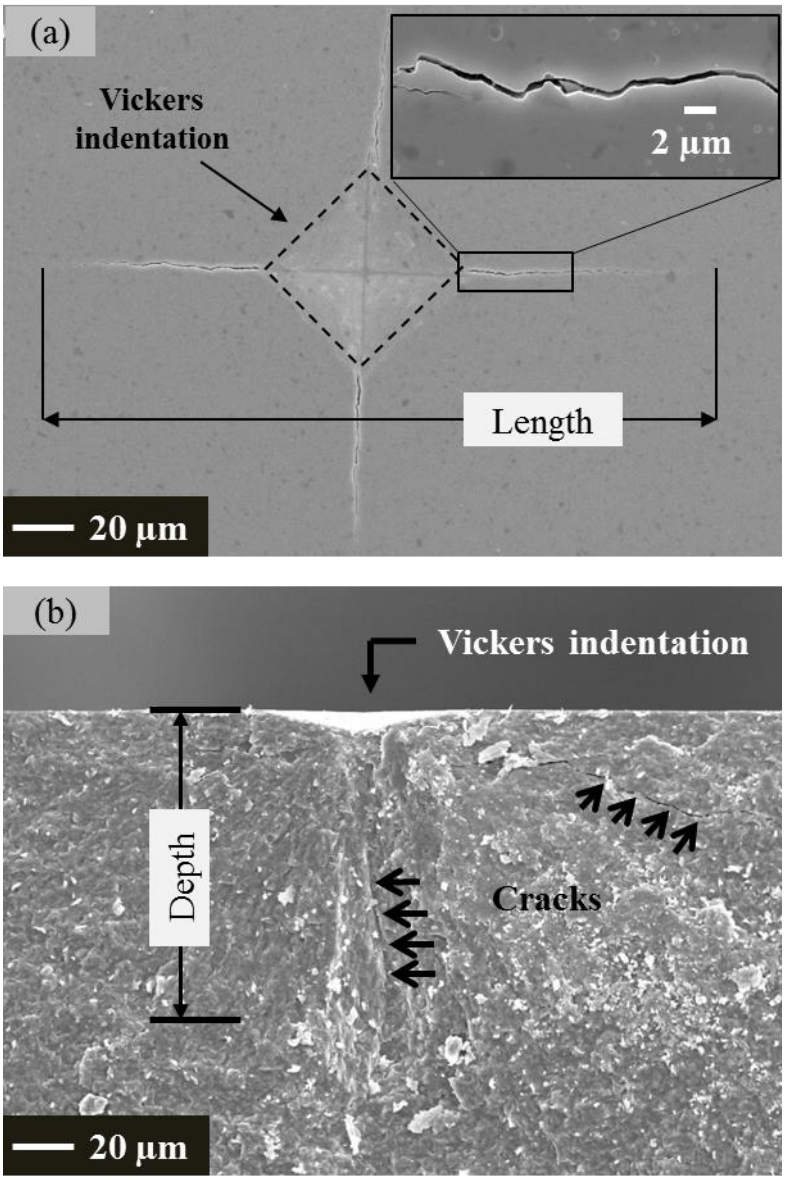

Figure 2.3 SEM images of the Vickers indentation from (a) the top view and (b) cross-sectional view of as-cracked sample

Investigation of strength recovery by surface crack-disappearance was conducted through bending tests at room temperature. Specimens used for bending test were cut into a rectangular shape with 3 x 4 x 24 mm in dimensions. The mirror polished surface was prepared by using a grinding wheel with 30 µm-diamond grains and polishing with 2 µm-diamond particles slurry. The polished samples are referred to as-sintered samples, hereafter. Three Vickers indentations were introduced at the

center of the sample tension surface by applying a load of 20 N for 10 s. The samples with introduced the indentations are referred to as-cracked samples, hereafter. As-healed samples were prepared by heat treatment of as-cracked samples. Three-point bending tests were conducted with a cross-head speed of 0.5mm/min at room temperature for as-sintered, as-cracked and as-healed specimens [68]. After bending test, surface of bended samples was observed by SEM to determine the fracture.

High-temperature oxidation tests at temperatures ranging from 1200 to 1400°C for 1 to 48 h of these composites were conducted as the following steps. The specimens were put on zirconia balls (2 mm in diameter) in an alumina crucible and oxidized at the targeted temperatures in air. The heating rate in the oxidation experiments were 400°C/h. Then oxidized samples were cross-sectioned and polished with slurry of diamond particles (2 μm). The microstructure of cross-section was observed by SEM to determine thickness of oxidized zone. The phase identification of oxidized samples was carried out by using XRD.

2.3 Results and discussion

2.3.1 Mechanical properties

Mechanical properties of 5 vol% SiC/Y_2SiO_5 composites at room temperature are shown in Table 2.1. Vickers hardness (H_v) of 5SiC/Y_2SiO_5 was measured to be 8.25±0.15 GPa. Fracture toughness (K_{IC}) of the composites calculated by applying Niihara's equation [72] was 5.93±0.15 MPam$^{1/2}$. Through the three-point bending tests conducted at room temperature, bending strength of the composites was 270±10 MPa. The mechanical properties of monolithic Y_2SiO_5 [69] are also shown in Table 2.1.

Table 2.1 Mechanical properties monolithic Y_2SiO_5 and $5SiC/Y_2SiO_5$ at room temperature

Sample	*R.D* (%)	H_v/GPa	K_{IC}/MPam$^{1/2}$	σ_b/MPa
Y_2SiO_5	98	5.3±0.1	1.85±0.17	116±3
$5SiC/Y_2SiO_5$	99.4	8.25±0.15	5.93±0.15	270±10

As shown in Table 2.1, the hardness and fracture toughness of the $5SiC/Y_2SiO_5$ composites are larger than that of the monolithic Y_2SiO_5. This fact indicates that dispersion of SiC in Y_2SiO_5 matrix gave considerable effect to their mechanical strength. The fracture toughness of the composites is significantly improved due to residual stress in Y_2SiO_5 matrix. The residual stress caused by the difference in CTE of SiC dispersoid and Y_2SiO_5 matrix at high temperatures.

2.3.2 Surface crack-disappearance

Figure 2.4 shows SEM images observed on surface of as-cracked samples before and after heat treatment for 1 h at various oxidation temperatures. The dash lines present the outline of the Vickers indentation. Before heat treatment, the cracks on surface of sample propagated from corners of the imaged Vickers indentation could be observed obviously, as shown in Figure 2.4 (a). After heat treatment at 1200°C for 1 h in air, sample surface was covered with oxidation products, as presented in Figure 2.4 (b). Surface cracks were healed partially. The surface crack disappearance was initially observed at the end of each crack and then the disappeared area extended to the corner of the Vickers indentation. Surface cracks were disappeared completely after heat treatment at 1300°C for 1 h in air, as shown in Figure 2.4 (c). Heat treatment at the same condition but in the Ar-1 %H_2 flow do not show any disappearance of the surface crack, as shown in Figure 2.4 (d).

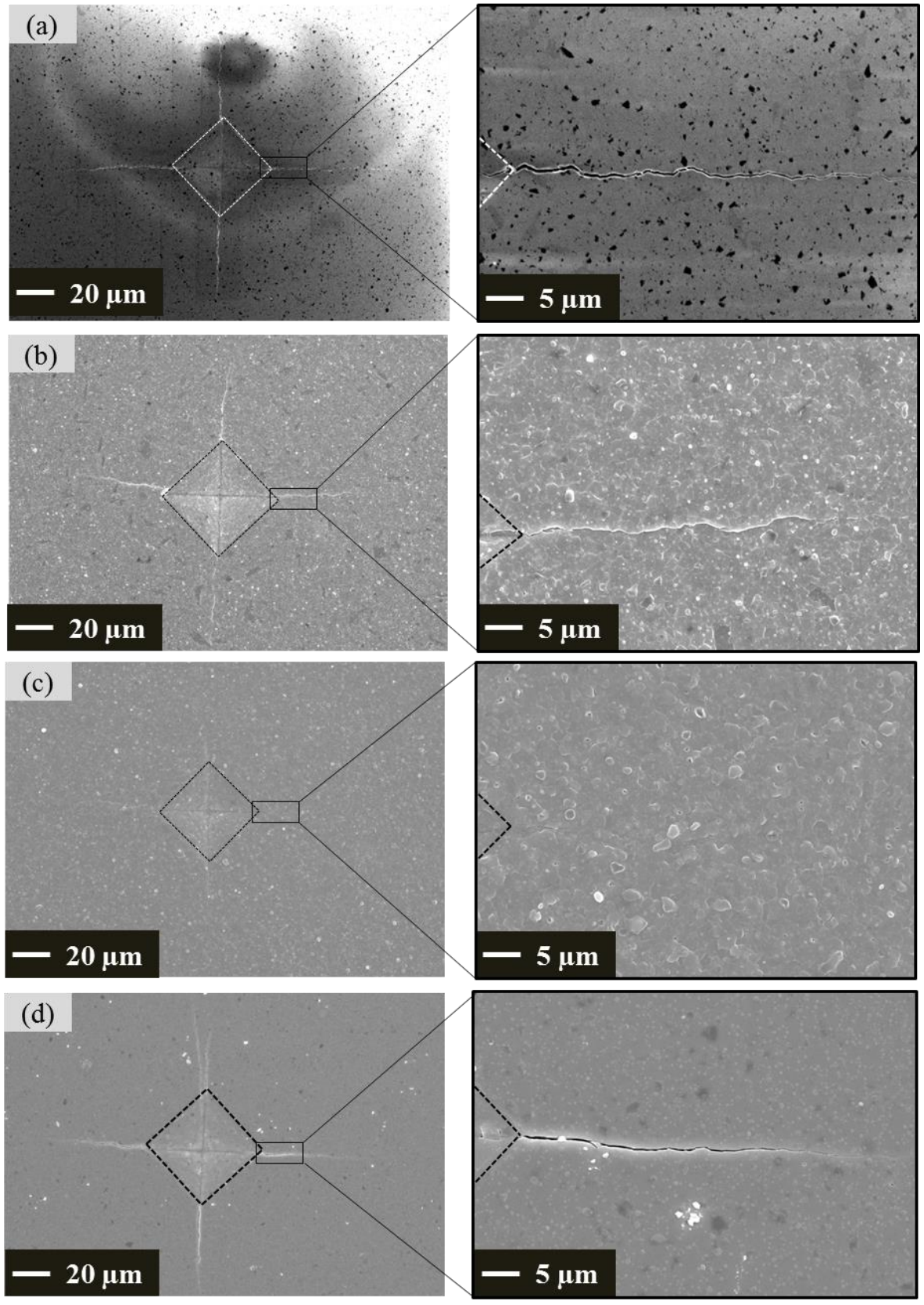

Figure 2.4 SEM images of surfaces of (a) as-cracked sample and samples heat-treated (b) 1200°C for 1 h in air, (c) 1300°C for 1 h in air, (d) 1300°C for 1 h in Ar-1%H_2 gas

Figure 2.5 represents the fraction of crack disappearance of specimens heat-treated in the logarithm of the reciprocal heat-treatment time as a function of the reciprocal heating temperature. Crack disappearance was categorized into three groups by less, partial and complete disappearance. This graph showed that fraction of crack disappearance was increased with increasing heat treatment temperature and time.

Figure 2.6 shows XRD patterns obtained from the sample surface before and after heat treatment for 1 h at various conditions. Figure 2.6 (a) shows the results for the as-sintered specimen in which only Y_2SiO_5 and SiC peaks were detected and no other crystalline phases were observed. The XRD patterns of samples heat-treated for 1 h at 1200 and 1300°C were respectively presented in Figures 2.6 (b) and (c). The results indicate that new peaks of oxidation product were detected on the surface of as-healed samples. Intensities of these new peaks became greater with higher heat-treated temperatures. The new phase appeared on surface of as-healed sample was identified to be $Y_2Si_2O_7$. The results mean that SiC particles were reacted with oxygen and Y_2SiO_5 matrix as the following equilibrium:

$$SiC + Y_2SiO_5 + 3/2O_2 = Y_2Si_2O_7 + CO \quad (2.1)$$

Because of the reduction environment without presence of oxygen, no changes were observed on surface of sample heat-treated at 1300°C for 1 h in the Ar-1 % H_2 gas mixture. No new peaks were detected, as shown in Figure 2.6 (d).

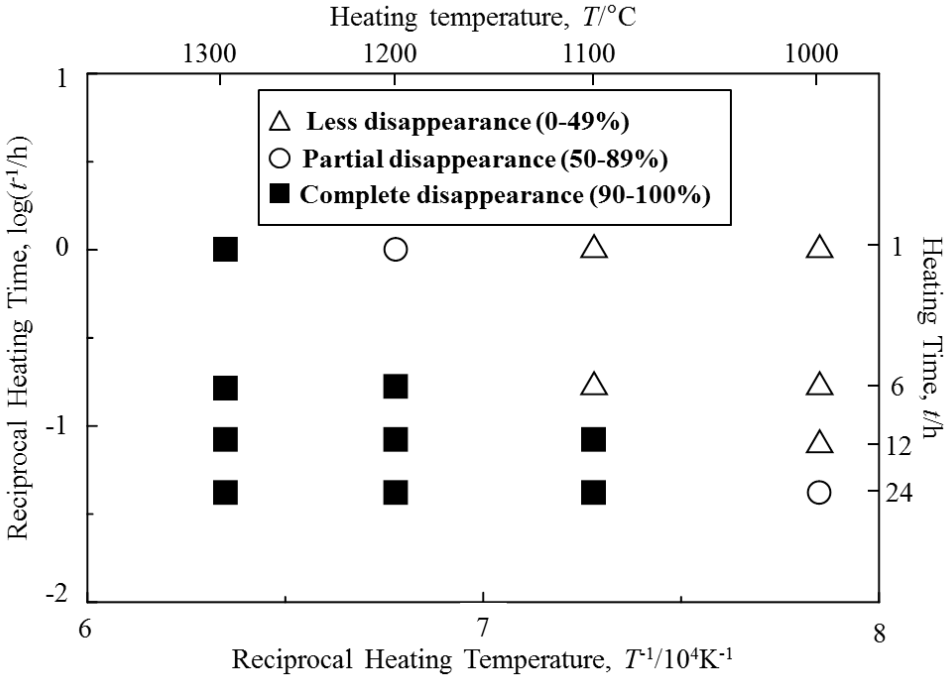

Figure 2.5 Dependence of crack disappearance on reciprocal time and temperatures

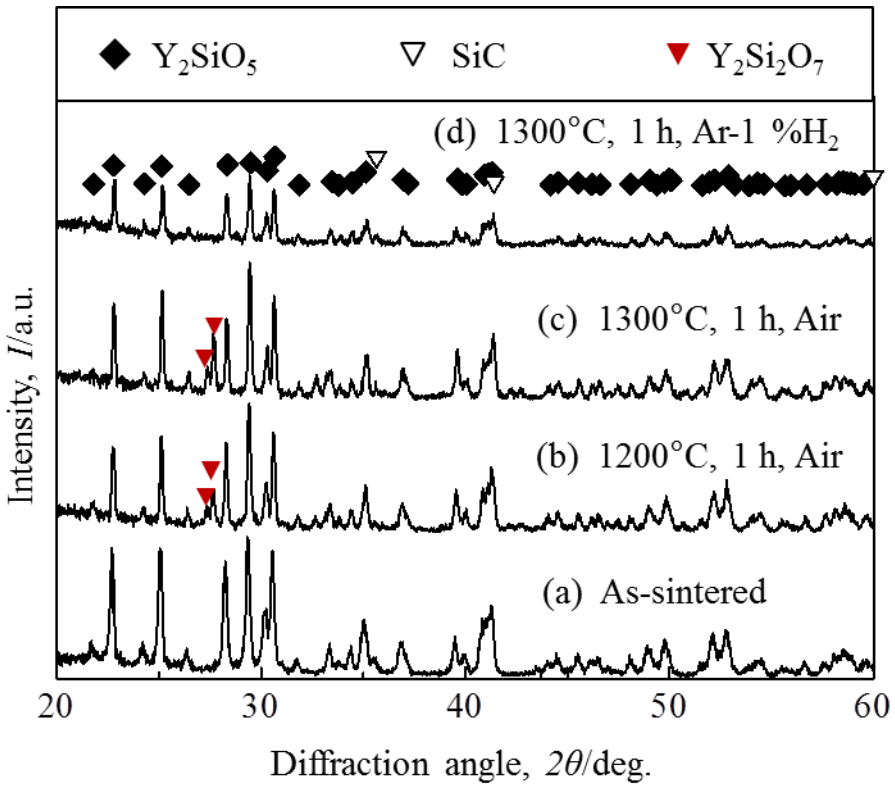

Figure 2.6 XRD patterns of surface samples before and after heat treatment at various heat treatments

In order to clarify the self-healing ability of SiC/Y_2SiO_5 composites, the crack-disappearance of the composites was compared with those of SiC/ceramic composites such as SiC/mullite [73] and SiC/Al_2O_3 composites [74]. In both case of SiC/mullite and SiC/Al_2O_3 composites, 20 vol% SiC were dispersed in mullite and Al_2O_3 matrices. And surface cracks with approximately 100 μm in length were completely healed after heat treatment at 1300°C for 1 h in air. In case of SiC/Y_2SiO_5 composites, 5 vol% SiC were dispersed in Y_2SiO_5 matrix. Surface cracks with approximately 200 μm could be completely disappeared after heat treatment at 1300°C for 1 h in air. Although surface cracks on those composites were completely healed at same condition, SiC/mulltie and SiC/Al_2O_3 composites needed more fraction of SiC for healing than SiC/Y_2SiO_5 composites. Crack-healing of SiC/mullite and SiC/Al_2O_3 composites was reported to be caused by formation of oxidation product, SiO_2, associated with a volume expansion. More SiC particles on crack surface are necessary to generate much SiO_2 phase which accompanies the volume expansion induced crack-healing of SiC/mullite and SiC/Al_2O_3 composites. Self-healing mechanism of SiC/Y_2SiO_5 composites is differed from that of SiC/mullite and SiC/Al_2O_3.

In terms of SiC/Y_2SiO_5 composites, the outward diffusion of Y^{3+} cations, which was responsible for formation of $Y_2Si_2O_7$ layer on the sample surface, plays the major role in the crack-healing effectiveness of SiC/Y_2SiO_5 composites. Inward diffusion of oxygen passing through the component causes the oxidation of SiC particles within Y_2SiO_5 matrix to form $Y_2Si_2O_7$ phase. This process induced a small volume expansion of 1.14 times. However, the small volume expansion could be not attributed to healing surface cracks. Only 5vol% SiC on the sample surface (including crack surface) was not enough to create the oxidation product filling in the cracks. The surface cracks were healed by filling and re-bonding with $Y_2Si_2O_7$ layer. The formation of $Y_2Si_2O_7$

layer on the initial surface is proposed by outward diffusion of Y^{3+} cations. The formation of sub-micron spherical voids after high-temperature oxidation is the evidence of the outward diffusion of the cations, as shown in Figure 2.10. Although the outward diffusion of cations could cause the formation of oxidation product layer on the sample surface, the oxidation product layer is not obviously observed on surface of SiC/Y_2SiO_5. This indicates that contribution of outward diffusion of cations in this ceramic composite may be not so strong for high-temperature oxidation. This assumption can be also explained through formation of short cracks after annealing, as shown in Figure 2.10. Inward diffusion of oxygen passing through Y_2SiO_5 matrix gives a volume expansion of SiC dispersion upon conversion to $Y_2Si_2O_7$. The volume expansion of $Y_2Si_2O_7$ causes the formation of the short cracks. If the outward diffusion of cations is much faster than inward diffusion of oxygen, the volume expansion would be completely compensated due to the formation of the voids in the inside of the sample. It means that volume change in the inside of oxidized zone will be negative. And the interior cracks will be not appeared. This behavior was observed in Ni/Al_2O_3 and Ni/MgO composites after high-temperature oxidation [75]. The determination of ions diffusivity in the Y_2SiO_5 matrix will be conducted in chapter VI to clarify this issue.

2.3.3 Strength recovery induced by self-healing

Figure 2.7 shows the bending strength of as-sintered, as-cracked and as-healed samples at room temperature. The as-sintered samples achieved approximately 270 MPa in bending strength. After three-Vickers indentations were introduced on sample surface, cracking decreased the bending strength to approximately 100 MPa. The sample with heat treatment at 1300°C for 1 h in air, as-healed exhibited a bending

strength of 330 MPa which is comparable with that of as-sintered samples.

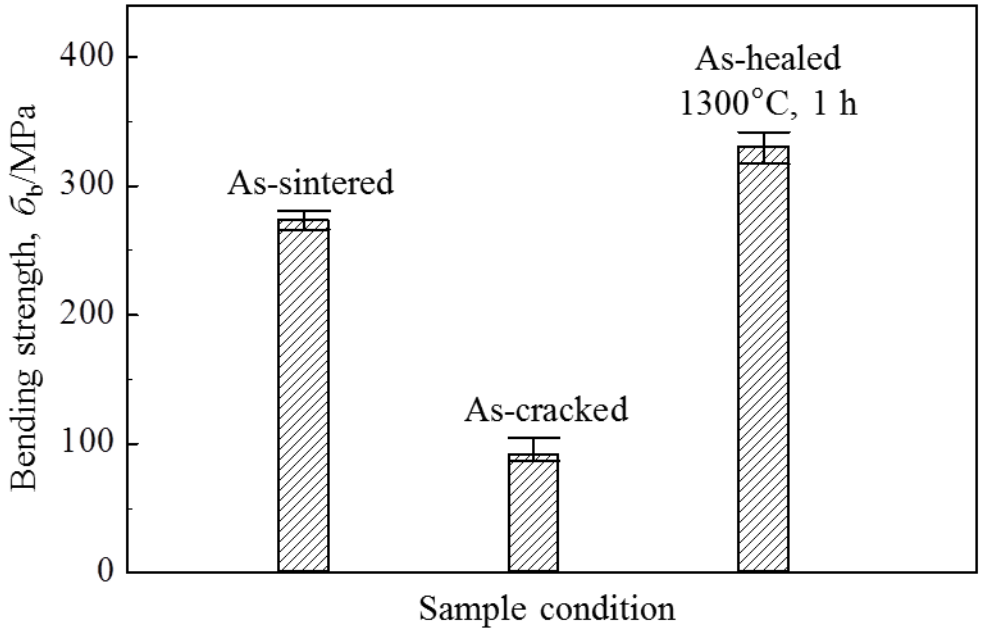

Figure 2.7 Bending strengths of as-sintered, as-cracked samples and samples heat treatment at 1300°C for 1 h in air

Figure 2.8 shows SEM images observed on surface of bending test samples. Fracture mechanism of as-cracked sample was shown in Figure 2.8 (a). The Vickers indentation outlined by dash lines indicates that as-cracked sample fractured across the indentations and along surface cracks introduced by the indentation during bending test. After heat treatment at 1300°C for 1 h in air, the surface cracks are completely healed by filling of the oxidation products. Figure 2.8 (b) shows fracture mechanism of as-healed sample was different from that of the as-cracked sample. The failure of as-healed sample did not occur along the Vickers indentation. This fact implies that fracture strength at cracked region was recovered up to the same level of the region without cracks. And the recovery of the strength caused by the crack-disappearance after heat treatment. Figure 2.9 shows the cross-sectional view of cracks after heat treatment at 1300°C for 1 h in air. It means that the cracks were not only healed from

the top view but also from the cross-sectional view.

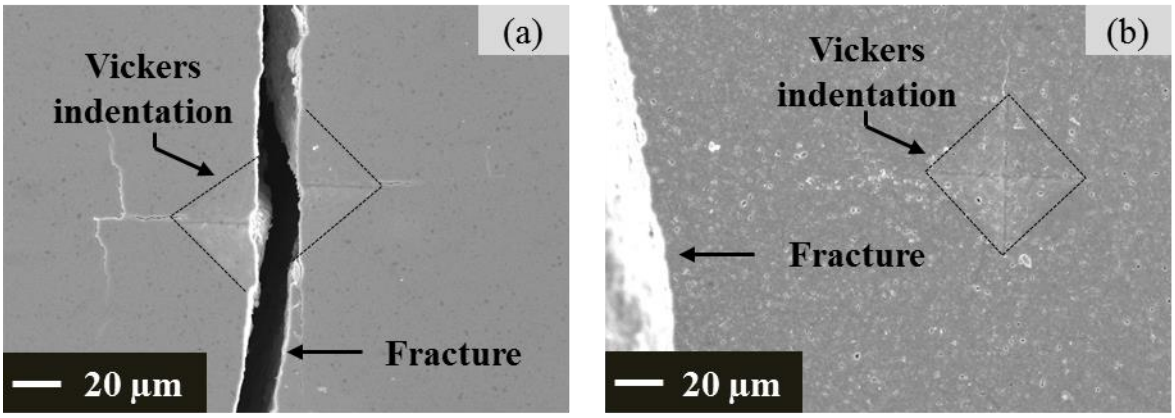

Figure 2.8 SEM images of fractures of samples after bending test at room temperature for (a) as-cracked and (b) as-healed sample

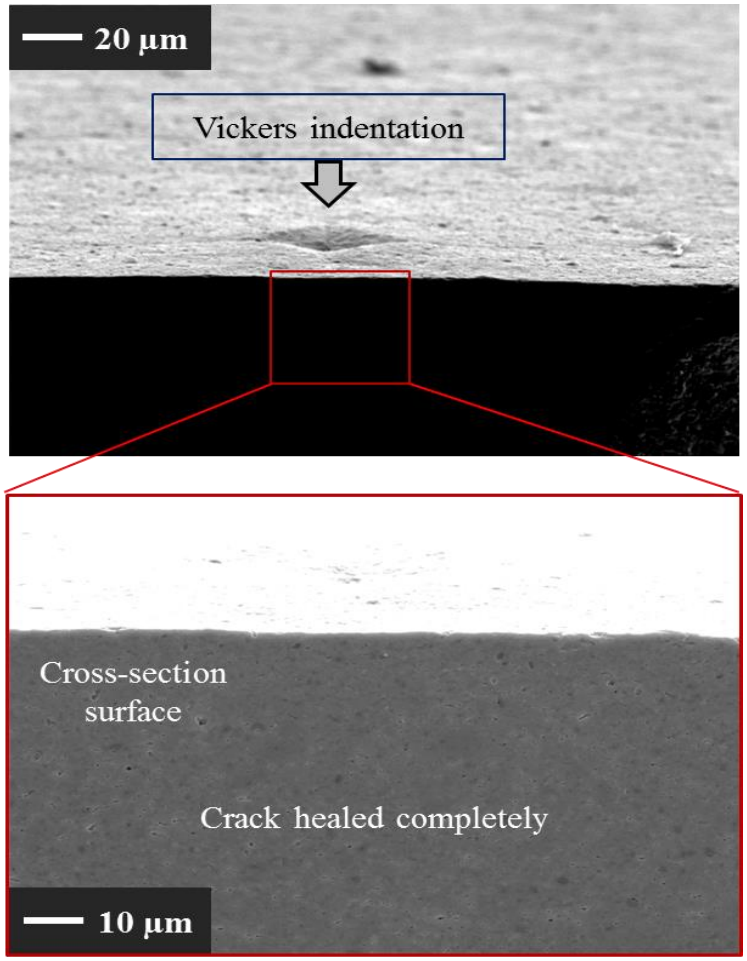

Figure 2.9 SEM images on cross-sectional view of the cracks after heat treatment at 1300°C for 1 h in air

2.3.4 Oxidation resistance

Figure 2.10 shows the SEM images of cross-sectioned surface of SiC/Y_2SiO_5, composites after oxidation at 1200, 1300 and 1400°C for 6 h. Oxidized zone was defined in which fine voids with sub-micro in diameter and small cracks parallel to the sample surface could be observed. In this region, SiC particles dispersed in the matrix were oxidized and disappeared partially or completely. In the region following the oxidized zone, no cracks and voids were observed. This region was defined as the non-oxidized zone where SiC particles can be observed clearly.

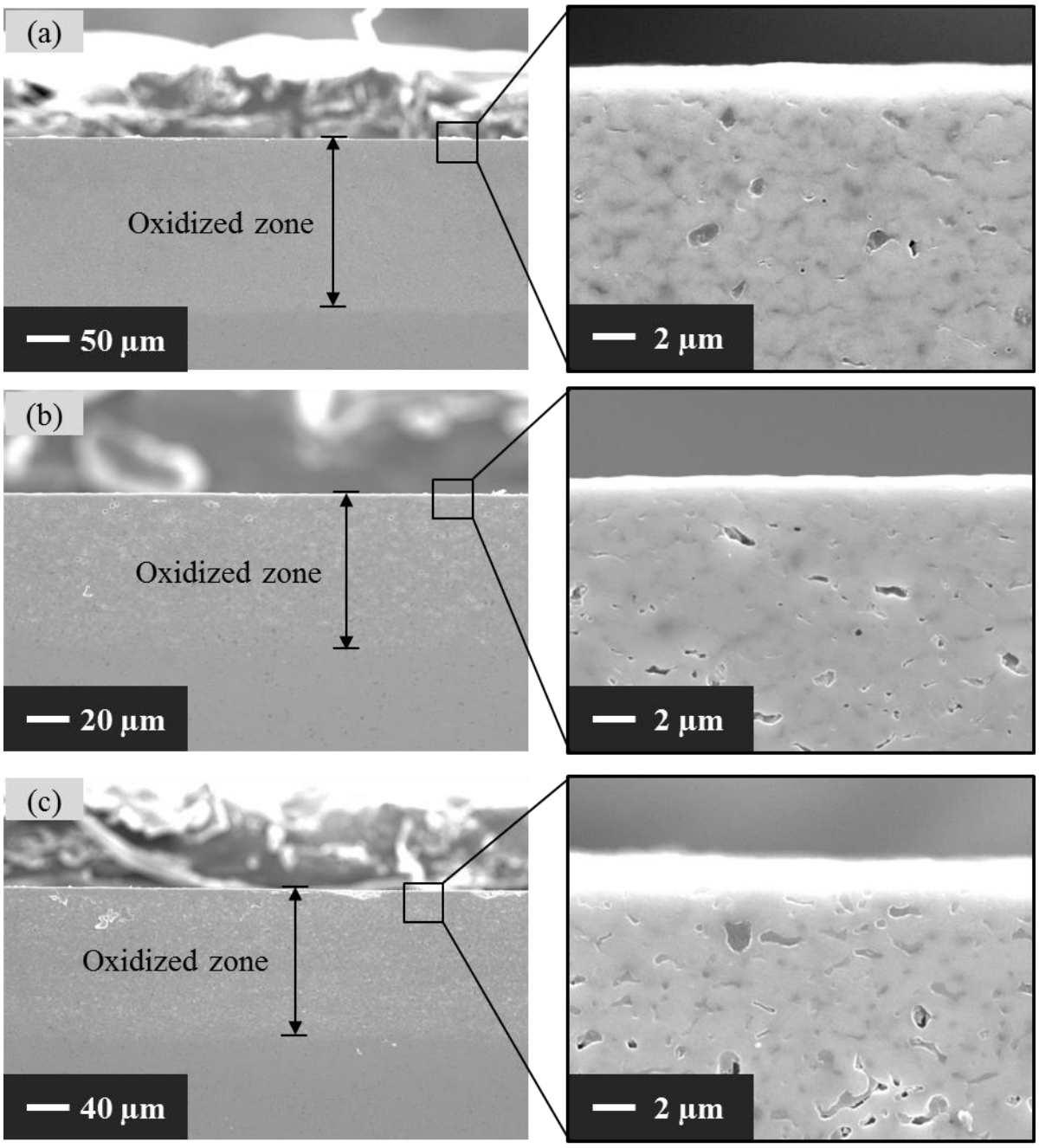

Figure 2.10 SEM images of cross-sectioned surface of SiC/Y_2SiO_5 composites after oxidation at (a) 1200, (b) 1300 and (c) 1400°C for 6 h in air

Figures 2.11 plot the thickness of the oxidized zone, *x*, as a function of oxidation time, *t*, at various oxidation temperatures for SiC/Y_2SiO_5. The thickness of the oxidized zone was increased with the increase in oxidation time as well as oxidation temperatures. The growth of oxidized zone seemed to obey the parabolic law:

$$x^2 = k_p t \tag{2.2}$$

where k_p is the parabolic rate constant. As the oxidized zone is almost dense, as shown in Figure 2.10, the mass transport in the oxidized zone is the predominant process for growth of the oxidized zone.

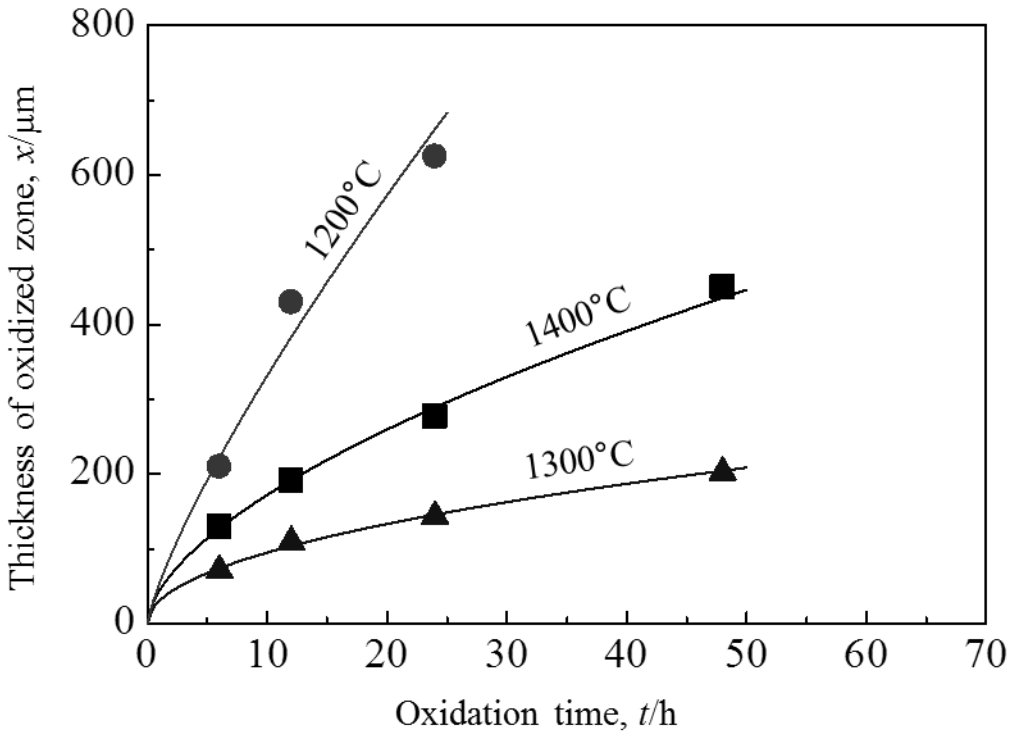

Figure 2.11 Thickness of oxidized zone as function of oxidation time at various temperatures for SiC/Y_2SiO_5 composites

The results in growth of the oxidized zone of SiC/Y_2SiO_5 composites indicate the oxidation rate of the composites at 1200°C is larger than that at 1300 and 1400°C. This phenomenon is caused by difference in oxidation mode of the composites at various temperatures. Schematic representations of oxidation mode on SiC/Y_2SiO_5 composites at various temperatures are revealed in Figure 2.12. The oxidation modes for SiC-reinforced ceramic matrix composite materials have been proposed by Luthra et al. [76]. At high temperatures, oxygen can penetrate into Y_2SiO_5 matrix and causes the oxidation reaction of SiC particles and Y_2SiO_5 matrix. This process results in

formation of oxidation product $Y_2Si_2O_7$ and development of the oxidized zone. The oxidation of the composites at 1200°C would occur when oxygen diffusion rate through Y_2SiO_5 matrix is much larger than that through the oxidation product. It means that the oxidation rate of Y_2SiO_5 matrix is much higher than that of $Y_2Si_2O_7$ product. Almost SiC particles in the oxidized zone are partially oxidized and developed a finite thickness of the oxidation product, as shown in Figure 2.12 (a). When the oxidation temperatures increased up to 1300 and 1400°C, the oxygen diffusion rates through the matrix and the oxidation product are also increased. At these oxidation temperatures, the oxidation rates of the matrix and the oxidation product are comparable. And almost SiC particles in the oxidized zone were fully oxidized. The interface between the oxidized and the non-oxidized zone is not sharp. There would be an area of the oxidized zone containing partially oxidized SiC particle, as shown in Figure 2.12 (b). This issue will be more clearly proved by a comparison of oxidation rates of Y_2SiO_5 and $Y_2Si_2O_7$ at high temperatures mentioned in next Chapter.

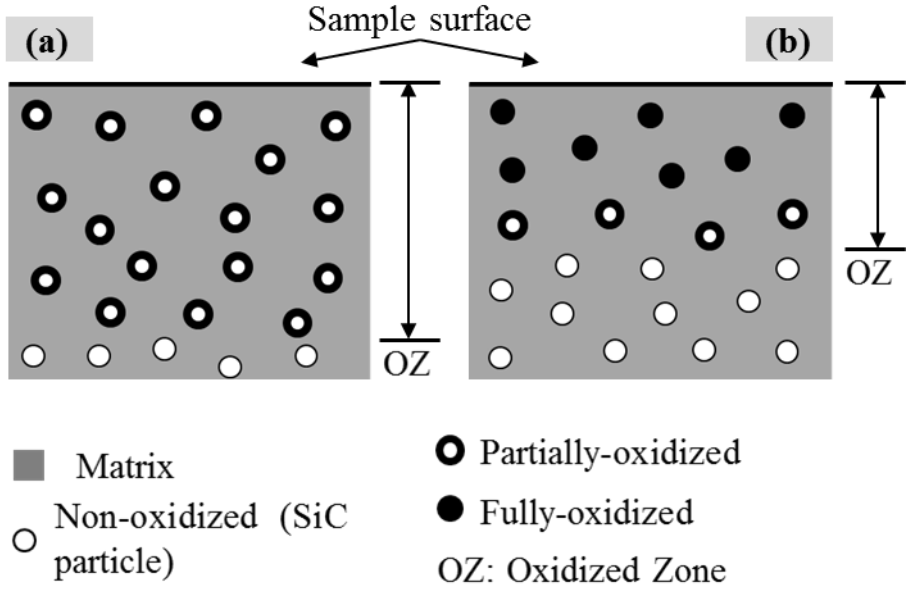

Figure 2.12 Schematic illustration of oxidation mode on SiC/Y_2SiO_5 composites at (a) 1200°C and (b) 1300 and 1400°C

Figure 2.13 plotted the parabolic rate constant k_p on growth of oxidized zone as function of reciprocal temperature for SiC/Y_2SiO_5 composites in comparison with previous study on Ni/Al_2O_3 [47] and Ni/mullite [50]. The apparent activation energy for growth of oxidized zone in SiC/Y_2SiO_5 was calculated to be 332 $kJmol^{-1}$. Oxidation resistance of SiC/Y_2SiO_5 could be comparable to that of Ni/Al_2O_3 at high temperatures such as 1300°C.

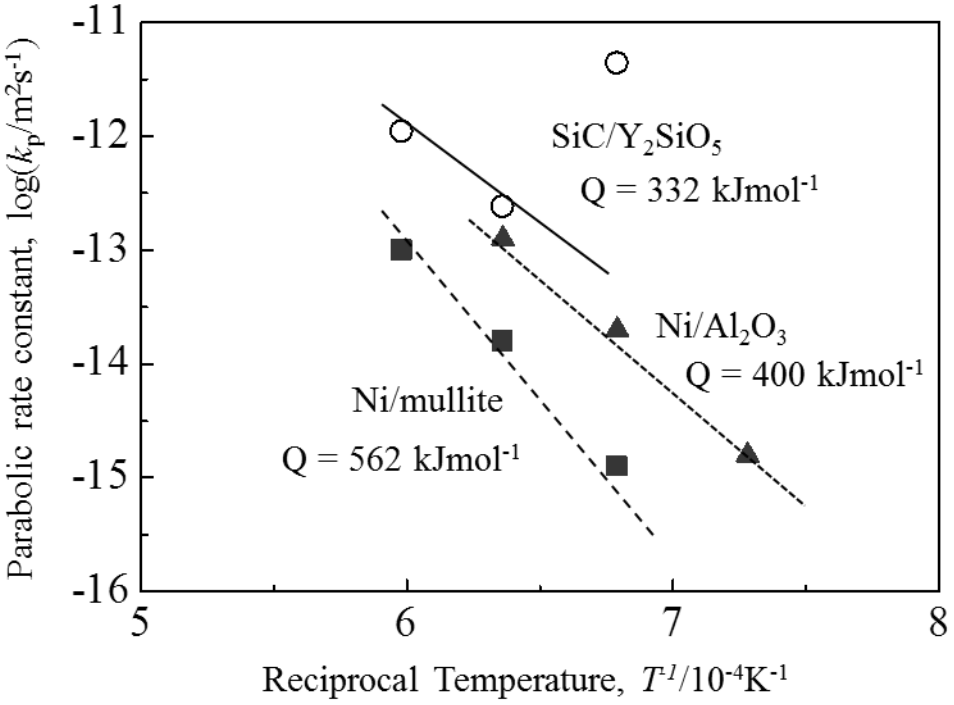

Figure 2.13 Temperature dependence of parabolic rate constant on oxidation of SiC/Y_2SiO_5

2.4 Conclusions

The single-phase X2-Y_2SiO_5 powder was successfully synthesized by using the solid-state reaction method at 1400°C for 20 h in air. Fully-densified Y_2SiO_5 composites with 5 vol% SiC particles were successfully fabricated by pulse electric current sintering technique to investigate their self-healing function. Investigation on mechanical properties on monolithic Y_2SiO_5 and SiC/Y_2SiO_5 composites indicated that

dispersion of SiC in Y_2SiO_5 matrix gave significant effect to their hardness and fracture toughness. The improvement in the fracture toughness may be caused by the difference in coefficient of thermal expansion between SiC dispersoid and Y_2SiO_5 matrix.

The SiC/Y_2SiO_5 composites possess a considerable self-healing ability. For example, surface cracks with a total length of 200 μm completely disappeared by heat treatment at 1300°C for 1 h in air. By heat treatment in Ar-1 % H_2 gas mixture at 1300°C for 1 h, surface cracks on SiC/Y_2SiO_5 samples did not disappeared. It clarifies the self-healing of SiC/Y_2SiO_5 is caused by oxidation of SiC phase within the Y_2SiO_5 matrix. The outward diffusion of Y^{3+} cations, which was responsible for formation of $Y_2Si_2O_7$ layer on the sample surface, plays the major role in the crack-healing effectiveness of SiC/Y_2SiO_5 composites.

Three-point bending tests were conducted at room temperature for as-sintered, as-cracks and as-healed samples to estimate the effectiveness of the self-healing on strength recovery. As the surface cracks completely disappeared by heat treatment at 1300°C for 1 h in air, the bending strength of as-healed samples was recovered from 100 MPa to 330 MPa which is comparable to that of as-sintered samples.

Oxidation resistance of SiC/Y_2SiO_5 composites was estimated through the growth rate of oxidized zone after heat treatment at temperatures ranging from 1200 to 1400°C for 1 to 48 h in air. Oxidation of SiC phase within Y_2SiO_5 matrix causes the formation of the oxidized zone. The growth of oxidized zone obeyed the parabolic law. The oxidation rate of samples oxidized at 1200°C was much larger than that of samples oxidized at 1300 and 1400°C. The oxidation of the composites at 1200°C would occur when oxygen diffusion rate through Y_2SiO_5 matrix is much larger than that through the oxidation product. All SiC particles in the oxidized zone were partially

oxidized and developed a finite thickness of the oxidation product. In case of the oxidation process at 1300 and 1400°C, the oxygen diffusion rate through the oxidation product is comparable to or somewhat lower than that through Y_2SiO_5 matrix. Almost SiC particles in the oxidized zone were fully oxidized.

Chapter III

Self-healing Function of SiC/$Y_2Si_2O_7$ Matrix Composites

3.1 Background

Among four polymorphs of yttrium disilicate (α, β, γ, and δ) (Table 1.2), γ-$Y_2Si_2O_7$ is a high-temperature phase that extremely stable over a wide temperatures ranging from room temperature to 1500°C [77]. Single-phase γ-$Y_2Si_2O_7$ (hereafter written as $Y_2Si_2O_7$ for brevity) was also successfully fabricated and studied for high-temperature applications [77-79]. $Y_2Si_2O_7$ ceramic has a variety of desirable properties such as chemical compatibility with Si-based ceramics, resistance to sodium molten salt, and an ability to withstand prolonged high temperature in an oxidizing atmosphere [80, 81]. Some preliminary investigations have demonstrated that this material can provide good protection for C/C-SiC composites when used as an oxidation-resistance coating [71]. However, several studies have reported that through-thickness cracks are formed in the EBCs during service time, causing the failure of the EBCs. This problem can be solved by healing the through-thickness cracks during service time. Furthermore, the self-healing function in some ceramic matrix composites dispersed with SiC particles was reported [73, 74]. Therefore, self-healing function in $Y_2Si_2O_7$ ceramic matrix composites dispersed with SiC particles could be an excellent candidate for EBC applications.

In this chapter, investigation of self-healing function for $Y_2Si_2O_7$ ceramic composites dispersed 5 vol% SiC was carried out. The fraction of crack-disappearance is estimated through length of surface cracks before and after heat treatment in air at temperatures ranging from 1100 to 1300°C for 1 to 24 h. Oxidation resistance of the

composites is investigated through the growth rate of oxidized zone induced by heat treatment in air at 1200 to 1400°C for 1 to 60 h. Self-healing mechanism of the composites is mentioned as well.

3.2 Experimental procedure

The single-phase $Y_2Si_2O_7$ powder was fabricated by solid-state reaction method from powder mixture containing Y_2O_3 (Nippon Yttrium Co., Ltd, 99.9% purity, d=1.1 μm) and SiO_2 powder (Nacalai Tesque, Inc., 99% purity). The mixture in a molar ratio 1:2 consisting of Y_2O_3 and SiO_2 powder was ball-milled in a plastic bottle with ethanol and alumina balls for 24 h. After drying and manual crashing, the mixture was annealed at 1500°C for 24 h in air. The received powder was phase-identified by using X-ray diffraction (XRD). Figure 3.1 shows XRD pattern of the powder fabricated by above procedure. Only single-phase $Y_2Si_2O_7$ is detected and it corresponds to standard pattern of $Y_2Si_2O_7$ (ICDD Card, No. 42-0167).

Samples used in this study were 5 % SiC/Y_2SiO_5 composites, fabricated by the following procedures. The starting powder mixture was prepared by making a slurry mixture consisting of 5 vol% SiC (Ibiden Co., Ltd, 99.9 % purity, 0.32 μm mean particle size), $Y_2Si_2O_7$ powder and ethanol. Afterward, the slurry mixture was ball-milled for 24 h in a plastic bottle with 5-mm-diameter alumina balls. Then the ceramic slurry was dried at 100°C for 10 h in air and milled manually by using an alumina mortar to eliminate the agglomeration of the particles. Consolidation of the powder mixture was conducted by PECS with a graphite die in vacuum at 1500°C under 70 MPa in uniaxial pressure for 5 min holding time. The density of the as-sintered sample was measured by the Archimedean method with toluene. The relative density of all the specimens fabricated by this procedure reached at least 99 %

of the theoretical value of the composites. Figure 3.2 shows fracture surface of an as-sintered sample observed by the scanning electron microscope (SEM). SiC particles, which could be observed as white dots, were homogeneously dispersed in $Y_2Si_2O_7$ matrix.

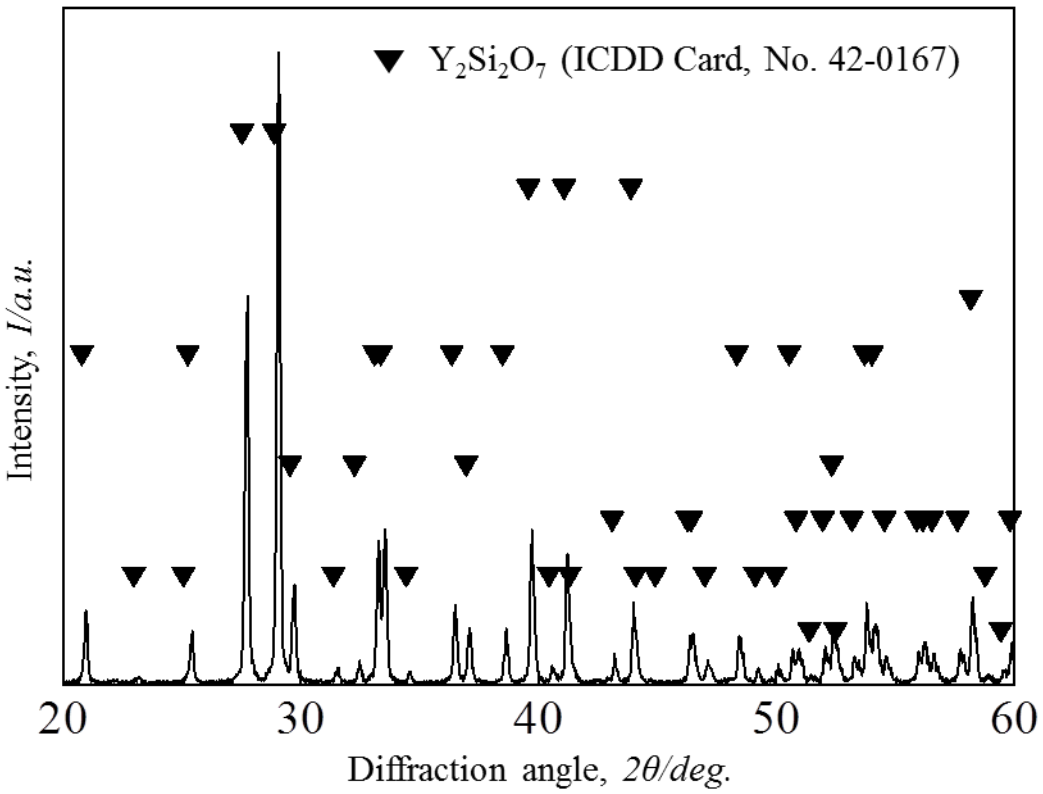

Figure 3.1 XRD patterns of $Y_2Si_2O_7$ powder obtained by solid-state reaction method

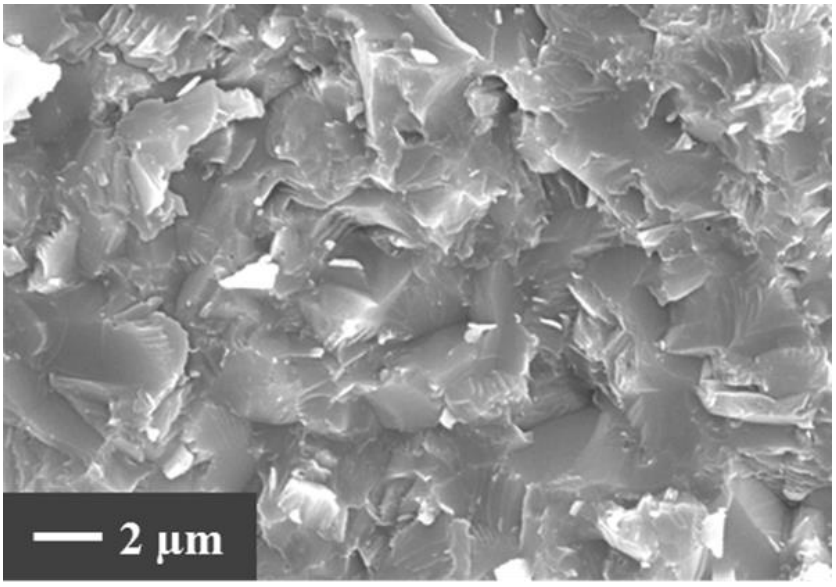

Figure 3.2 SEM image of fracture surface of as-sintered sample

Evaluation of the specimens was conducted as the following steps. The as-sintered specimens were ground by using a grinding wheel with 30 µm diamond grains and then polished with 2 µm diamond slurry. For investigation of self-healing function of $5SiC/Y_2Si_2O_7$ composites, three Vickers indentations were introduced on polished surface of the sample by applying a load of 20 N for 10s. Each Vickers indentation produces four surface pre-cracks at their corners, as shown in Figure 3.3. The crack size in total is approximately 200 µm in length. Effectiveness of surface crack-disappearance after heat treatment at 1100 to 1300°C for 1 to 24 h was estimated by using SEM and XRD for phase identification. The details of evaluation method for surface crack-disappearance were described by Maruoka et al. [67]. For investigation of oxidation resistance of the composites, oxidation tests were conducted at temperatures ranging from 1200 to 1400°C for 1 to 60 h in the air with a heating rate of 400°C/h. The tested samples were put on zirconia balls (2 mm in diameter) in an alumina crucible and exposed in the air at the investigated conditions. Oxidized samples were then cross-sectioned and polished with 2 µm diamond slurry. Phase

identification for the oxidized samples was carried out by XRD. Oxidation evolution of the heat-treated samples was evaluated through the growth rate of oxidized zone observed on cross-sectioned surface by SEM.

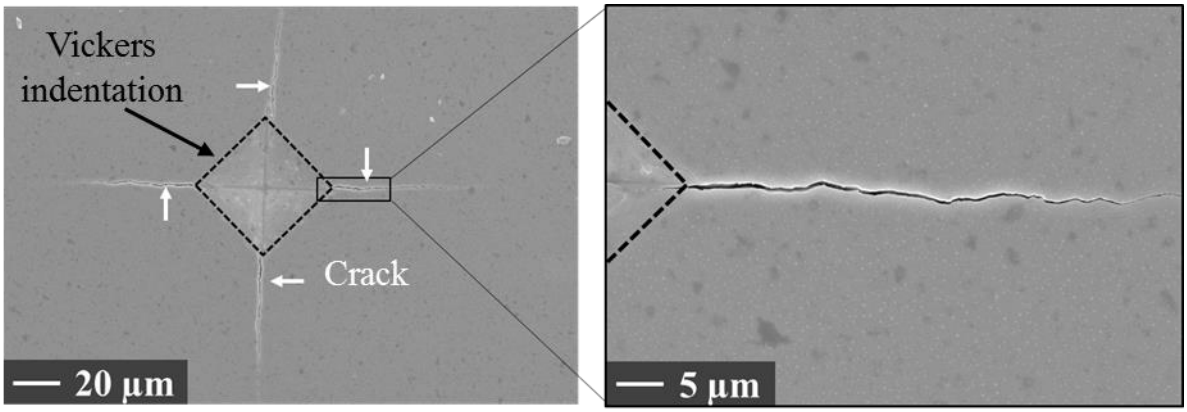

Figure 3.3 SEM images of the top view of Vickers indentation and surface cracks of as-cracked sample

3.3 Results and discussion

3.3.1 Surface crack-disappearance

Figure 3.4 shows SEM images of sample surfaces with introduced cracks after heat treatment at various conditions. Dash lines present the outline of Vickers indentations. Without heat treatment in air, surface cracks that are indicated by white arrows could be observed clearly as shown in Figure 3.3. At 1200°C, surface cracks partially disappeared after heat treatment for 1 and 6 h (Figure 3.4 (a) and (b)). The fraction of crack-disappearance is increased with increasing in heat treatment time. Heat treatment at 1200°C for 1 h in air, 30±13% cracks disappeared on sample surface, as shown in Figure 3.4 (a). And 60±10% cracks disappeared after heat treatment at 1200°C for 6 h in air, as shown in Figure 3.4 (b). By increasing the annealing temperature, the surface cracks completely disappeared at 1300°C for 1 h in air, as shown in Figure 3.4 (c).

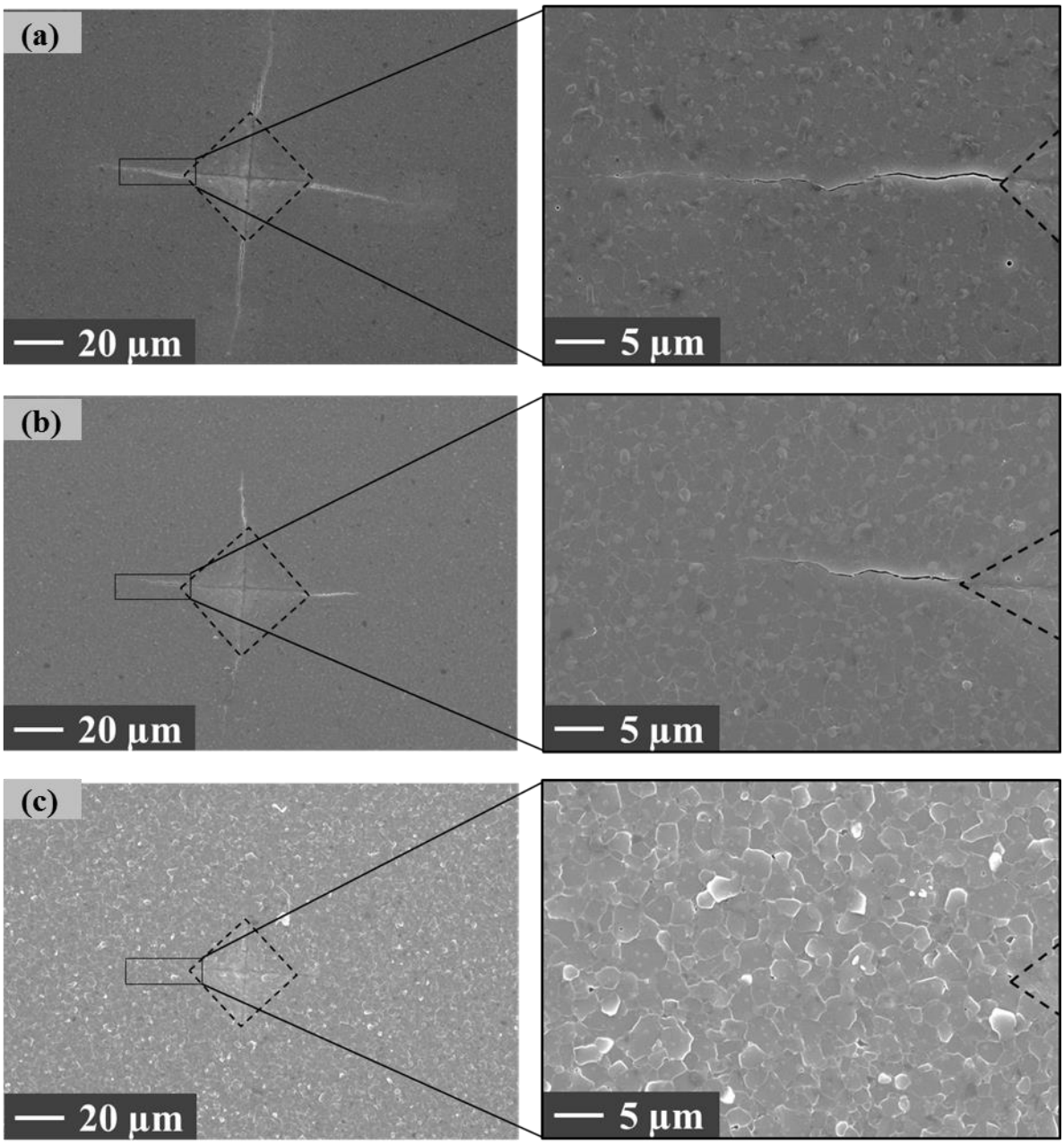

Figure 3.4 SEM images of surfaces of samples heat-treated at (a) 1200°C for 1 h, (b) 1200°C for 6 h and (c) 1300°C for 1 h in air

Figure 3.5 show XRD patterns of sintered samples before and after heat treatment in air in order to identify compounds formed on sample surface. Before heat treatment, there were two dominant substances that were $Y_2Si_2O_7$ and SiC detected on sample surface (Figure 3.5 (a)). After heat treatment at 1200 and 1300 °C for 1 h in air, no new peaks were detected, as shown in Figure 3.6 (c) and (d). However, intensity of

SiC peaks was decreased. This fact implies that the SiC particles were oxidized into SiO_2 as an amorphous phase, following equation (1.1). Thus, it could be not detected.

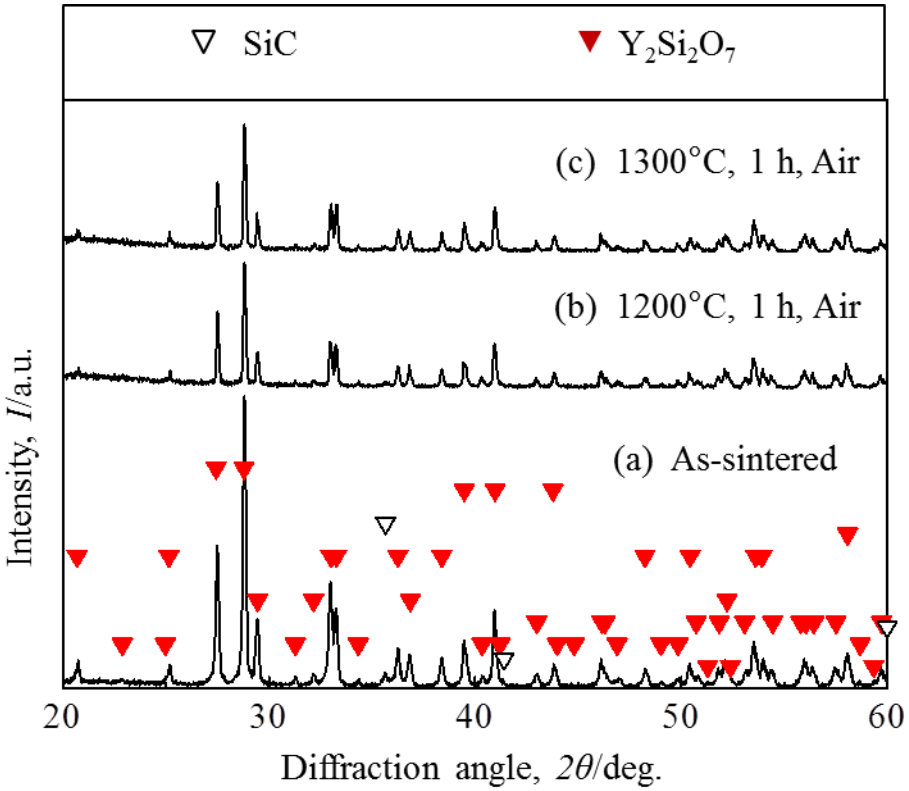

Figure 3.5 XRD patterns of the sintered $SiC/Y_2Si_2O_7$ samples before and after heat treatment at various conditions

Figure 3.6 shows the fraction of surface crack-disappearance as a function of heat treatment temperatures for $5SiC/Y_2Si_2O_7$ and the previously reported results on $5SiC/Y_2SiO_5$ (in chapter II). Both of composites required same heat treatment temperature and time, at 1300°C for 1 h, for complete disappearance of surface cracks. However, healing rate of $5SiC/Y_2Si_2O_7$ composites is less than that of $5SiC/Y_2SiO_5$ composites at lower temperatures. For example, $SiC/Y_2Si_2O_7$ achieved 30% of the fraction of crack-disappearance after heat treatment at 1200°C for 1 h while

SiC/Y_2SiO_5 achieved 80% of the fraction of crack-disappearance. This phenomenon is caused by the difference of crack-healing mechanism of the two composites.

As mentioned in previous chapter, the outward diffusion of Y^{3+} cations, which was responsible for formation of $Y_2Si_2O_7$ layer on the sample surface, plays the major role in the crack-healing effectiveness of SiC/Y_2SiO_5 composites. However, the dominant factor cause the self-healing of $SiC/Y_2Si_2O_7$ composites would be the volume expansion which was accompanied by oxidation of SiC dispersoid into amorphous SiO_2 phase. Figure 3.8 (b) shows the cross-sectional view of a sample after heat treatment at 1300°C for 48 h in air. A lot of short cracks parallel to the sample surface are generated in the inside of the oxidized zone. Similar cracks were observed in Y_2O_3 partially-stabilized ZrO_2 composites dispersed with Ni particles after oxidation process at high temperatures [82]. The cracks appeared in the inside of the oxidized zone of $SiC/Y_2Si_2O_7$ composites would be formed by oxidation of SiC dispersoid into SiO_2 which accompanies a volume expansion during high-temperature oxidation process. Theoretical value of the volume expansion of oxidation of SiC into SiO_2 is approximately equal to be two. This volume expansion caused the closure of surface cracks. Besides, the healing of surface cracks can be caused by the formation of amorphous SiO_2. The SiC dispersoid was oxidized into amorphous SiO_2. The amorphous SiO_2 subsequently migrated along surface cracks leading to full filling of the cracks. Same mechanism was observed in yttria stabilized zirconia composites dispersed with $MoSi_2$ [83]. Moreover, as shown in Figure 38 (b), some spherical voids can be observed in the oxidized zone as well. The formation of these voids was caused by outward diffusion of Y^{3+} cations. A comparison between the cracks and voids appeared in the inside of the oxidized zone indicates that the volume change in the oxidized zone will be positive. It means that the outward diffusion of cations in the

$Y_2Si_2O_7$ matrix is much slower than the inward diffusion of oxygen. The outward diffusion of cations, therefore, displays the minor role in crack-healing performance of $SiC/Y_2Si_2O_7$composites.

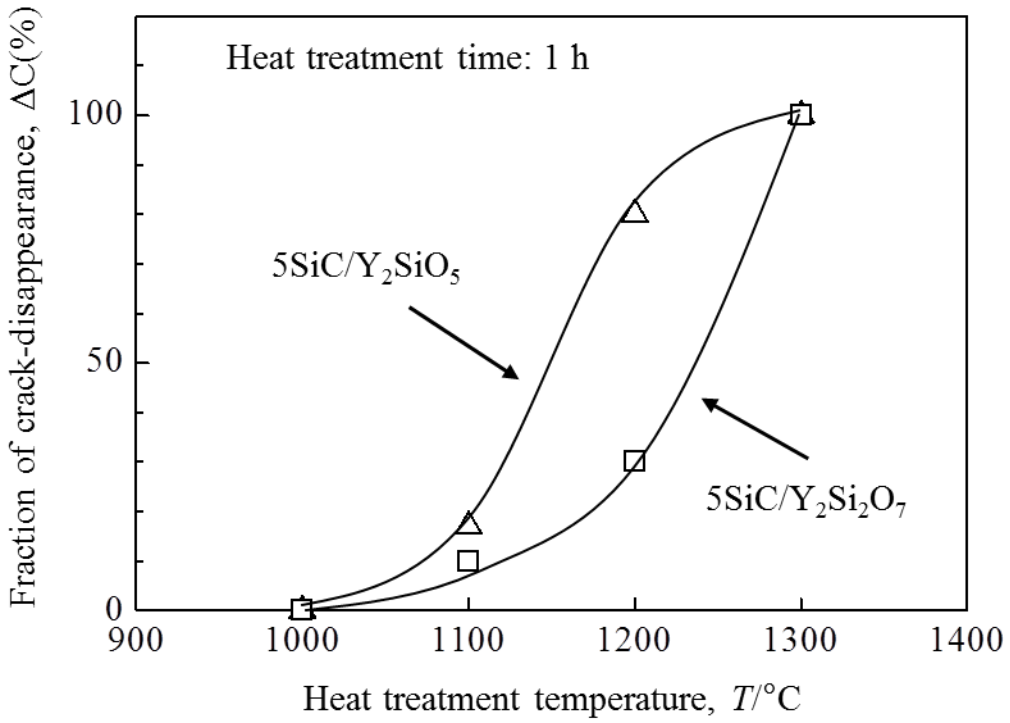

Figure 3.6 Fraction of crack-disappearance as a function of heat treatment temperatures for $5SiC/Y_2SiO_5$ and $5SiC/Y_2Si_2O_7$

3.3.2 Oxidation resistance

Figures 3.7, 3.8 and 3.9 show SEM images observed on cross-sectioned surface of $SiC/Y_2Si_2O_7$ samples after oxidation at various conditions. The oxidized zone was defined to be the region containing the matrix, oxidation product and short cracks parallel to the sample surface. In this region, SiC particles dispersed in the matrix were almost oxidized. Thickness of oxidized zone, *x*, was determined. In the region following the oxidized zone, no cracks were observed. This region was considered as the non-oxidized zone where SiC particles can be observed clearly.

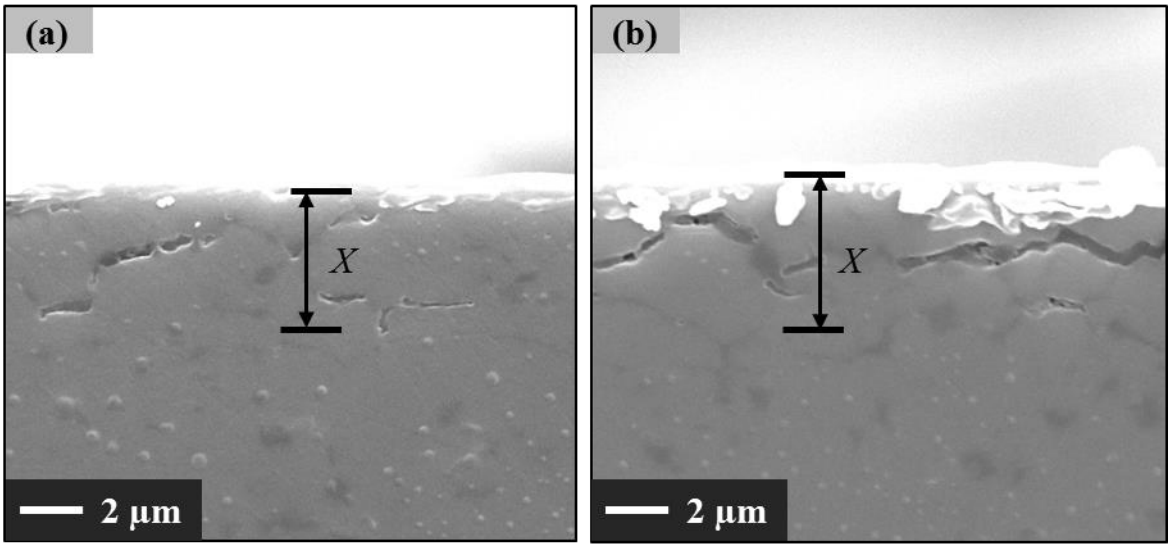

Figure 3.7 SEM images of the cross-sectioned surfaces of $SiC/Y_2Si_2O_7$ samples after oxidation at 1200°C for (a) 24 h and (b) 48 h

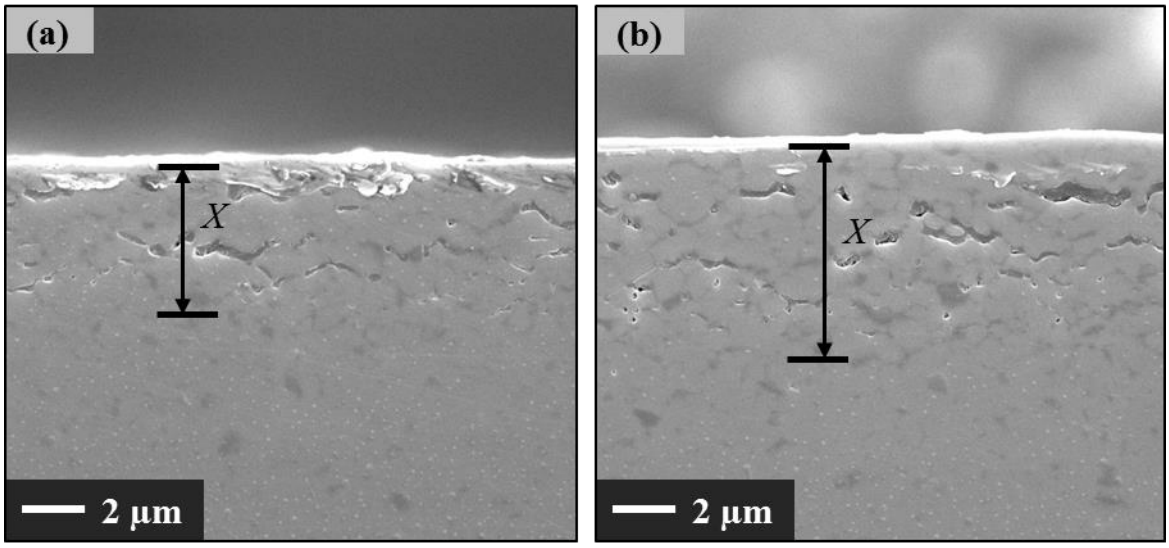

Figure 3.8 SEM images of the cross-sectioned surfaces of $SiC/Y_2Si_2O_7$ samples after oxidation at 1300°C for (a) 24 h and (b) 48 h

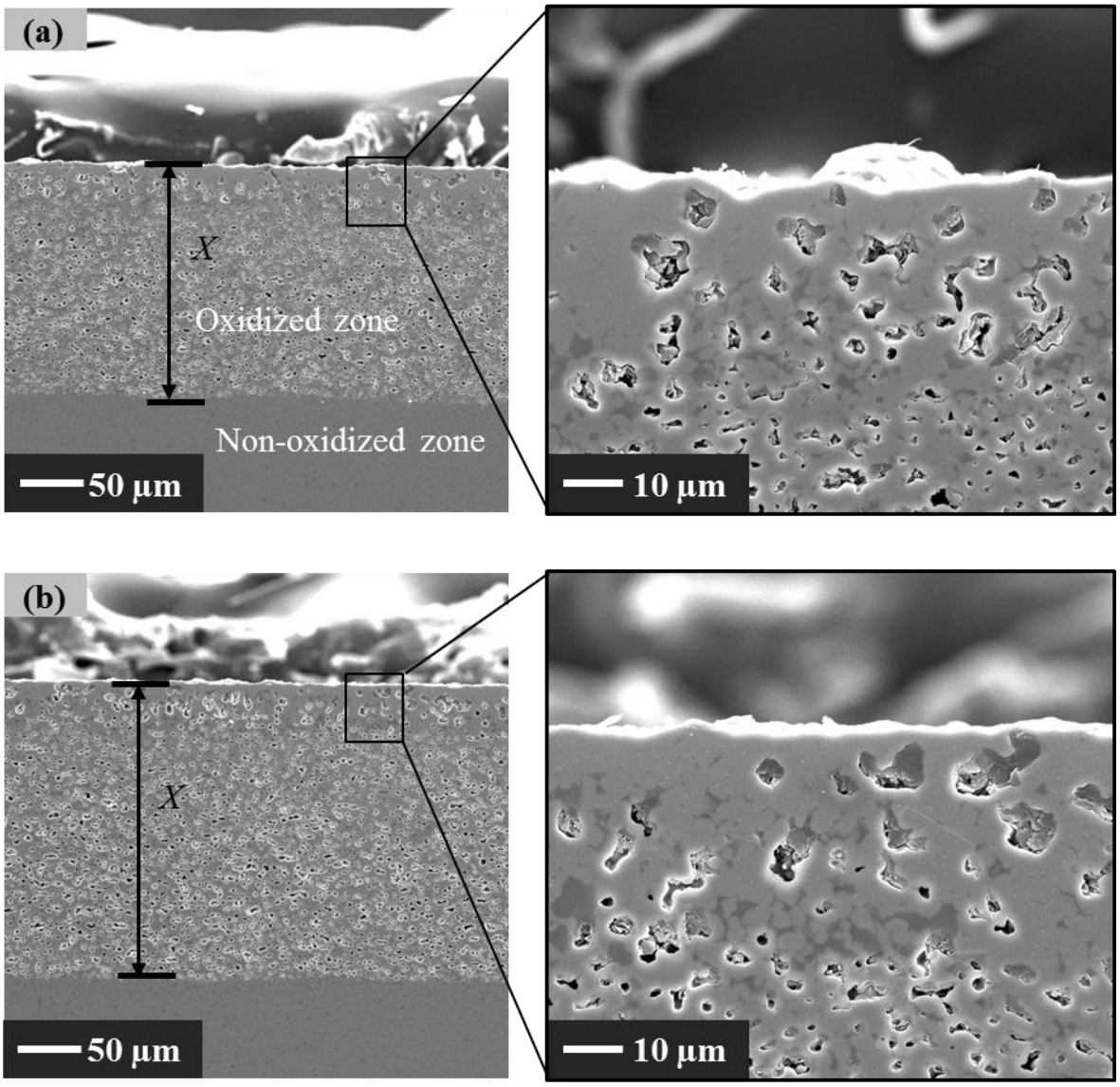

Figure 3.9 SEM images of the cross-sectioned surfaces of $SiC/Y_2Si_2O_7$ samples after oxidation at 1400°C for (a) 24 h and (b) 48 h

Figure 3.10 plotted the thickness of oxidized zone as function of oxidation time. With increasing oxidation time, the thickness of oxidized zone was increased. The growth of oxidized zone obeyed the parabolic law. Figure 3.11 shows the parabolic rate constant, k_p, of $SiC/Y_2Si_2O_7$ as a function of reciprocal oxidation temperature. The value of apparent activation energy for growth rate of oxidized zone in $SiC/Y_2Si_2O_7$ was calculated to be 735 $kJmol^{-1}$. As shown Figure 3.11, the oxidation rate of $Y_2Si_2O_7$

matrix is much lower than that of Y_2SiO_5 matrix at 1200 °C. At higher oxidation temperatures such as 1300 and 1400 °C, the oxidation rate of $Y_2Si_2O_7$ is comparable or somewhat lower than that of Y_2SiO_5. This comparison indicates that the discussion on oxidation mode of the SiC/Y_2SiO_5 composites at various temperatures mentioned in Chapter II is reasonable. The comparison also implies that oxidation resistance of $SiC/Y_2Si_2O_7$ composites is better than that of SiC/Y_2SiO_5 composites.

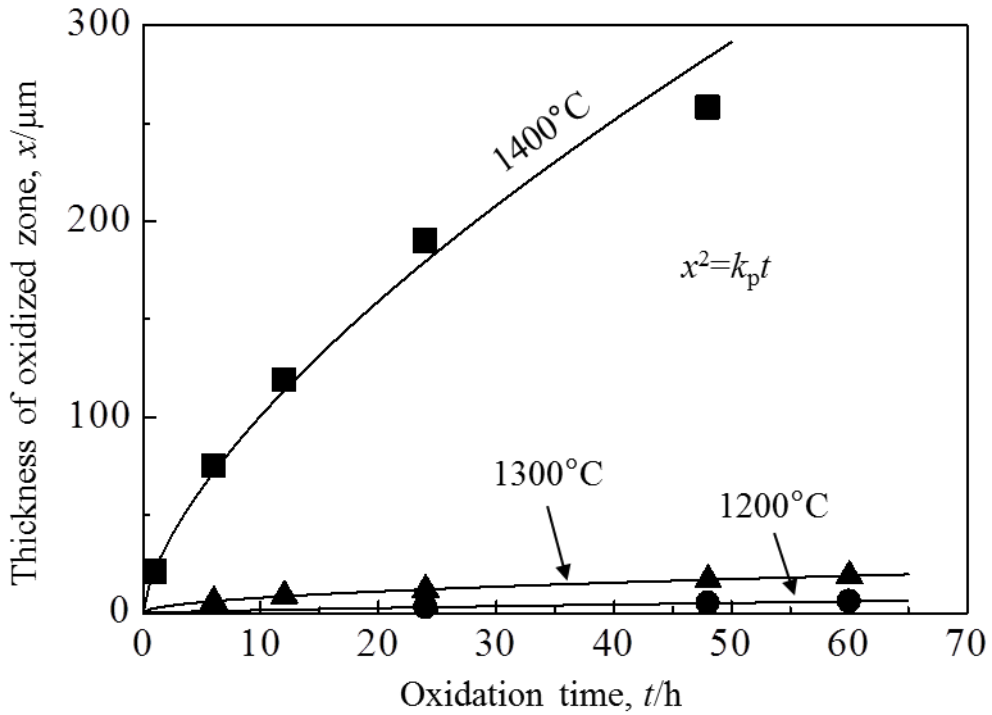

Figure 3.10 Thickness of oxidized zone as a function of oxidation time at various temperatures for $SiC/Y_2Si_2O_7$ composites

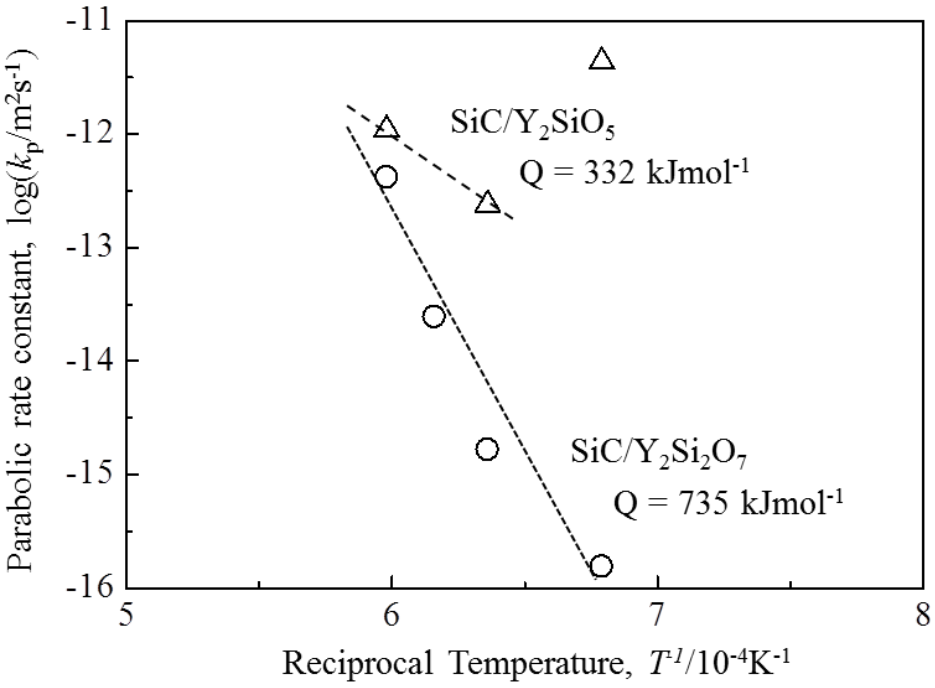

Figure 3.11 Temperature dependence of parabolic rate constant on oxidation of SiC/Y_2SiO_5 and $SiC/Y_2Si_2O_7$ composites

3.4 Conclusions

The single-phase γ-$Y_2Si_2O_7$ powder could be successfully synthesized by using the solid-state reaction method at 1500°C for 24 h in air. Consolidated 5 vol% $SiC/Y_2Si_2O_7$ specimens were successfully fabricated by PECS to investigate the self-healing function and oxidation resistance.

The investigation of surface crack-disappearance by heat treatment in air was conducted at temperatures ranging from 1100 to 1300°C for 1 to 24 h. Results of the investigation indicated the surface crack-disappearance achieved by heat treatment at 1300°C of $5SiC/Y_2Si_2O_7$ was similar with that of $5SiC/Y_2SiO_5$. By heat treatment at lower than 1300°C, the healing rate of $5SiC/Y_2Si_2O_7$ was lower than that of $5SiC/Y_2SiO_5$. The dominant factor cause the self-healing of $SiC/Y_2Si_2O_7$ composites would be the volume expansion which was accompanied by oxidation of SiC dispersoid into amorphous SiO_2 phase.

Oxidation tests for $SiC/Y_2Si_2O_7$ were conducted at temperatures ranging from 1100 to 1300°C for 1 to 24 h. Oxidation resistance of $SiC/Y_2Si_2O_7$ composites was examined through the growth rate of oxidized zone after annealed in air. The oxidized zone was considered as a region in which short cracks parallel to the sample surface were appeared due to the volume expansion caused by oxidation of SiC phase in to amorphous SiO_2 phase in the matrix. The growth of oxidized zone obeyed the parabolic law. The apparent activation energy for growth of the oxidized zone was determined to be 735 $kJmol^{-1}$. Oxidation rate of $SiC/Y_2Si_2O_7$ composites is one order of magnitude lower than that of SiC/Y_2SiO_5 composites. In other words, oxidation resistance of $SiC/Y_2Si_2O_7$ composites is better than that of SiC/Y_2SiO_5 composites.

Chapter IV

Self-healing Function of SiC/Y_2SiO_5-$Y_2Si_2O_7$ Matrix Composites

4.1 Background

The key limitation in the applicability of the EBCs for SiC-based composites is the CTE mismatch between the coating and the substrate. Because a large difference in CTE of the coating and the substrates leads to mismatch stress between the coating and substrates induced cracks in the coating. In order to reduce the mismatch stress, CTE of the selected coating need to be closest to that of the substrates. While Y_2SiO_5 has large CTE mismatch with SiC whereas $Y_2Si_2O_7$ possesses a good match to SiC(Table 1.2). Furthermore, as reported in Chapter 4, the self-healing ability of SiC/Y_2SiO_5 is better than that of $SiC/Y_2Si_2O_7$ whereas oxidation resistance of $SiC/Y_2Si_2O_7$ is better than that of SiC/Y_2SiO_5. From above reasons, Y_2SiO_5 and $Y_2Si_2O_7$ ceramic can be mixed together to fabricate a ceramic displaying the CTE closest to that of the substrate. Some preliminary investigations have also demonstrated that the Y_2SiO_5-$Y_2Si_2O_7$ ceramic can provide good oxidation protection for C/C-SiC composites when used as an oxidation-resistance coating [71, 84]. And Y_2SiO_5-$Y_2Si_2O_7$ coating with composition (in mass %) $70Y_2Si_2O_7$-$30Y_2SiO_5$ provide suitable protection against the oxidation of SiC-based composites at 1600°C. Therefore, Y_2SiO_5-$Y_2Si_2O_7$ matrix composites dispersed SiC particles is expected to exhibit better self-healing capability and oxidation resistance which is suitable for self-healing EBC applications.

In this chapter, the investigation of self-healing function for $70Y_2Si_2O_7$-$30Y_2SiO_5$ (hereafter written as YS for brevity) matrix composites dispersed

5 vol% SiC particles is conducted. The self-healing capability is evaluated through fraction of surface crack-disappearance before and after heat treatment in air at 1100 to 1300°C for 1 to 24 h. In order to clarify the oxidation resistance of the composites, oxidation test are carried out at temperatures ranging from 1200 to 1400°C for 6 to 48 h in air. To investigate effects of SiC volume fraction on self-healing ability and oxidation resistance, the self-healing and oxidation test are conducted at same above conditions for 10 vol% SiC/70$Y_2Si_2O_7$-30Y_2SiO_5 (10SiC/YS) and 20 vol% SiC/70$Y_2Si_2O_7$-30Y_2SiO_5 (20SiC/YS) composites.

4.2 Experimental procedure

Specimens used in this study were 5, 10 and 20 vol% SiC/70$Y_2Si_2O_7$-30Y_2SiO_5, fabricate by following procedures. Slurry mixtures containing SiC (Ibiden Co., Ltd, 99.9% impurity, 0.32 μm mean particle size) , the YS ceramic powder and ethanol were prepared by ball-milling for 24 h in a plastic bottle with alumina balls (5mm in diameter). The slurries then were dried at 100°C for 10 h in air. Afterward, the powder mixtures were manually crashed by a mortar for reduce the agglomeration of the powder. The powder mixtures were consolidated with a graphite die by PECS in vacuum for 5 min holding time and under 70 MPa in uniaxial pressure at 1550°C. The density of the as-sintered sample was measured by the Archimedean method with toluene. The relative density of all the specimens fabricated by this procedure reached at least 99 % of the theoretical value of the composites. Figure 4.1 shows SEM images representative for the fracture surface of the as-sintered sample of 5SiC/YS composites. SiC particles are visible as the bright dots dispersed homogeneously into YS matrix.

Evaluation of the specimens was conducted as the following steps. The as-sintered specimens were ground by using a grinding wheel with 30 μm diamond

grains and then polished with 2 μm diamond slurry. For investigation of self-healing function of 5SiC/YS, 10SiC/YS and 20SiC/YS composites, three Vickers indentations were introduced on polished surface of the sample by applying a load of 20 N for 10s. Each Vickers indentation produces four surface pre-cracks at their corners, as shown in Figure 4.2. Effectiveness of surface crack-disappearance after heat treatment at 1100 to 1300°C for 1 to 24 h was estimated by using SEM and XRD for phase identification. The details of evaluation method for surface crack-disappearance were described by Maruoka et al. [67]. For investigation of oxidation resistance of the composites, oxidation tests were conducted at temperatures ranging from 1200 to 1400 °C for 1 to 48 h in air. The tested samples were put on zirconia balls (2 mm in diameter) in an alumina crucible and exposed at the test temperatures in air. The heating rate in the oxidation experiments were 400°C/h. Oxidized samples were then cross-sectioned and polished with 2 μm diamond slurry. Phase identification for the oxidized samples was carried out by XRD. Oxidation evolution of the oxidized samples was evaluated through the growth rate of oxidized zone observed on cross-sectioned surface by SEM.

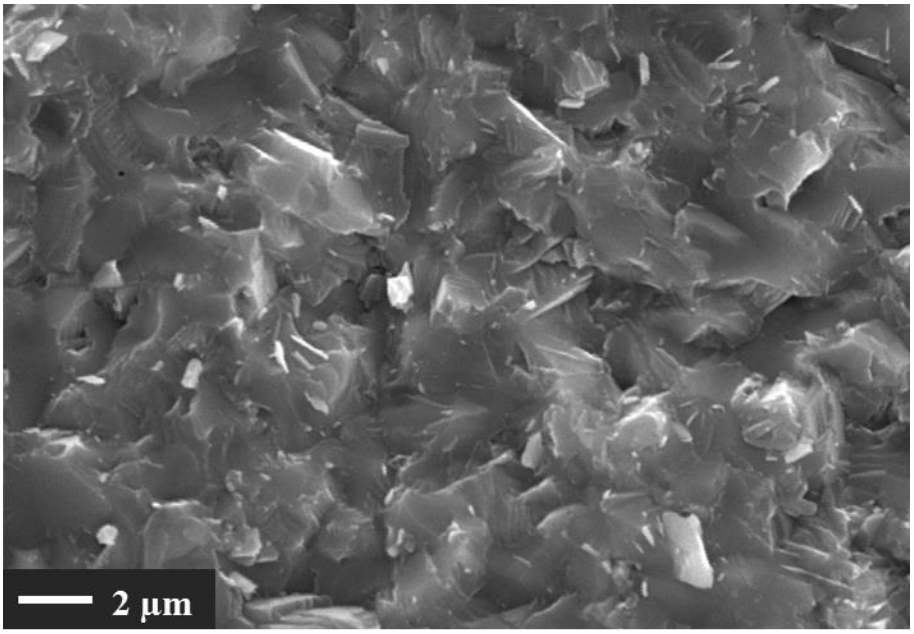

Figure 4.1 SEM image of the fractured surface of an as-sintered sample of 5SiC/YS composites

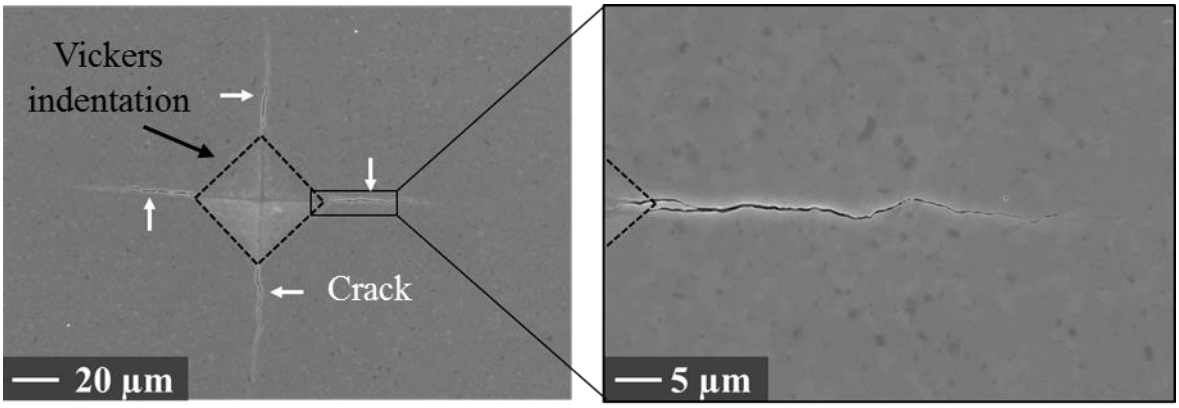

Figure 4.2 SEM images of the pre-cracks induced by Vickers indentation from top view

4.3 Results and discussion

4.3.1 Crack-disappearance of 5SiC/YS composites

Figure 4.3 presents SEM images of the introduced cracks on sample surfaces after heat treatment at various conditions. The dashed lines indicate the edges of Vickers indentations. From each corner of the Vickers indentation, a crack with 60 µm

in length propagated as observed in Figure 4.2. After heat treatment at 1100°C for 6 h in air, the surface cracks partially disappeared as the fraction of crack-disappearance was determined to be 30%. As shown in Figure 4.3 (a), some newly created phases were observed on sample surface. For higher heat treatment temperature, heat treatment at 1200°C for 6 h in air, surface cracks still partially disappeared as the fraction of crack-disappearance was determined to be 80%., as shown in Figure 4.3 (b). At 1300°C, complete surface crack-disappearance can be achieved with a short heat treatment time such as 1 h, as presented in Figure 4.3 (c). Heat treatment at 1300°C for 6 h in air makes significant formation of oxidation products, as shown in Figure 4.3 (d).

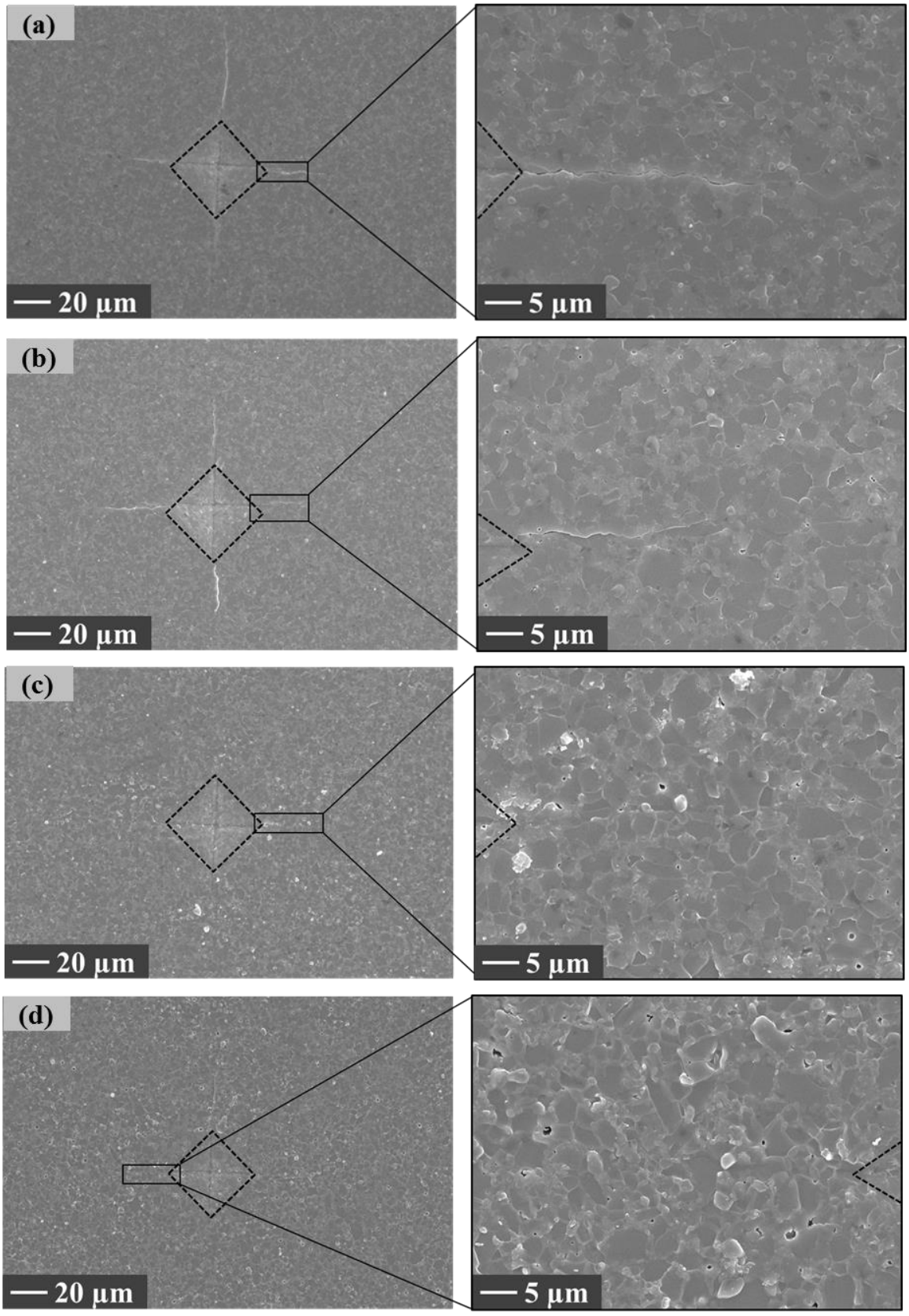

Figure 4.3 SEM images of surfaces of samples heat-treated at (a) 1100°C for 6 h, (b) 1200°C for 6 h, (c) 1300°C for 1 h and (d) 1300°C for 6 h in air

Figure 4.4 shows XRD patterns for phase identification of the exposed surface before and after heat treatment at various conditions. Three dominant compounds which are Y_2SiO_5, $Y_2Si_2O_7$ and SiC were detected in as-sintered sample. No new peaks were detected on the surface of heat-treated samples. Intensity of Y_2SiO_5 and SiC peaks were decreased after heat treatment. Oxidation reaction which occurred in the heat-treated process is similar to that of SiC/Y_2SiO_5. The oxidation of SiC into amorphous SiO_2 could be occurred as well.

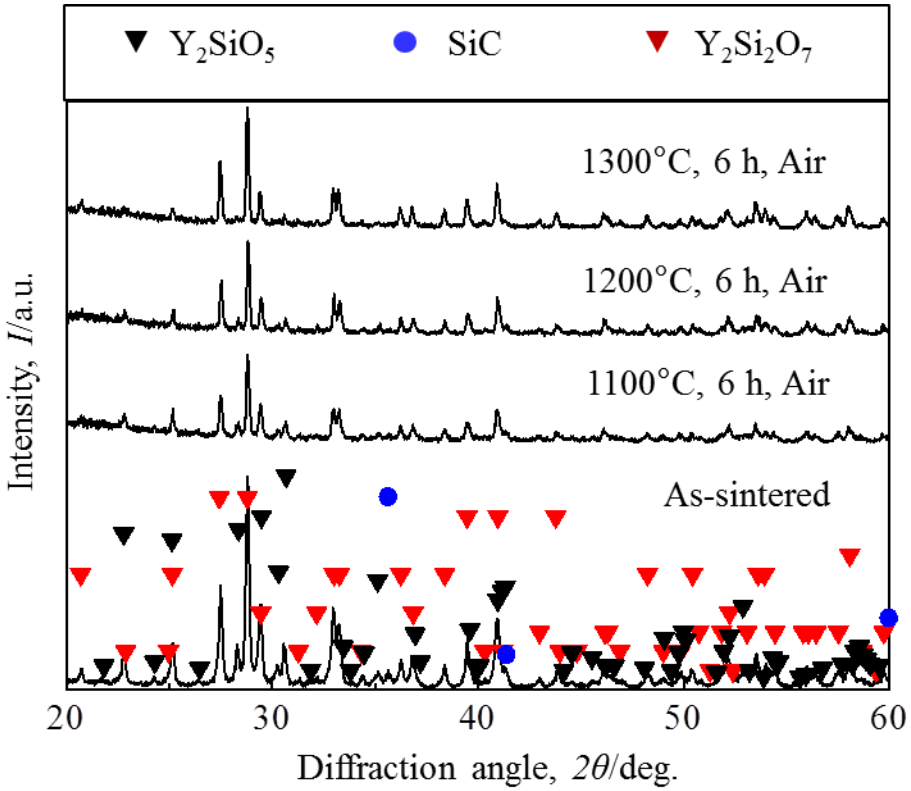

Figure 4.4 XRD patterns of the sample surface before and after heat treatment at various conditions

Figure 4.5 shows the fraction of surface crack-disappearance as a function of heat treatment temperatures for 5SiC/YS and the previously reported results on $5SiC/Y_2SiO_5$ (in chapter II) and $5SiC/Y_2Si_2O_7$ (in Chapter III). The comparison in

crack-disappearance performance of three composites indicates that the crack-healing rate of SiC/Y_2SiO_5-$Y_2Si_2O_7$ is in the middle of that of SiC/Y_2SiO_5 and SiC/$Y_2Si_2O_7$. Taking account of the previous discussion on the crack-healing mechanism of SiC/Y_2SiO_5 and SiC/$Y_2Si_2O_7$ composites, the crack-healing mechanism of SiC/Y_2SiO_5-$Y_2Si_2O_7$ composites is illustrated as Figure 4.6. The closure of surface cracks is considered as the consequence of outward diffusion of cations caused formation of $Y_2Si_2O_7$ outer layer, and SiC oxidation in the matrix to form the amorphous SiO_2 which accompanies the volume expansion.

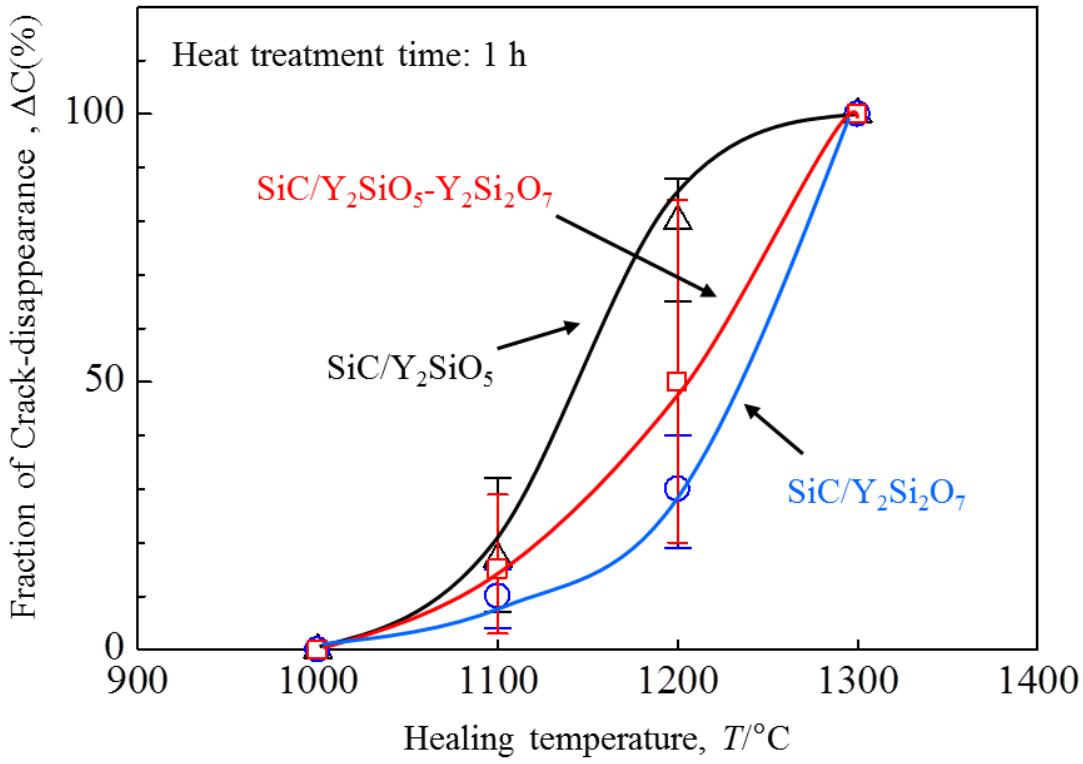

Figure 4.5 Fraction of crack-disappearance as a function of heat treatment temperatures for 5SiC/Y_2SiO_5, 5SiC/$Y_2Si_2O_7$ and 5SiC/YS

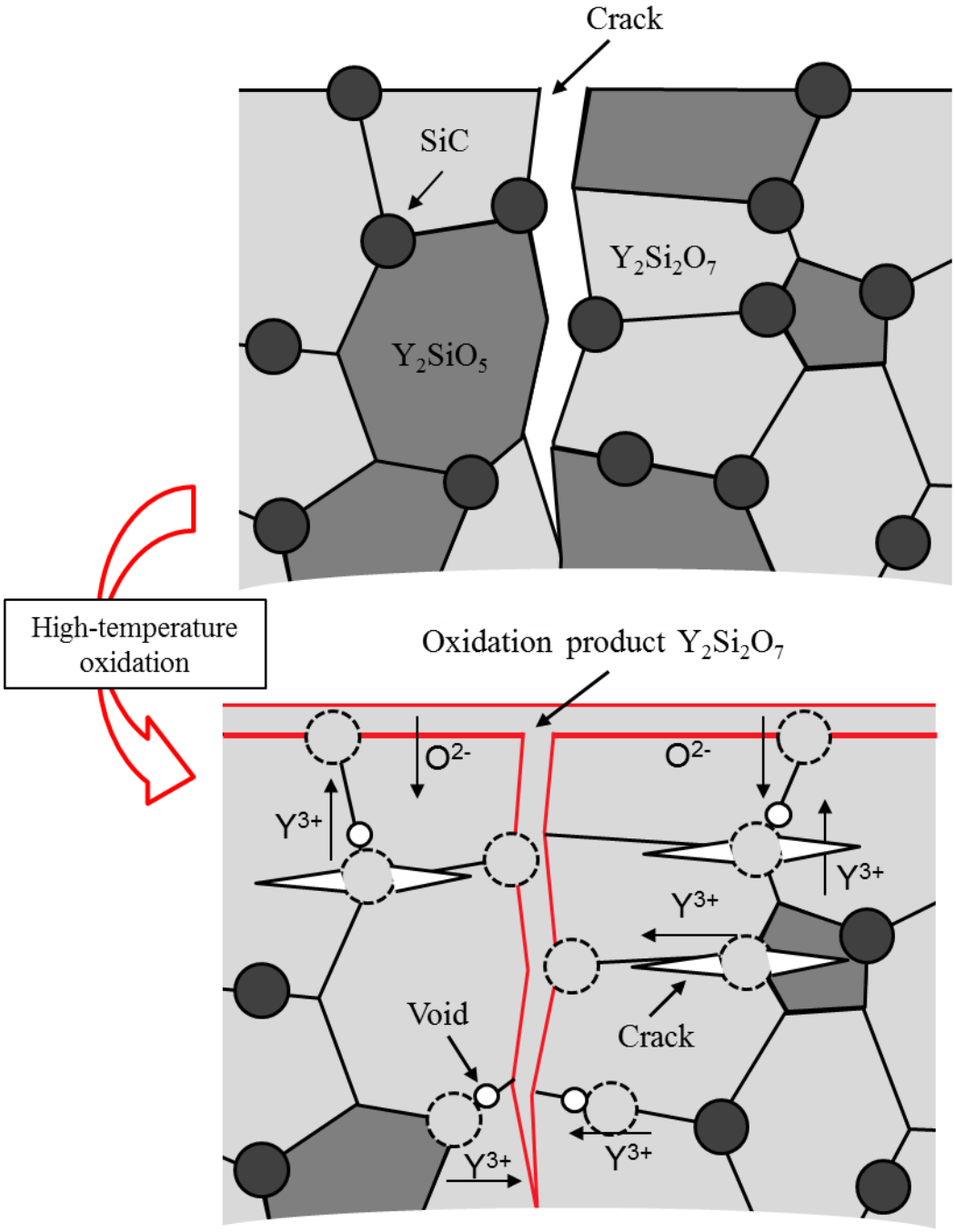

Figure 4.6 Schematic illustration of self-healing mechanism of SiC/Y_2SiO_5-$Y_2Si_2O_7$ composites

4.3.2 Oxidation resistance of 5SiC/YS composites

Figure 4.7 shows the SEM images of cross-sectioned surface of 5SiC/YS composites after oxidation at 1200, 1300 and 1400°C for 24 h in air. As shown in

Figure 4.7 (a), oxidation at 1200°C for 24 h in air, the region from the surface to the depth of 40 μm was considered as the oxidized zone. In this region, SiC particles were partially oxidized. Some short cracks caused by the volume expansion of oxidation products such as $Y_2Si_2O_7$ and SiO_2 were observed. Spherical voids caused by outward diffusion of yttrium cations were also appeared. After oxidation at 1300°C for 24 h in air, the thickness of the oxidized zone was slightly increased to be 60 μm. Almost SiC particles were completely oxidized. This leaded to increasing of amount of the cracks and voids in this region, as shown in Figure 4.7 (b). The thickness of the oxidized zone was significantly increased after oxidation at 1400°C for 24 h in air, as shown in Figure 4.7 (c). In the region following the oxidized zone, no cracks, voids and new phases were observed. This region was considered as the non-oxidized zone where SiC particles can be observed clearly.

Figure 4.8 plotted the thickness of oxidized zone as a function of oxidation time at various temperatures. With increasing oxidation time, the thickness of oxidized zone was increased. The growth of oxidized zone followed the parabolic law. Figure 4.9 shows the parabolic rate constant, k_p, as a function of reciprocal oxidation temperature for the growth of oxidized zone for SiC/Y_2SiO_5, SiC/$Y_2Si_2O_7$ and SiC/YS composites. The apparent activation energy for growth of oxidized zone in SiC/YS was calculated to be 383 kJmol^{-1}, which is higher than that of SiC/Y_2SiO_5 composites (332 kJmol^{-1}). Although Y_2SiO_5 only possesses 30 vol% of the mixed matrix, difference in the activation energy for growth of oxidized zone for SiC/Y_2SiO_5 and SiC/YS composites is not significant. This implies that the inward diffusion of oxide ions through Y_2SiO_5 ceramic is the major contribution to develop the oxidized zone of SiC/Y_2SiO_5-$Y_2Si_2O_7$ composites, in particular, at low temperatures such as 1200°C.

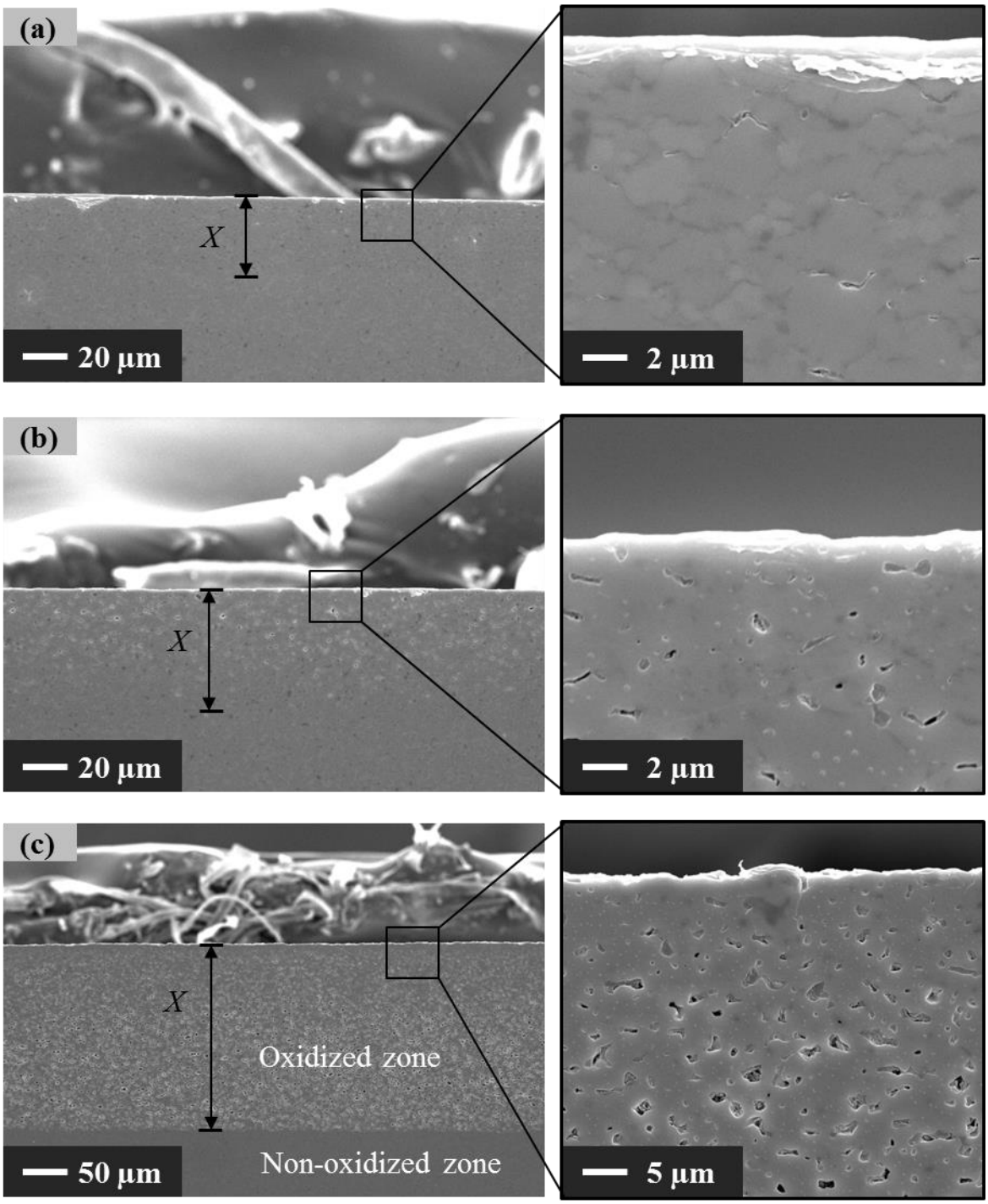

Figure 4.7 SEM images of the cross-sectioned surface of 5SiC/YS composites after oxidation at (a) 1200°C, (b) 1300°C and (c) 1400°C for 24 h in air

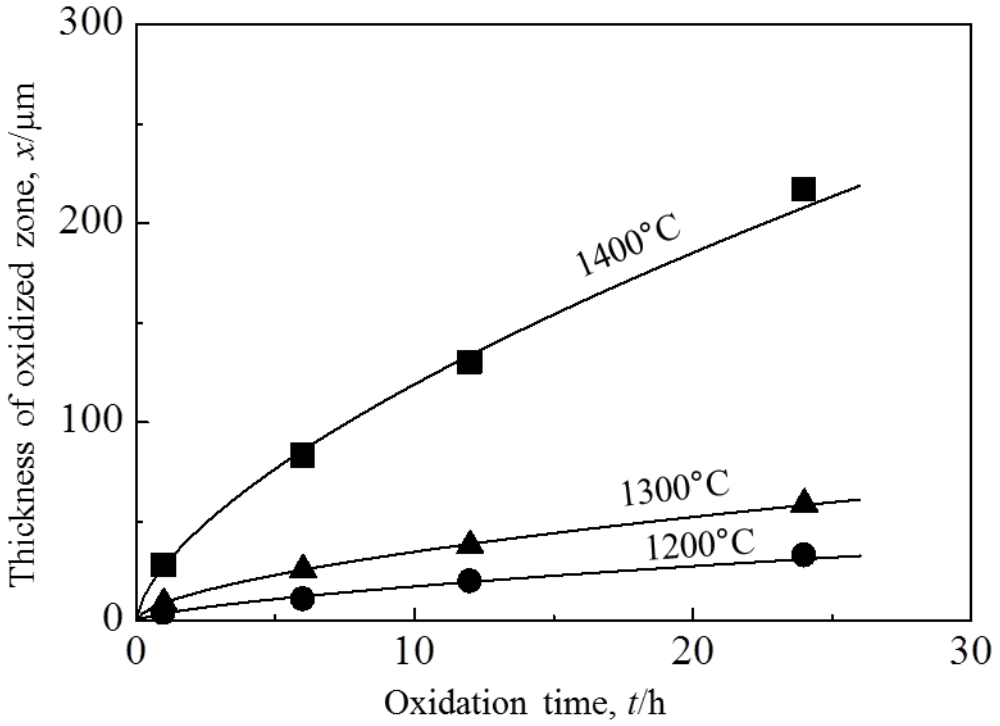

Figure 4.8 Thickness of oxidized zone as a function of oxidation time at various temperatures for 5SiC/YS composites

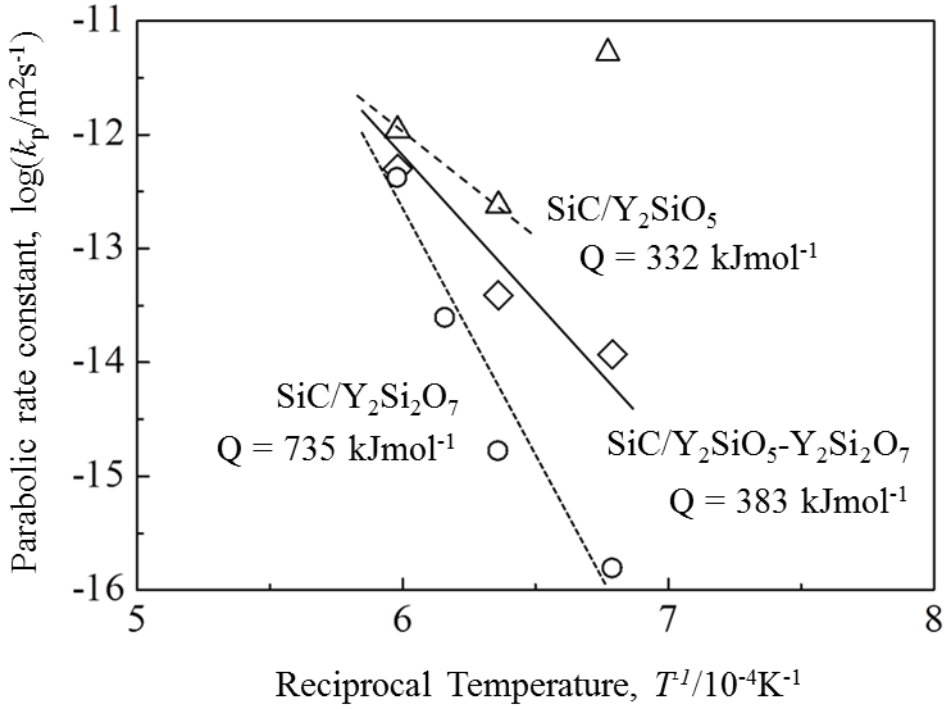

Figure 4.9 Temperature dependence of parabolic rate constant on oxidation of 5SiC/YS in comparison with $5SiC/Y_2SiO_5$ and $5SiC/Y_2Si_2O_7$

4.3.3 Effect of SiC volume fraction on self-healing ability of SiC/YS composites

4.3.3.1 Crack-disappearance of 10SiC/YS and 20SiC/YS composites

Figure 4.10 presents SEM images of 10SiC/YS sample surfaces with introduced surface cracks before and after heat treatment at various conditions. Dash lines present the outline of Vickers indentation. Without heat treatment, surface cracks propagated from the corners of the indentation could be observed clearly as shown in Figure 4.10 (a). After heat treatment at 1200°C for a short time such as 1 or 6 h, the surface cracks were partially disappeared, as shown in Figure 4.10 (b) and (c). The fraction of crack-disappearance was increased with increasing heat treatment time. At higher heat treatment temperatures, 1300°C for 1 h, surface cracks were completely healed, as shown in Figure 4.10 (d).

Figure 4.11 shows SEM images of the introduced cracks on 20SiC/YS sample surface before and after heat treatment. From each corner of the indentation, a crack propagated as observed in Figure 4.11 (a). After heat treatment at 1200°C for 1 h, the surface crack was almost disappeared. The fraction of crack-disappearance at this condition was determined to be 80%, shown in Figure 4.11 (b). For longer heat treatment time, heat treatment at 1200°C for 6 h, cracks on sample surface completely disappeared as shown in Figure 4.11 (c). Higher heat treatment temperatures and shorter heat treatment time, such as 1300°C for 1 h, would also cause complete disappearance of surface cracks, as shown in Figure 4.11 (d).

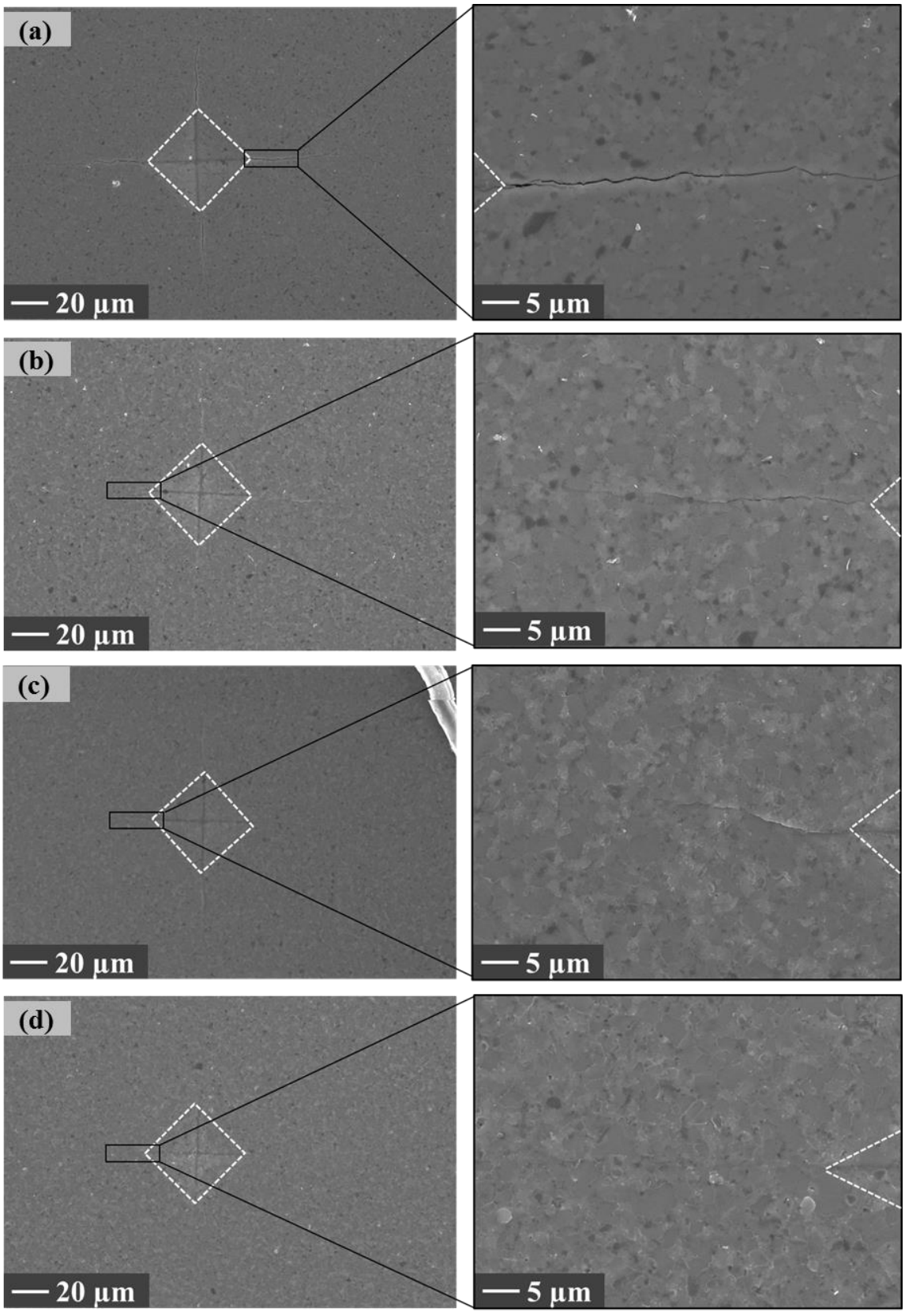

Figure 4.10 SEM images of surfaces of 10SiC/YS samples after (a) cracking and heat treatment at (b) 1200°C for 1 h (c) 1200°C for 6 h and (d) 1300°C for 1 h in air

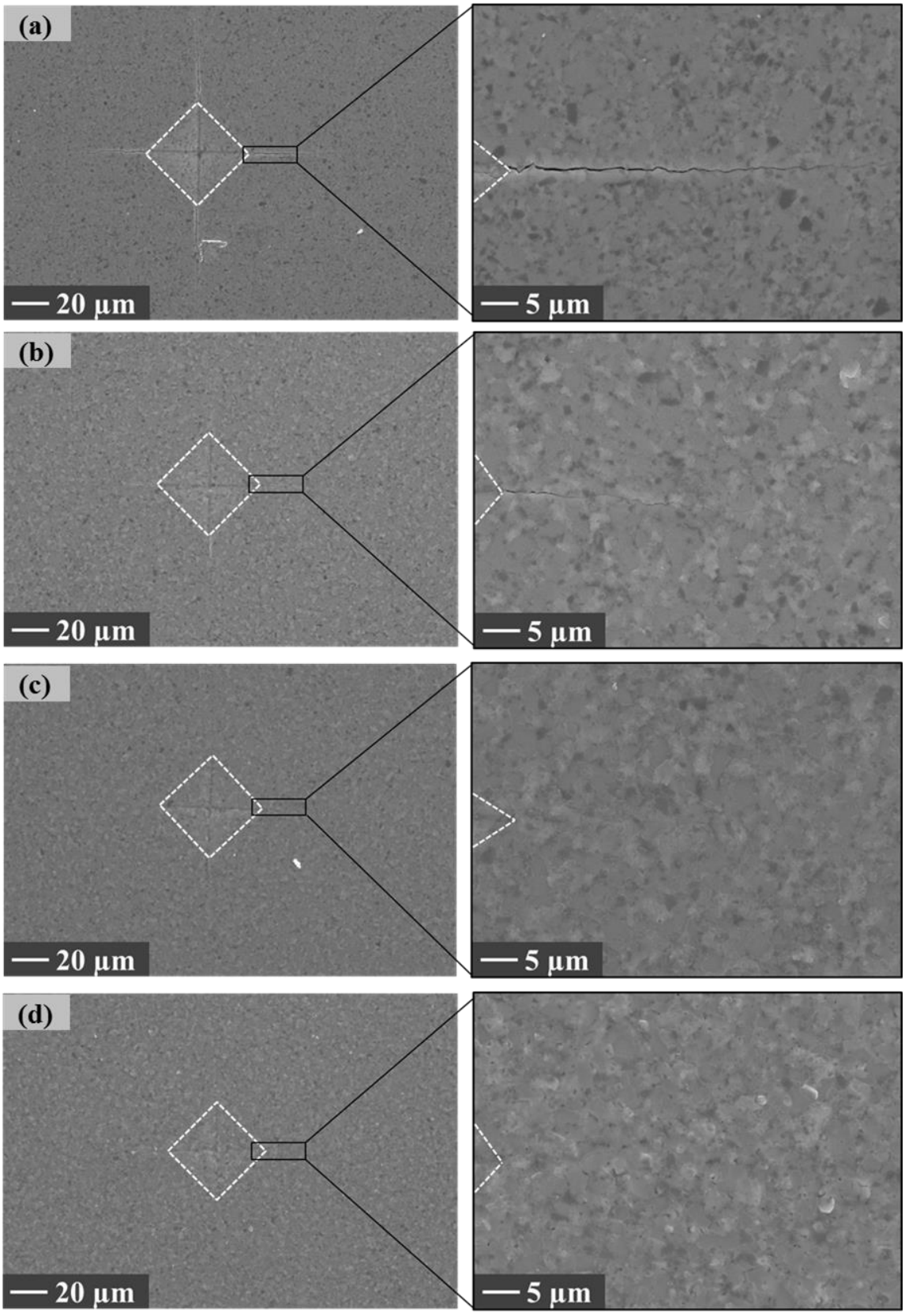

Figure 4.11 SEM images of surfaces of 20SiC/YS samples after (a) cracking and heat treatment at (b) 1200°C for 1 h (c) 1200°C for 6 h and (d) 1300°C for 1 h in air

Figure 4.12 plotted the crack-disappearance as a function of heat treatment temperature for 5SiC/YS, 10SiC/YS and 20SiC/YS composites. A comparison in crack-disappearance performance of these composites indicates that the healing rate of 20SiC/YS composites is larger than that of the other ones. The results imply that the self-healing ability of the composites is proportional to the volume fracture of SiC dispersoid. Taking into account the function of these composites, volume fraction of SiC dispersed in the matrices should be controlled because a large volume fraction of SiC disperoid will affects the lifetime and provided protection of SiC/YS composites in combustion environments.

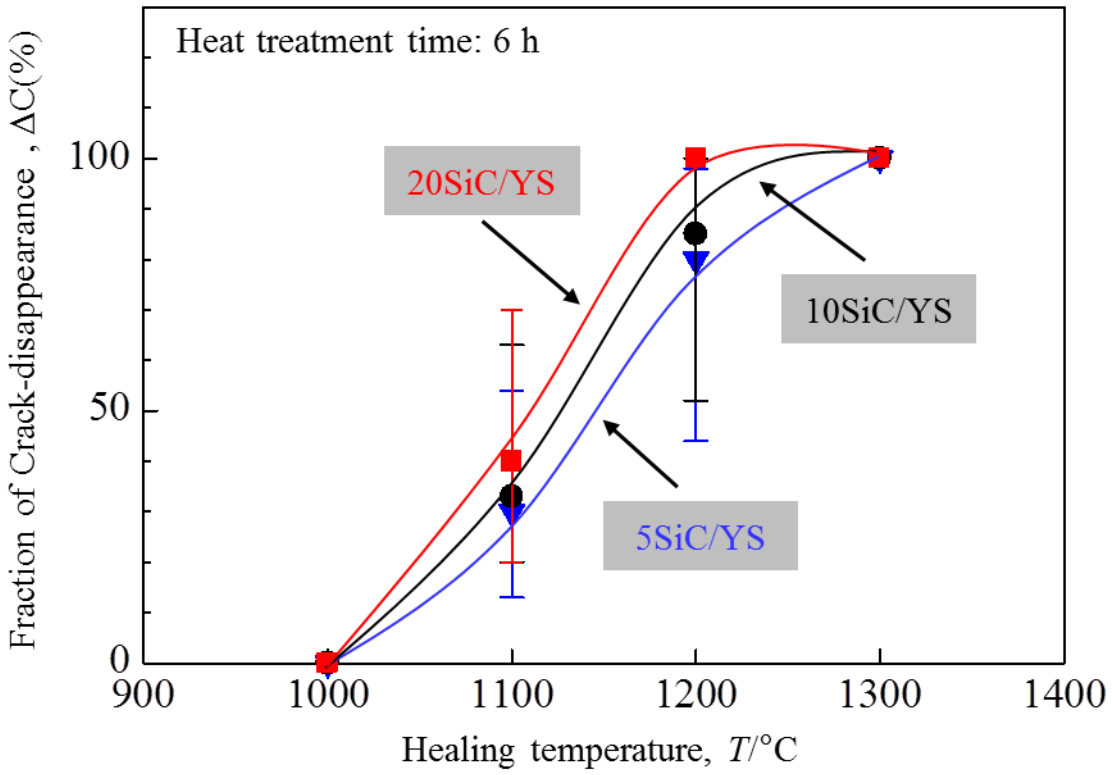

Figure 4.12 Fraction of crack-disappearance as a function of heat treatment temperature for 5SiC/YS, 10SiC/YS and 20SiC/YS composites

4.3.3.2 Oxidation resistance of 10SiC/YS and 20SiC/YS composites

Figures 4.13 and 4.14 show SEM images observed on cross-sectioned surface of

10SiC/YS and 20SiC/YS samples after oxidation at 1200, 1300 and 1400°C for 24 h in air. The oxidized zone was considered as a region consisting of $Y_2Si_2O_7$ and SiO_2 phases. The amorphous SiO_2 was formed not only on/near the sample surface but also inside of the oxidized zone, as clearly shown in Figures 4.13 and 4.14 (c). The crystalline SiO_2 was also formed in the SiO_2 regions inside of the oxidized zone [85]. The pores and short cracks were also detected in the oxidized zone. Some large pores near the sample surface were produced by CO gas evolution, according to Equation (2.1) and (3.1), as shown in Figure 4.14 (c). This phenomenon was reported in oxidation behavior of Si/mullite composites [86] as well.

Figures 4.15 and 4.16 present the thickness of oxidized zone as a function of oxidation time at various oxidation temperatures for 10SiC/YS and 20SiC/YS composites, respectively. The results indicate the thickness of oxidized zone was increased with increasing oxidation time as well as oxidation temperatures. The growth of oxidized zone obeyed the parabolic law.

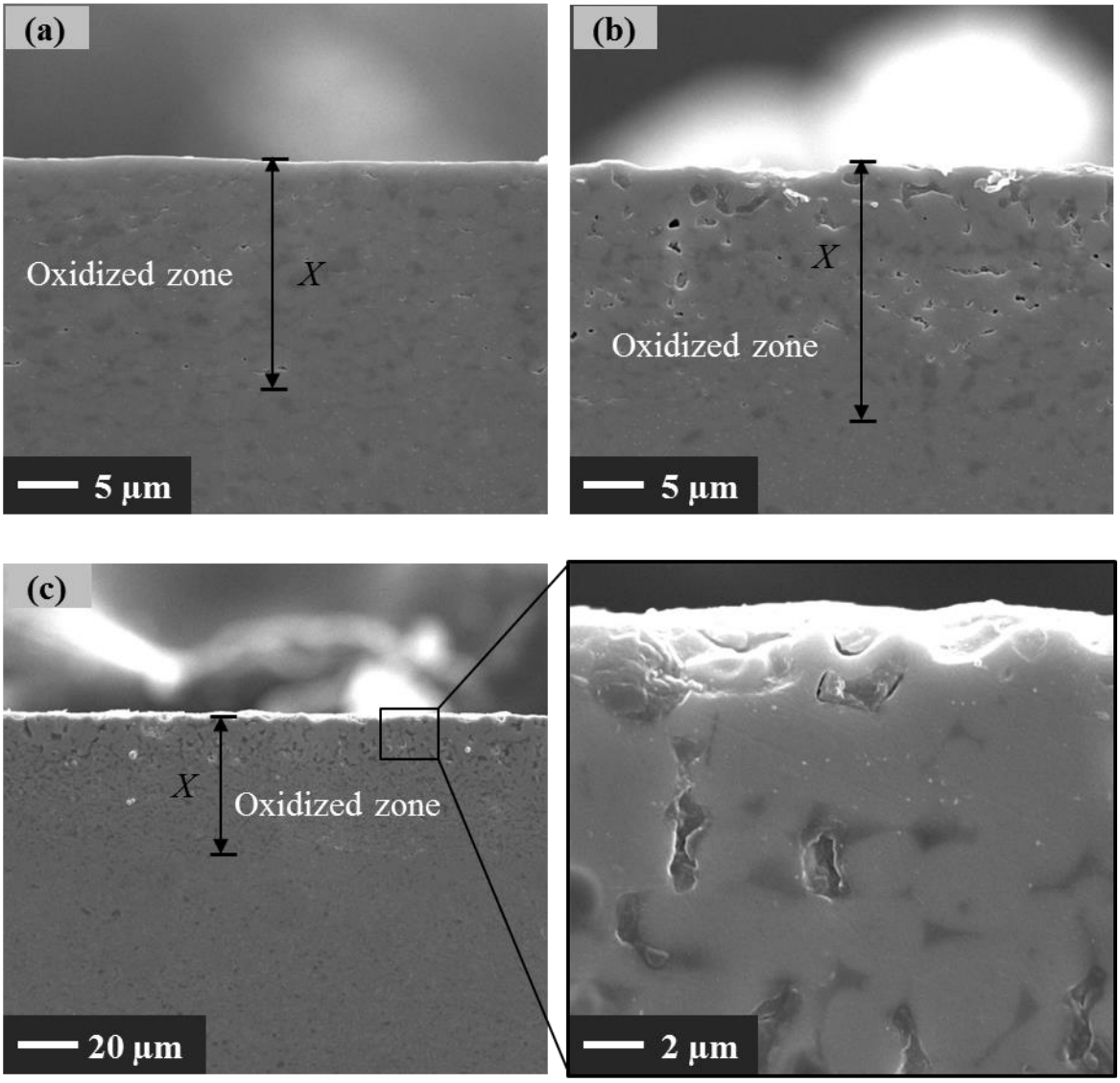

Figure 4.13 SEM images of the cross-sectioned surface of 10SiC/YS composites after oxidation at (a) 1200°C, (b) 1300°C and (c) 1400°C for 24 h in air

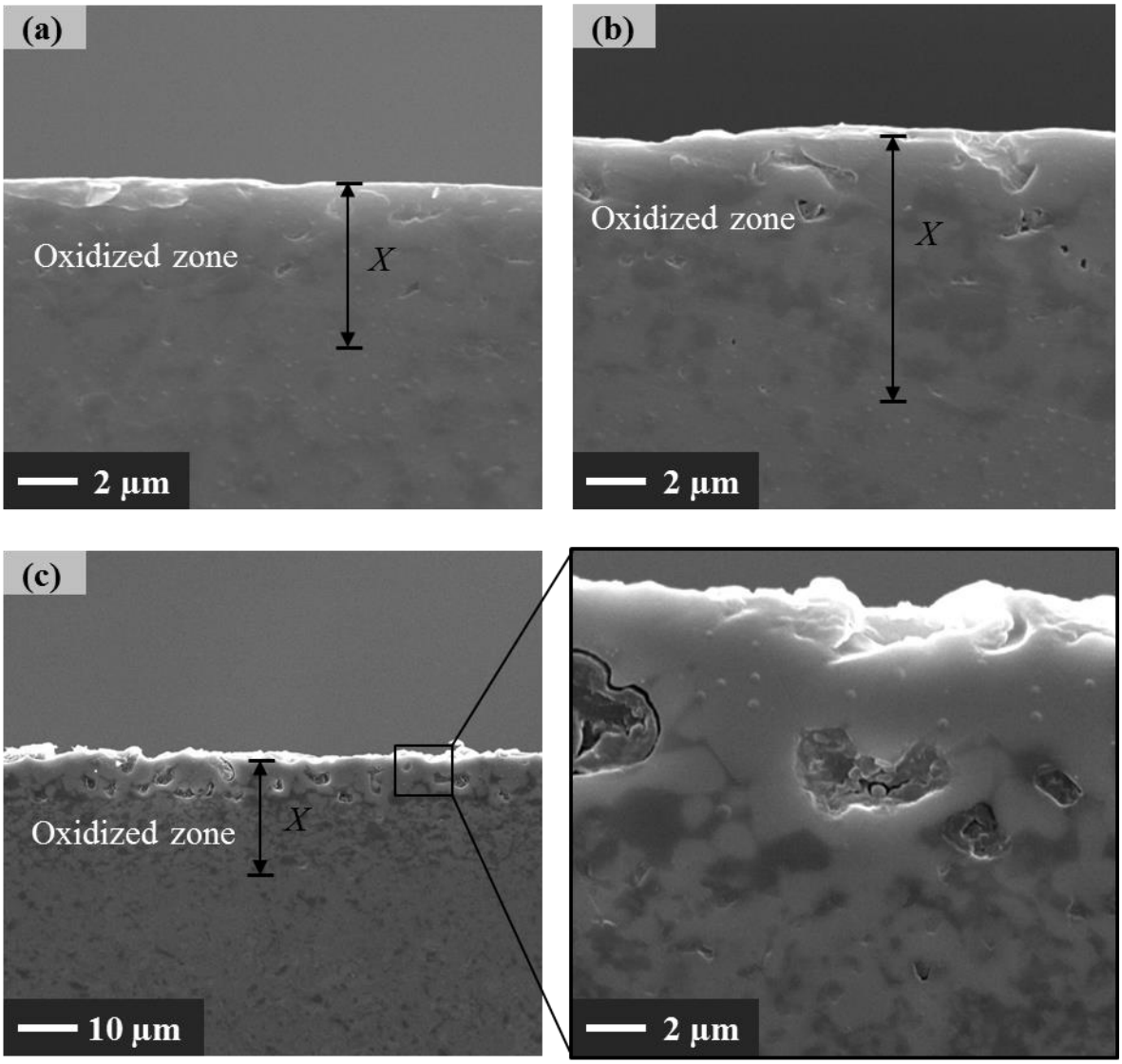

Figure 4.14 SEM images of the cross-sectioned surface of 20SiC/YS composites after oxidation at (a) 1200°C, (b) 1300°C and (c) 1400°C for 24 h in air

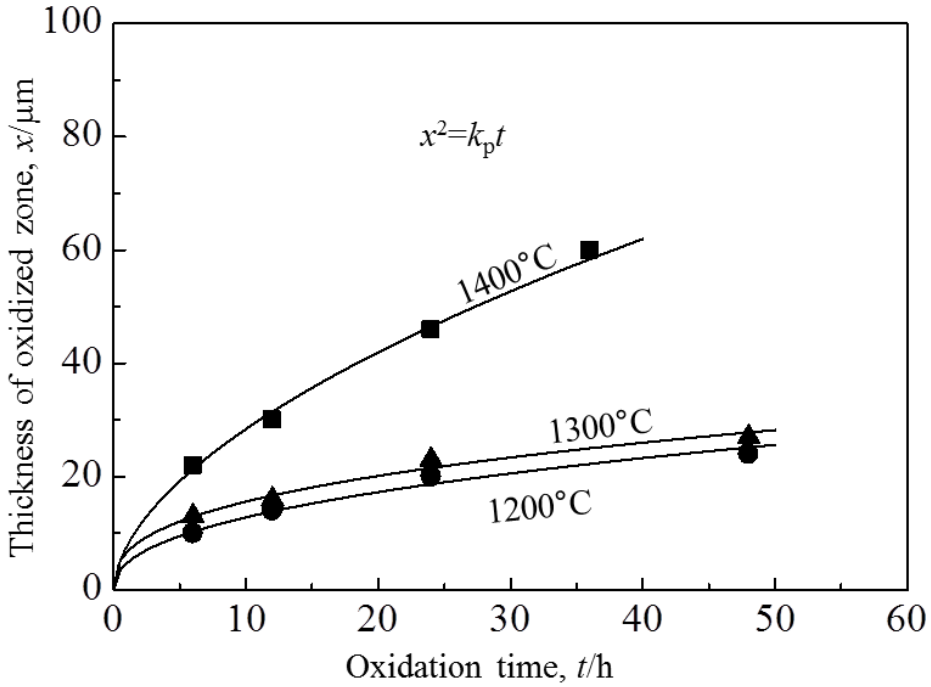

Figure 4.15 Thickness of oxidized zone as a function of oxidation time at various temperatures for 10SiC/YS composites

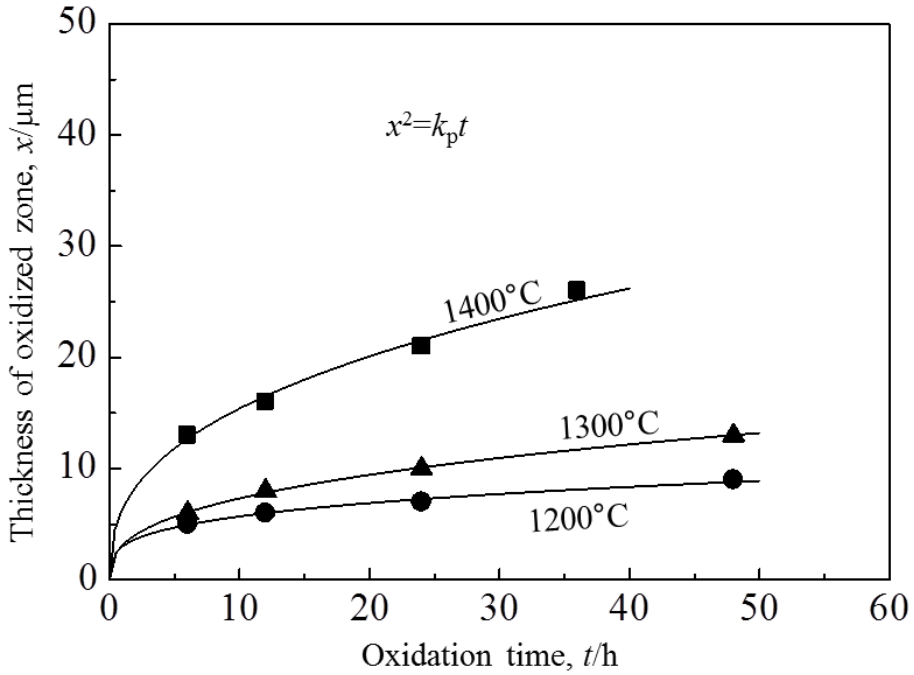

Figure 4.16 Thickness of oxidized zone as a function of oxidation time at various temperatures for 20SiC/YS composites

Figure 4.17 plotted the parabolic rate constant k_p on the growth of oxidized zone as a function of reciprocal oxidation temperature for 10SiC/YS and 20SiC/YS composites. The comparison in oxidation rate of these composites indicates that oxidation resistance of the composites is increased with increasing the volume fraction of SiC dispersoid. The oxidation rate of 20SiC/YS composites is lower than those of the other ones.

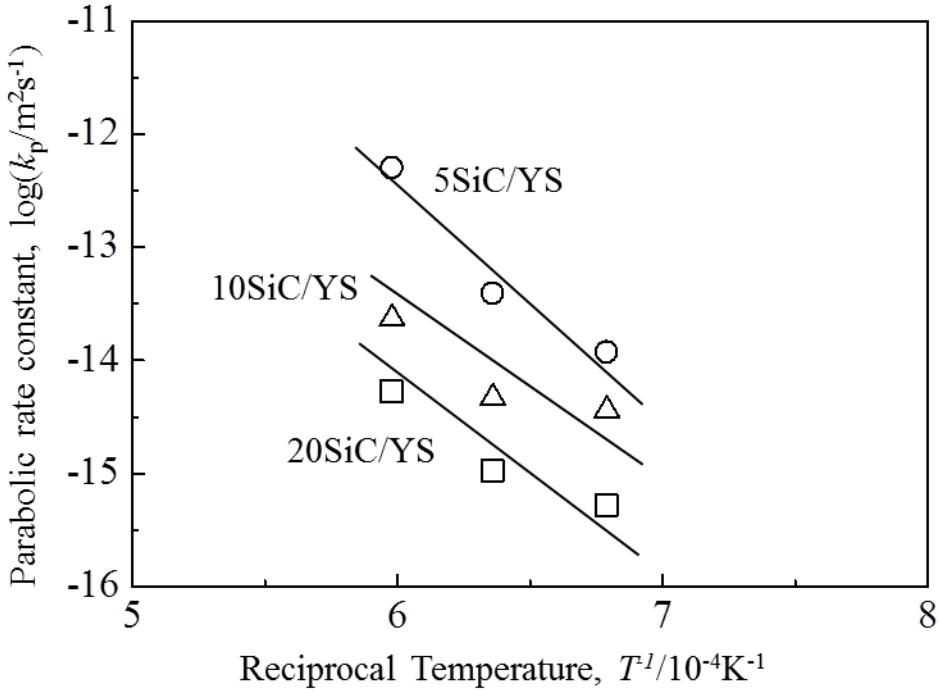

Figure 4.17 Temperature dependence of parabolic rate constant on oxidation of 5SiC/YS, 10SiC/YS and 20SiC/YS composites

4.4 Conclusions

Full densified 5 vol% SiC particles dispersed in the Y_2SiO_5-$Y_2Si_2O_7$ (mixing in a volume ratio of 3:7) matrix composites were fabricated by PECS to investigate the self-healing function. The investigation on self-healing is conducted at the temperatures ranging from 1100 to 1300°C for 1 to 24 h in air. The complete disappearance of cracks on 5SiC/YS sample surface would be caused by heat

treatment at 1300°C for 1h in air. The healing rate of 5SiC/YS is the middle order of magnitude of 5SiC/$Y_2Si_2O_7$ and 5SiC/Y_2SiO_5. The formation of oxidation product layer and the volume expansion are responsible for closure of the surface cracks. The formation of the outer layer was considered as the outward diffusion of Y^{3+} cations. The oxidation of SiC dispersoid into SiO_2 caused the volume expansion.

Investigation for oxidation behavior of 5SiC/YS composites was conducted at 1200 to 1400°C for 1 to 60 h in air. Oxidation resistance of the composites was examined through growth rate of oxidized zone after heat treatment in air. Oxidation of SiC particles within the matrix creates the formation of the oxidized zone. The growth of oxidized zone follows the parabolic law. The inward diffusion of oxygen through the Y_2SiO_5 components is the major contribution to develop the oxidized zone of 5SiC/YS composites, in particular, at low temperatures such as 1200°C. The apparent activation energy for the growth of oxidized zone was determined to be 383 $kJmol^{-1}$. Oxidation rate value of 5SiC/YS is the middle value of 5SiC/$Y_2Si_2O_7$ and 5SiC/Y_2SiO_5.

Consolidated 10 and 20 vol% SiC/YS samples were fabricated by PECS to investigate the effect of SiC volume fraction on self-healing ability of SiC/YS composites. The investigation of surface crack-disappearance for 10SiC/YS and 20SiC/YS was carried out by heat treatment at 1100 to 1300°C for 1 to 24 h in air. Results of the investigation indicated the healing rated of 20SiC/YS composites is larger than that of the other ones. The self-healing ability of SiC/YS composites is proportional to the volume fracture of SiC dispersoid. Investigation for oxidation resistance of 10SiC/YS and 20SiC/YS composites was conducted at temperatures ranging from 1200 to 1400°C for 6 to 48 h in air. The oxidation in air resulted in the formation of the oxidized zone consisting of $Y_2Si_2O_7$ and SiO_2. The growth of

oxidized zone obeyed the parabolic law. The oxidation rate was controlled by the diffusion of oxygen through the amorphous SiO_2 scale, in particular at high temperatures such as 1400°C. The oxidation resistance of SiC/YS is increased with increasing volume fraction of SiC dispersoid.

Chapter V

Diffusivity of Ions in Yttrium Monosilicate

5.1 Background

As mentioned in the previous chapters, the mass transport in the oxidized zone is the predominant process for growth of the oxidized zone. Solid-state diffusion is responsible for mass transport. In other words, ions diffusion in the oxidized zone determine rate-controlling for growth of the oxidized zone. For understanding the high-temperature oxidation behavior as well as self-healing mechanism of SiC/Y_2SiO_5, SiC/$Y_2Si_2O_7$ and SiC/YS composites, the diffusion coefficient of yttrium ions in yttrium silicates have to be known. However, no yttrium diffusivity in yttrium silicates has been reported previously. In this study, diffusion coefficient of Y^{3+} cation in yttrium silicates will be determined.

Several researches on diffusion coefficient of cations in rare earth chromites ($RECrO_3$) were reported such as those of Y^{3+} in $YCrO_3$ [87], La^{3+} in $LaCrO_3$ [88] and Nd^{3+} in $NdCrO_3$ [89]. The rate of a solid state reaction gives the diffusion coefficient of the rate-determining ion as a function of the activities of the components. The diffusivity of Y^{3+} in $YCrO_3$ was determined from the solid state reaction between Y_2O_3 and Cr_2O_3 [87]. The solid state reaction between La_2O_3 and Cr_2O_3 was examined to estimate the diffusion coefficient of La^{3+} in $LaCrO_3$ [88]. The examination of the solid state reaction was conducted by investigation for a diffusion couple made by facing the polished surface plates of two oxides. As shown in Figure 5.1, the different mechanisms are given for the hypothetical reaction of a diffusion couple of AX and BX compound [90], where A and B are the cations (such as Ni^{2+} and Al^{3+} in $NiAlO_4$)

and X is the common anion (such as O^{2-} in $NiAlO_4$). It is assumed that single crystal AX and BX react to form a compact product ABX_2, which separates the reactants from each other. As shown in Figure 5.1 (b), the formation of reaction layer of ABX_2 is caused by the parallel diffusion of B and X ions from the BX/ABX_2 interface to the AX/ABX_2 interface. After the reaction, the marker particles are observed in the in vicinity of the AX/ABX_2 interface. If the parallel diffusion of A and X ions is responsible for the formation of ABX_2 layer, the markers will be located at the interface of BX and ABX_2, as shown in Figure 5.2 (c). As shown in Figure 5.1 (d), the marker is observed in the reaction layer ABX_2. It means that the formation of the reaction layer is caused by the counter diffusion of A and B ions.

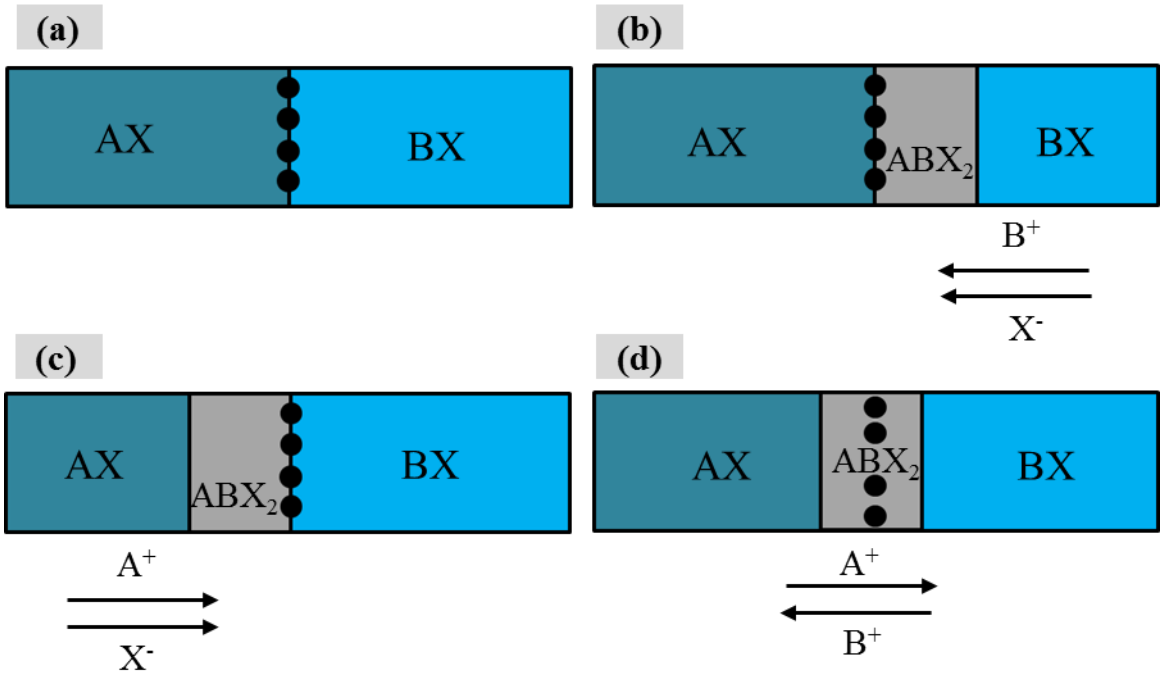

Figure 5.1 Basic mechanism of the reaction: $AX + BX \rightarrow ABX_2$

(a) Reactants

(b) $AX + B^+ + X^- \rightarrow ABX_2$

(c) $BX + A^+ + X^- \rightarrow ABX_2$

(d) $2AX + B^+ \rightarrow ABX_2 + A^+$

$2BX + A^+ \rightarrow ABX_2 + B^+$

● Cross section of a particle marker

According to the Y_2O_3-SiO_2 phase diagram, shown in Figure 1.4, Y_2O_3 and Y_2SiO_5 could be existed together in the equilibrium whereas Y_2O_3 does not coexist with $Y_2Si_2O_7$. In this chapter, diffusion coefficient of Y^{3+} cations in Y_2SiO_5 ceramic is estimated through investigation for $Y_2Si_2O_7$-Y_2O_3 diffusion couple. The diffusion coefficient of oxygen in the Y_2SiO_5 matrix is also calculated and compare to that of Y^{3+} to clarify the self-healing and oxidation process of SiC/Y_2SiO_5 composites.

5.2 Experimental procedure

Specimens used in this study were $Y_2Si_2O_7$ and Y_2O_3, prepared by the following procedure. The single phase $Y_2Si_2O_7$ powder was synthesized by using the solid-state reaction method, as mentioned in chapter 3. The $Y_2Si_2O_7$ powder was consolidated with a graphite die by PECS at die temperature of 1500°C for 5 min in holding time under 70 MPa in uniaxial pressure in a vacuum. The relative density of fabricated samples attained at least 99% of theoretical density. The Y_2O_3 bulk samples were purchased from Japan Yttrium Co., Japan. The surface of $Y_2Si_2O_7$ and Y_2O_3 plates were ground by using a grinding wheel with 30 μm diamond grains and then polished with 2μm diamond slurry. $Y_2Si_2O_7$ plate samples were coated with a slurry mixture containing platinum (Pt) particles with 3 μm in average and ethanol on the polished surface.

A diffusion couple was made by facing the polished plates of $Y_2Si_2O_7$ and Y_2O_3. The diffusion couple was placed in a sample holder with a push rod to obtain an intimate contact, as shown in Figure 5.2. The solid state reactions were conducted at 1300°C for 2 and 3 d in air. After the reaction, the diffusion couple was mounted in epoxy resin, cut perpendicular to the reaction interface, and polished with 2 μm diamond particle slurry. The cross-sectioned surfaces were observed by using high

speed optical microscope (OM) and SEM. The phase identification on surface of samples was carried out by using XRD.

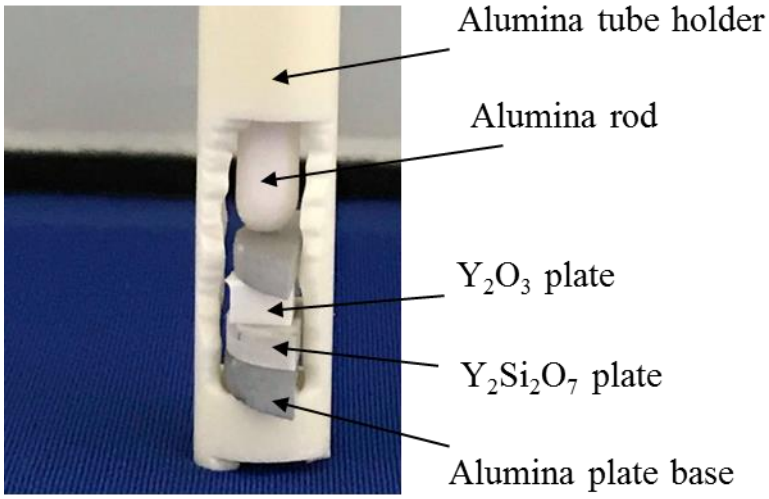

Figure 5.2 Picture of the $Y_2Si_2O_7$-Y_2O_3 diffusion couple

5.3 Results and discussion

5.3.1 Diffusion coefficient of yttrium ions in Y_2SiO_5

Figure 5.3 shows OM images of typical cross-sectional view of the diffusion couples after reaction at 1300°C for 2 and 3 d. The interface of Y_2SiO_5/$Y_2Si_2O_7$ was separated during cooling so that the epoxy resin penetrates between Y_2SiO_5 and $Y_2Si_2O_7$. The Pt marker was clearly observed in the vicinity of the Y_2SiO_5/Y_2O_3 interface. This result indicates that yttrium and oxygen are transported from the Y_2SiO_5/Y_2O_3 interface to the Y_2SiO_5/$Y_2Si_2O_7$ interface. Since the diffusion of oxygen anions is generally much faster than that of cations [87], it is assumed that the diffusion of Y^{3+} in Y_2SiO_5 layer controls the rate of the solid state reaction between Y_2O_3 and $Y_2Si_2O_7$.

The thickness of the Y_2SiO_5 layer was estimated through observation of cross-sectioned surfaces of the diffusion couple by SEM, as shown in Figure 5.4. After

heated at 1300°C for 3 d, the reaction layer achieved approximately 13 μm. With shorter heating time, 1300°C for 2 d, the thickness of the Y_2SiO_5 layer was approximately 10 μm. Figure 5.5 plotted the thickness of the reaction layer as a function of reaction time at 1300°C. The growth of the product layer obeys the parabolic law.

Figure 5.6 shows XRD patterns for phase identification of $Y_2Si_2O_7$ sample surface after reaction at 1300°C for 3 d. The detected phases are not only $Y_2Si_2O_7$ but also Y_2SiO_5 phase. It means that the reaction layer formed between $Y_2Si_2O_7$ and Y_2O_3 plates is the Y_2SiO_5 layer.

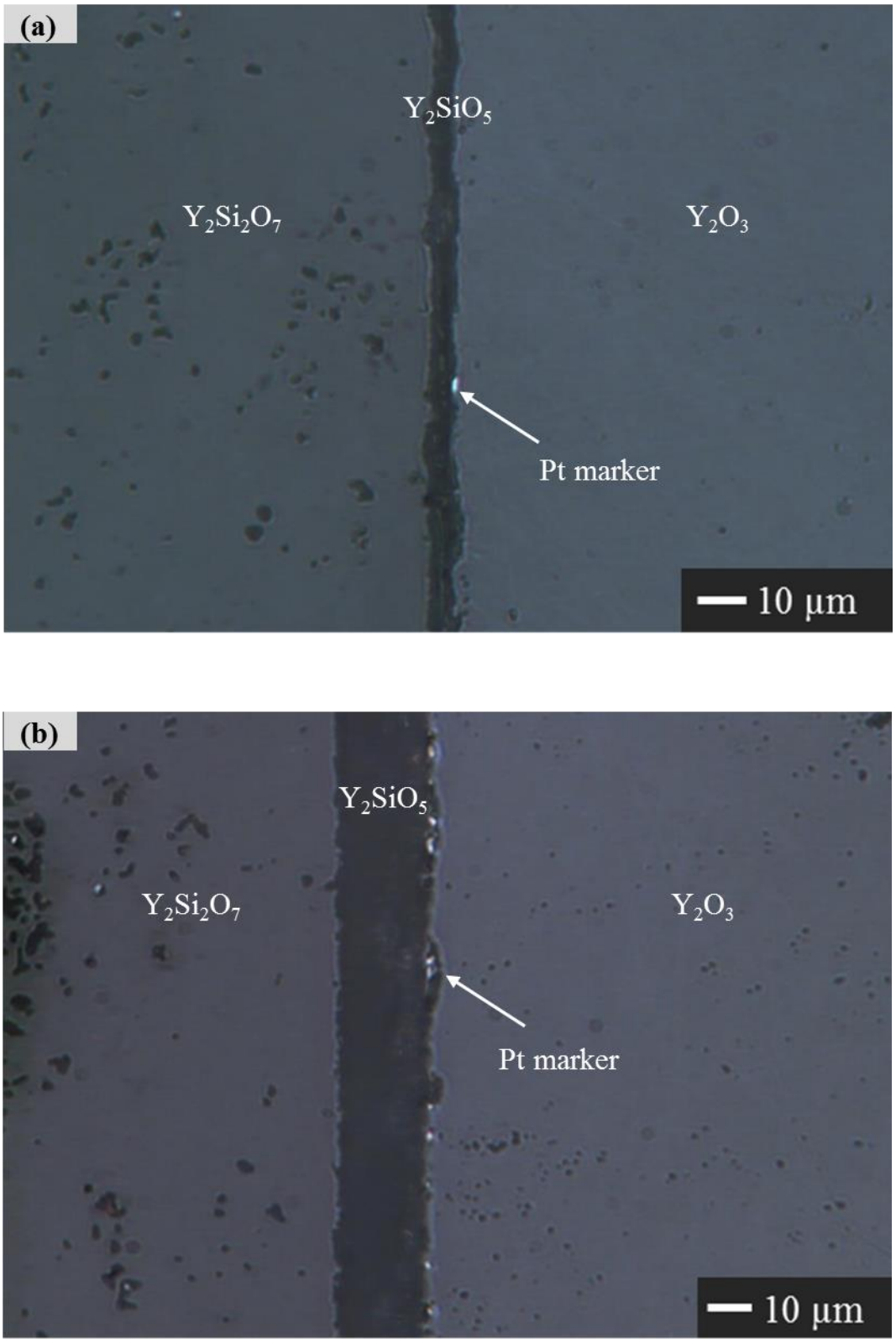

Figure 5.3 OM images of cross-sectioned surfaces of the diffusion couple after heated at 1300°C for (a) 2 d and (b) 3 d in air

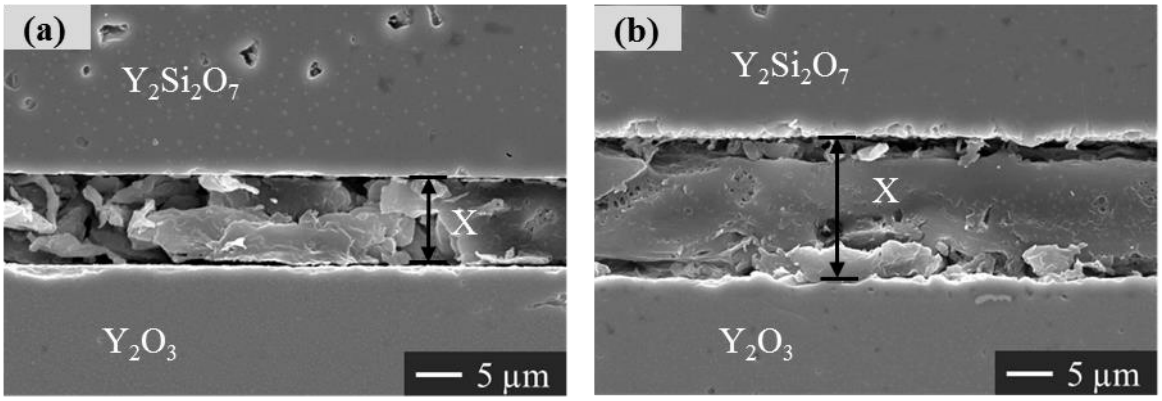

Figure 5.4 SEM images of cross-sectional view of the diffusion couple after heated at 1300°C for (a) 2 d and (b) 3 d in air

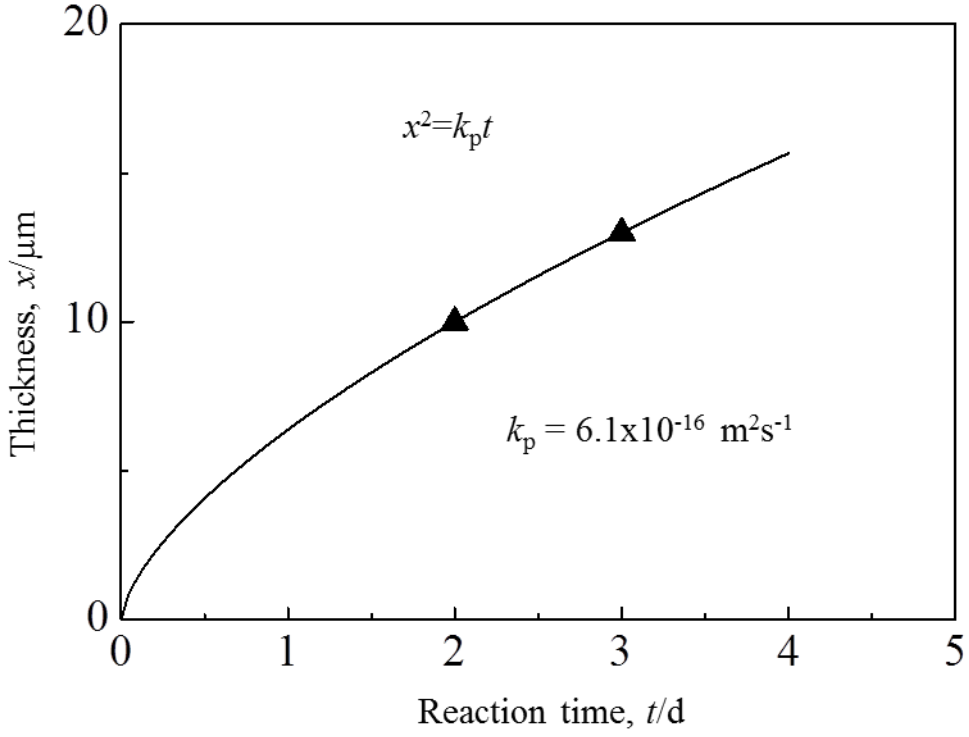

Figure 5.5 Thickness of reaction layer as function of reaction time at 1300°C

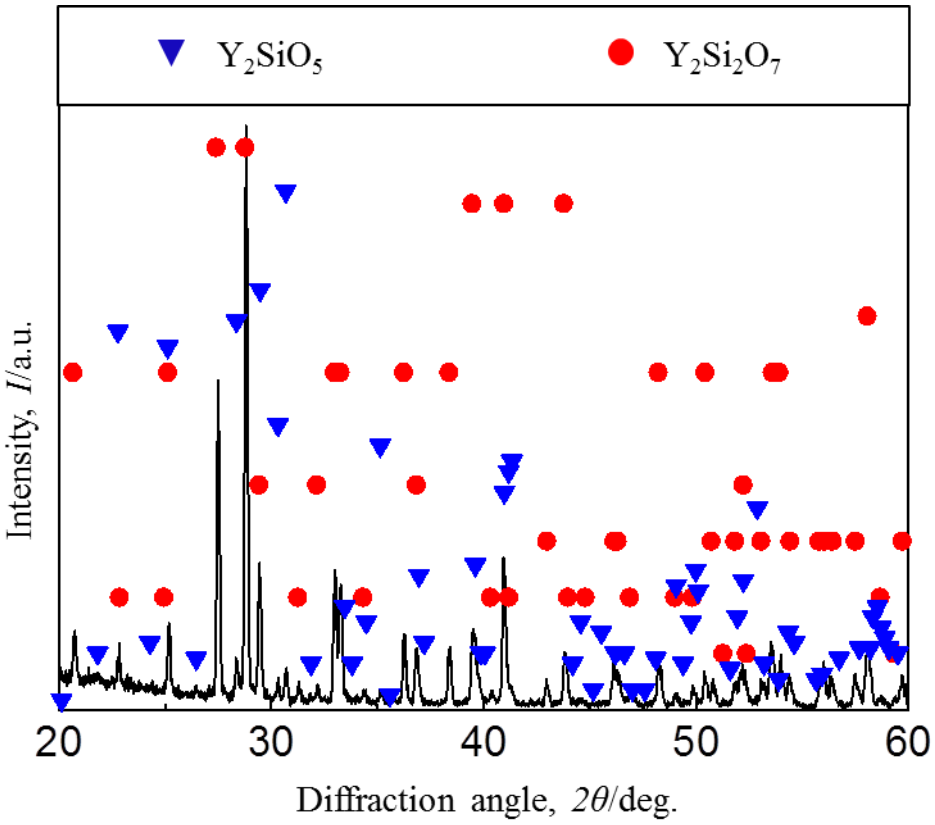

Figure 5.6 XRD patterns of $Y_2Si_2O_7$ sample surface after reaction at 1300°C for 3 d in air

As mentioned above, the formation of Y_2SiO_5 layer was caused by transportation of yttrium and oxygen from the Y_2SiO_5/Y_2O_3 interface to the $Y_2SiO_5/Y_2Si_2O_7$ interface. The reaction between $Y_2Si_2O_7$ and Y_2O_3 to form Y_2SiO_5 layer is following equilibrium:

$$\frac{1}{2}Y_2Si_2O_7 + \frac{1}{2}Y_2O_3 = Y_2SiO_5 \quad (5.1)$$

Figure 5.7 shows the illustration of the solid state reaction kinetic of the diffusion couple. The difference of Y_2O_3 activity between the interface I and II is driving force for diffusion of Y^{3+} and O^{2-} ions from the interface II to the interface I. From the Fick's 1st law, the diffusion flux of Y ions can be expressed as:

$$J_Y = \frac{-D_Y C_Y}{RT}\frac{d\mu_Y}{dx} \quad (5.2)$$

where J_Y is diffusion flux of Y^{3+} cation through the reaction layer, D_Y diffusion coefficient, C_Y molar concentration, R gas constant , T temperature, μ_Y chemical potential, x thickness of the reaction layer.

Chemical potential in formation of Y_2O_3:

$$2\mu_Y + \frac{3}{2}\mu_{O_2} = \mu_{Y_2O_3} \tag{5.3}$$

The present diffusion couple experiments were carried out in constant P_{O_2} condition. Then the deferential of Eq. (5.3) is:

$$2\mathrm{d}\mu_Y = \mathrm{d}\mu_{Y_2O_3} \tag{5.4}$$

From Gibbs energy of chemical potential of Y_2O_3:

$$\mathrm{d}\mu_{Y_2O_3} = RT\mathrm{d}\ln a_{Y_2O_3} \tag{5.5}$$

where $a_{Y_2O_3}$ is activity of Y_2O_3. From (5.2), (5.4) and (5.5), the diffusion flux of Y ions becomes:

$$J_Y = \frac{-D_Y C_Y}{2}\frac{\mathrm{d}\ln a_{Y_2O_3}}{\mathrm{d}x} \tag{5.6}$$

Integrating Eq. (5.6):

$$J_Y = \frac{-D_Y C_Y}{2x}\ln\left(\frac{a^{I}_{Y_2O_3}}{a^{II}_{Y_2O_3}}\right) \tag{5.7}$$

where $a^{I}_{Y_2O_3}$ is the activity of Y_2O_3 at the interface of $Y_2SiO_5/Y_2Si_2O_7$, $a^{II}_{Y_2O_3}$ the activity of Y_2O_3 at the interface of Y_2SiO_5/Y_2O_3, as shown in Figure 5.7.

Furthermore, it assumed that the diffusion of oxygen is much faster than that of yttrium. The diffusion of Y^{3+} in Y_2SiO_5 layer controls the rate of the solid state reaction between Y_2O_3 and $Y_2Si_2O_7$. According to the Eq. (5.1), 1 molar of Y ion diffuses in the Y_2SiO_5 layer to the interface $Y_2SiO_5/Y_2Si_2O_7$ and react with $Y_2Si_2O_7$ for generating 1 molar of Y_2SiO_5. Thus, the relationship between the flux Y cation and the growth rate of Y_2SiO_5 is expressed as:

$$J_{\mathrm{Y}} = \frac{\mathrm{d}n_{\mathrm{Y}}}{A\mathrm{d}t} = \frac{1}{V_{\mathrm{Y_2SiO_5}}}\frac{\mathrm{d}x}{\mathrm{d}t} \tag{5.8}$$

where A is cross-section area of the reaction layer, $V_{\mathrm{Y_2SiO_5}}$ molar volume of Y_2SiO_5, and *x* thickness of the reaction layer.

From equations (5.7) and (5.8):

$$\frac{-D_{\mathrm{Y}}C_{\mathrm{Y}}}{2x}\ln\left(\frac{a^{\mathrm{I}}_{\mathrm{Y_2O_3}}}{a^{\mathrm{II}}_{\mathrm{Y_2O_3}}}\right) = \frac{1}{V_{\mathrm{Y_2SiO_5}}}\frac{\mathrm{d}x}{\mathrm{d}t} \tag{5.9}$$

Assuming that D_{Y} and C_{Y} are constant for x and t, then integrating Eq. (5.9):

$$x^2 = D_{\mathrm{Y}}C_{\mathrm{Y}}V_{\mathrm{Y_2SiO_5}}\ln\left(\frac{a^{\mathrm{II}}_{\mathrm{Y_2O_3}}}{a^{\mathrm{I}}_{\mathrm{Y_2O_3}}}\right)\mathrm{t} = k_{\mathrm{p}}t \tag{5.10}$$

The activity of Y_2O_3 in Y_2SiO_5 at the Y_2O_3/Y_2SiO_5 interface is:

$$a^{\mathrm{II}}_{\mathrm{Y_2O_3}} = 1 \tag{5.11}$$

The activity of Y_2O_3 at the $Y_2Si_2O_7/Y_2SiO_5$ interface can be calculated from the standard Gibbs energy change of reaction (5.1), $\triangle G^{\mathrm{o}}$. Since the activity of $Y_2Si_2O_7$ in Y_2SiO_5 at the $Y_2Si_2O_7/Y_2SiO_5$ interface is unity ($a_{\mathrm{Y_2Si_2O_7}} = 1$), the activity of Y_2O_3 at the $Y_2Si_2O_7/Y_2SiO_5$ interface is expressed as:

$$a^{\mathrm{I}}_{\mathrm{Y_2O_3}} = \exp\left(\frac{2\Delta G^{\mathrm{o}}}{RT}\right) \tag{5.12}$$

From equations (5.10), (5.11) and (5.12), the diffusion coefficient of Y ion can be expressed:

$$D_{\mathrm{Y}} = \frac{x^2}{t}\frac{1}{C_{\mathrm{Y}}V_{\mathrm{Y_2SiO_5}}}\frac{-RT}{2\Delta G^{\mathrm{o}}} = k_{\mathrm{p}}\frac{1}{C_{\mathrm{Y}}V_{\mathrm{Y_2SiO_5}}}\frac{-RT}{2\Delta G^{\mathrm{o}}} \tag{5.13}$$

By using thermodynamic data of yttrium silicates reported previously [56, 91], the standard Gibbs energy change of the reaction (5.1) is calculated to be approximately -89 kJmol^{-1}. At 1300°C, the value of k_{p} is equal to be 6.1x10^{-16} m^{2}s^{-1}. Thus, the diffusion coefficient of Y ions in Y_2SiO_5 at 1300°C can be determined to be approximately 4 x10^{-17} m^{2}s^{-1}. There have been no yttrium diffusivity studies on Y_2SiO_5

reported in literature therefore no direct comparison can be made to assess the validity of this result.

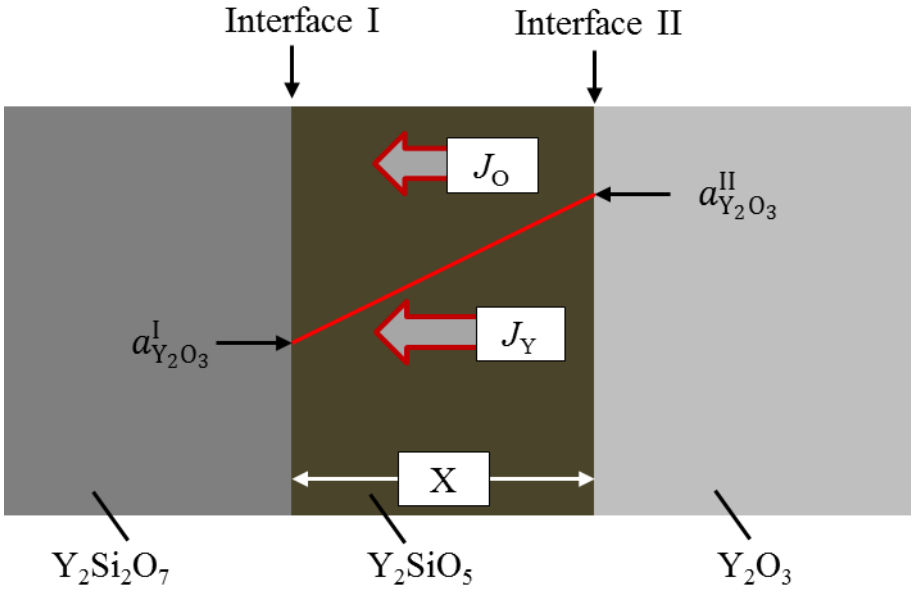

Figure 5.7 Schematic illustration of the solid state reaction kinetic of the diffusion couple

5.3.2 Diffusion coefficient of oxygen ions in Y_2SiO_5

As mentioned in chapter II, in the oxidation process of SiC/Y_2SiO_5 composites, oxygen inward diffused and reacted with SiC particles within the Y_2SiO_5 matrix at high temperature to form oxidation product as the Eq. (2.1). The illustration of the oxidation kinetic of SiC/Y_2SiO_5 composites is shown in Figure 5.8. The inward diffusion of oxygen ions is caused by the difference of oxygen pressure between the sample surface and the oxidized/non-oxidized interface. According to the Fick's first law, the diffusion flux of oxygen ions can be expressed:

$$J_O = \frac{-D_O C_O}{RT}\frac{d\mu_O}{dx} \quad (5.15)$$

where J_O is diffusion flux of oxygen ions, D_O diffusion coefficient, C_O molar concentration, R gas constant, T temperature, μ_O chemical potential of oxygen, x

thickness of the oxidized zone.

From the Gibbs energy of chemical potential oxygen:

$$\mu_{O_2} = \mu^0_{O_2} + RT\ln P_{O_2} \tag{5.16}$$

where $\mu^0_{O_2}$ is chemical potential in a given standard state (constant), P_{O_2} oxygen partial pressure. Considering $\mu_{O_2} = 2\mu_O$, then the deferential of Eq. (5.16) is:

$$\mathrm{d}\mu_O = \frac{RT}{2}\mathrm{d}\ln P_{O_2} \tag{5.17}$$

From equations (5.15) and (5.17):

$$J_O = \frac{-D_O C_O}{2}\frac{\mathrm{d}\ln P_{O_2}}{\mathrm{d}x} \tag{5.18}$$

Integrating the Eq. (5.18):

$$J_O = \frac{-D_O C_O}{2x}\ln\left(\frac{P^{II}_{O_2}}{P^{I}_{O_2}}\right) \tag{5.19}$$

where $P^{I}_{O_2}$ is the oxygen partial pressure at the sample surface, $P^{II}_{O_2}$ the oxygen partial pressure at the interface between the oxidized zone and the non-oxidized zone.

In addition, the inward diffusion of oxygen ions controlled the growth of the oxidized zone. According to the Eq. (2.1), 3 molar of oxygen ions diffused in the Y_2SiO_5 matrix to the oxidized/non-oxidized interface to react with SiC dispersoids and the matrix for forming 1 molar of $Y_2Si_2O_7$. Thus, the flux oxygen ions can be expressed as:

$$J_O = \frac{\mathrm{d}n_O}{A\mathrm{d}t} = \frac{3f_{V_{SiC}}}{V_{Y_2SiO_5}}\frac{\mathrm{d}x}{\mathrm{d}t} \tag{5.20}$$

where $f_{V_{SiC}}$ is volume fraction of SiC, $V_{Y_2SiO_5}$ molar volume of the Y_2SiO_5 matrix, and *x* thickness of the oxidized zone.

From equations (5.19) and (5.20):

$$\frac{-D_O C_O}{2x}\ln\left(\frac{P^{II}_{O_2}}{P^{I}_{O_2}}\right) = \frac{3f_{V_{SiC}}}{V_{Y_2SiO_5}}\frac{\mathrm{d}x}{\mathrm{d}t} \tag{5.21}$$

Assuming that D_O and C_O are constants for x and t, then integrating Eq. (5.21):

$$x^2 = D_O C_O \frac{V_{Y_2SiO_5}}{3f_{V_{SiC}}} \ln\left(\frac{P^I_{O_2}}{P^{II}_{O_2}}\right) t = k_p t \tag{5.22}$$

From Eq. (522), the diffusion coefficient of oxygen ion, D_O, can be expressed as:

$$D_O = \frac{x^2}{t} \frac{3f_{V_{SiC}}}{V_{Y_2SiO_5}} \frac{1}{C_O} \frac{1}{\ln\left(\frac{P^I_{O_2}}{P^{II}_{O_2}}\right)} = k_p \frac{3f_{V_{SiC}}}{V_{Y_2SiO_5}} \frac{1}{C_O} \frac{1}{\ln\left(\frac{P^I_{O_2}}{P^{II}_{O_2}}\right)} \tag{5.23}$$

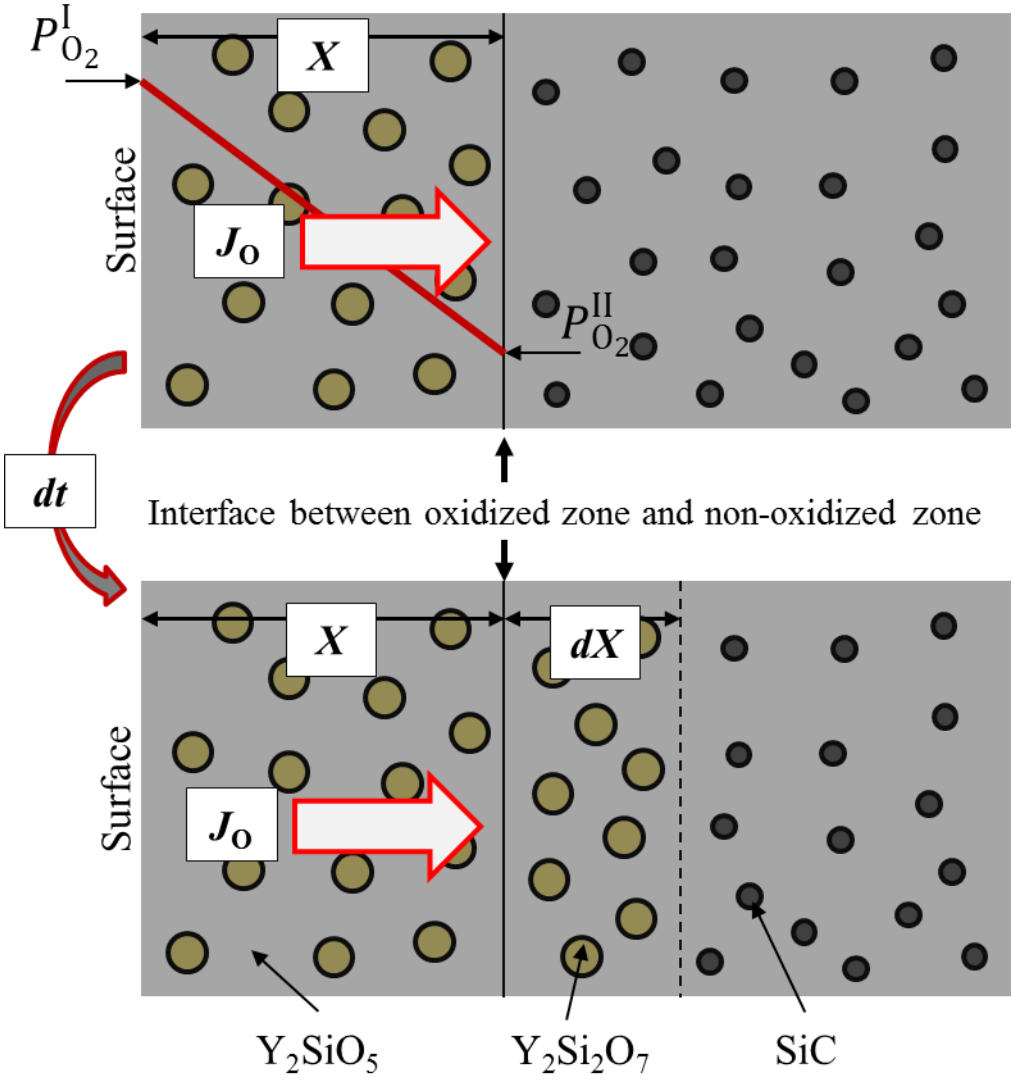

Figure 5.8 Schematic illustration of oxidation kinetic of SiC/Y_2SiO_5

As the high-temperature oxidation results of SiC/Y_2SiO_5 composites mentioned in Chapter 2, the values of k_p at 1300 and 1400 °C are equal to be $2.4x10^{-13}$ and $1.1x10^{-12}$ m^2s^{-1}, respectively. Thus, the diffusion coefficients of oxygen ion in Y_2SiO_5 matrix are calculated to be approximately $2.8x10^{-16}$ m^2s^{-1} at 1300°C, and $1.0x10^{-15}$ m^2s^{-1} at 1400°C. Figure 5.9 plots oxygen diffusivity as a function of reciprocal temperature for Y_2SiO_5 of this study in comparison to other previous reports. The diffusion coefficients of oxygen ions in Y_2SiO_5 single crystals found by Argirusis et al. [92] are 1~2 order of magnitude lower than that in the Y_2SiO_5 matrix calculated in this study. The diffusion coefficient of oxygen in the Y_2SiO_5 matrix estimated in this study is in good agreement with those in Y_2SiO_5 polycrystalline which are obtained with isotope method given by Golden et al. [85]. This demonstrates that the value for diffusion coefficient of oxygen in the Y_2SiO_5 matrix calculated in this study is reasonable. Y_2SiO_5 has a lower oxygen diffusivity than SiO_2 [94] and single crystal Y_2O_3 [95] which are the constituents of Y_2SiO_5.

Oxygen diffusivity in Y_2SiO_5 is enhanced with decreasing grain size. The grain sizes of Y_2SiO_5 in the Golden' study (~7 μm) and oxidation experiments of this study (~5 μm) are able to be comparable. Thus, the oxygen diffusivities in the Golden' study and the oxidation experiments are in a good agreement as mentioned above. In case of diffusion couple, the thickness of Y_2SiO_5 layer is just 13 μm after reaction for 3 d. It means that the grain size of Y_2SiO_5 layer should be finer than that in the oxidation experiments. This implies that diffusion of O ions in the diffusion couple is faster than that in the oxidation experiments. Besides, the above results of Y and O diffusivity indicated that diffusivity if O ions is larger than that of Y ions. These mean that diffusion of O ions is faster than that of Y ions in diffusion couple. This proved that the above assumption is reasonable.

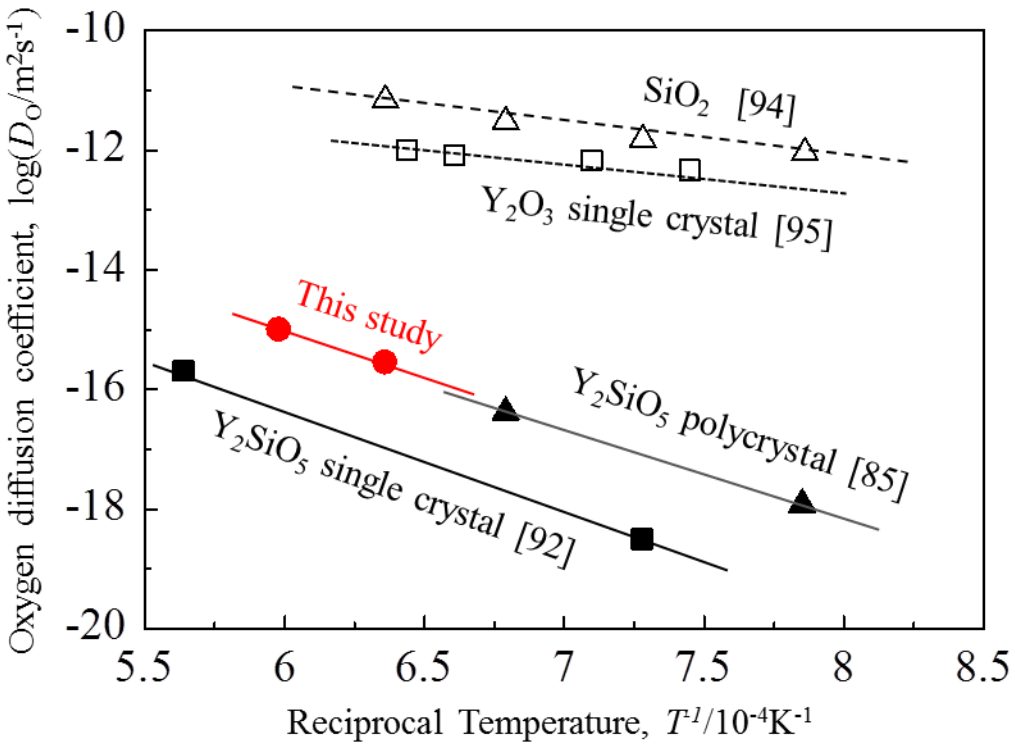

Figure 5.9 Temperature dependence of oxygen diffusivity for several oxides

A comparison in diffusion coefficients of yttrium and oxygen ion indicates that the discussion on the self-healing mechanism of SiC/Y_2SiO_5 composites mentioned in Chapter II is reasonable. The lower outward diffusion of yttrium ions does not give significant contribution for high-temperature oxidation therefore the formation of the outer layer is not obviously observed on the sample surface. The volume expansion caused by formation of the oxidation products would be not completely compensated by formation of the voids caused by outward diffusion of Y ions. The volume change in the inside of the oxidized zone is positive therefore short carks are appeared. The oxidation of SiC/Y_2SiO_5 composites are mainly caused by the oxygen diffusion. The outward diffusion of yttrium ions may possess a minor role in the oxidation process of the composites because yttrium diffusion is not much lower than oxygen diffusion.

5.4 Conclusions

Investigation for solid state reaction between $Y_2Si_2O_7$ and Y_2O_3 was conducted at 1300°C in air to determine the diffusivity of Y^{3+} cations in Y_2SiO_5. The diffusion of Y^{3+} in Y_2SiO_5 determines the rate of the solid-state reaction between $Y_2Si_2O_7$ and Y_2O_3. The diffusion coefficient of Y^{3+} cations in Y_2SiO_5 is calculated to be approximately $4x10^{-17}$ m^2s^{-1}. There have been no yttrium diffusivity studies on Y_2SiO_5 reported in literature therefore no direct comparison can be made to assess the validity of this result.

Calculation of diffusivity of oxygen in Y_2SiO_5 was carried out to find out the major diffusion controlled the high-temperature oxidation process of SiC/Y_2SiO_5 composites. The diffusion coefficient of oxygen in Y_2SiO_5 matrix at 1300°C was estimated to be approximately $2.8x10^{-16}$ m^2s^{-1}. The diffusion of oxygen ions is faster than that of yttrium ions. The high-temperature oxidation of SiC/Y_2SiO_5 composites is mainly cause by the inward diffusion of oxygen ions. The diffusion of Y ions possesses a minor role in the oxidation process of the composites.

Chapter VI

General Conclusions

The overall objective of this dissertation is to study and develop self-healing ceramic matrix composites (CMCs) for environmental barrier coatings (EBCs) which are protecting Si-based ceramic substrates from water vapor corrosion in combustion environments. Three CMCs material concepts studied in the present dissertation include SiC/Y_2SiO_5, $SiC/Y_2Si_2O_7$ and SiC/Y_2SiO_5-$Y_2Si_2O_7$ composites. The self-healing ability and high-temperature oxidation behavior of these composites were investigated and discussed from the kinetic point of view. The solid state reaction of the diffusion couple was investigated for determining diffusivity of ions in the matrix which is the rate controlling process of the oxidation of the composites. The major conclusions are summarized as follows:

6.1 Self-healing function of SiC/Y_2SiO_5 composites

Fully-densified Y_2SiO_5 composites dispersed with 5 vol% SiC particles possesses a considerable crack-healing ability. Surface cracks with total length of 200 μm were completely disappeared by heat treatment at 1300°C for 1 h in air. With heat treatment in Ar-1%H_2 gas at 1300°C for 1 h, cracks on sample surfaces did not show any disappearance. It clarified that the self-healing function of the composites was induced by high-temperature oxidation process. In comparison with self-healing of SiC/ceramic composites such as SiC/mullite and SiC/Al_2O_3, the self-healing performance of SiC/Y_2SiO_5 is better than those of the other ones. The self-healing mechanism of SiC/Y_2SiO_5 is considered as major cause of outward diffusion of Y^{3+}

cations created the surface layer which is responsible for closure of surface cracks. The formation of the surface layer was not observed clearly due to the low diffusivity of yttrium ions.

Investigation of strength recovery obtained by the self-healing effects was conducted by three point bending test at room temperature for as-sintered, as-cracked and as-healed specimens. Bending strength of the as-cracked samples which were prepared with three Vickers indentations on the tensile surface achieved 100MPa. After the surface cracks disappeared by heat treatment, as-healed samples exhibited a recovered bending strength of 330 MPa which was comparable to that of as-sintered samples (270MPa).

The oxidation of SiC/Y_2SiO_5 was mainly occurred by oxygen diffusion. The diffusivity of yttrium ions gives a minor role in the oxidation process. Oxidation of SiC phase within Y_2SiO_5 matrix causes the formation of the oxidized zone. The growth of oxidized zone obeyed the parabolic law. The oxidation rate of samples oxidized at 1200°C was much larger than that of samples oxidized at 1300 and 1400°C. The oxidation of the composites at 1200°C would occur when oxygen diffusion rate through Y_2SiO_5 matrix is much larger than that through the oxidation product. All SiC particles in the oxidized zone were partially oxidized and developed a finite thickness of the oxidation product. With the oxidation process at 1300 and 1400°C, the oxygen diffusion rate through the oxidation product is comparable to or somewhat lower than that through Y_2SiO_5 matrix. Almost SiC particles in the oxidized zone were fully oxidized.

6.2 Self-healing function of $SiC/Y_2Si_2O_7$ composites

The surface crack-disappearance obtained by heat treatment in the air of

$SiC/Y_2Si_2O_7$ composites was similar to that of SiC/Y_2SiO_5 composites at 1300°C or higher temperatures. At lower heat treatment temperatures, healing rate of $SiC/Y_2Si_2O_7$ was lower than that of SiC/Y_2SiO_5. For example, surface crack-disappearance of $SiC/Y_2Si_2O_7$ achieved approximately 30% after heat treatment at 1200°C for 1 h. While surface cracks on SiC/Y_2SiO_5 sample were disappeared 80% by heat treatment at the same condition. The dominant factor cause the self-healing of $SiC/Y_2Si_2O_7$ composites would be the volume expansion which was accompanied by oxidation of SiC into amorphous SiO2 phase. The outward diffusion of yttrium ions was also considered as the minor role in crack-healing performance of $SiC/Y_2Si_2O_7$composites.

Results of the investigation for oxidation resistance indicated the $SiC/Y_2Si_2O_7$ had a greater oxidation resistance than that of SiC/Y_2SiO_5, in particular, at low temperature such as at 1200°C. The oxidation of $SiC/Y_2Si_2O_7$ could occur by the inward diffusion of oxygen through the oxidized zone. Thus, the oxidized zone was defined as a region in which short cracks parallel to the sample surface were appeared due to the volume expansion caused by the oxidation of SiC into amorphous SiO_2 in the matrix. The growth of oxidized zone followed the parabolic law with the apparent activation energy of 735 $kJmol^{-1}$. The growth rate of oxidized zone in $SiC/Y_2Si_2O_7$ was lower than that of SiC/Y_2SiO_5.

6.3 Self-healing function of SiC/Y_2SiO_5- $Y_2Si_2O_7$ (SiC/YS) composites

In a comparison to the self-healing of $5SiC/Y_2SiO_5$ and $5SiC/Y_2Si_2O_7$ composites, the healing rate of 5SiC/YS is middle order of magnitude of $5SiC/Y_2SiO_5$ and $5SiC/Y_2Si_2O_7$. The complete disappearance of surface cracks on 5SiC/YS sample could be also caused by heat treatment at 1300°C for 1 h in air. The self-healing mechanism of 5SiC/YS was determined as the consequence of the formation of

oxidation product layer and the volume expansion. The formation of the outer layer was considered as the outward diffusion of Y ion. The oxidation of SiC into SiO_2 caused the volume expansion.

Oxidation resistance of 5SiC/YS was worse than that of 5SiC/$Y_2Si_2O_7$ and greater than that of 5SiC/Y_2SiO_5, in particular, at low temperatures such as at 1200°C. The inward diffusion of oxygen through the Y_2SiO_5 component is the major contribution to develop the oxidized zone of 5SiC/YS. The formation of the oxidized zone was caused by oxidation of SiC particles within the matrix. The growth of oxidized zone in 5SiC/YS obeyed the parabolic law with the apparent activation energy of 383 $kJmol^{-1}$which is little higher than that in 5SiC/Y_2SiO_5.

The self-healing function and oxidation resistance of 10SiC/YS and 20SiC/YS were investigated to clarify the effects of SiC volume fraction on self-healing function of SiC/YS composites. Results of the investigation for self-healing function indicated the healing rate of SiC/YS composites is proportional to the volume fraction of SiC dispersoid. For example, surface cracks on 20SiC/YS sample were completely disappeared by heat treatment at 1200°C for 6 h in air. While surface crack-disappearance of 5SiC/YS and 10SiC/YS achieved 80 and 85% after heat treatment at the same condition, respectively. The investigation for oxidation resistance suggests that the oxidation resistance of SiC/YS composites was increased with increasing the SiC volume fraction dispersed in the matrix. Results of the investigation show that oxidation rate of 20SiC/YS was lower than that of 5 and 10SiC/YS. Although both self-healing ability and oxidation resistance of SiC/YS composites was improved by increasing the volume fraction of SiC dispersoid, the amount of SiC dispersion should be in an equilibrium with self-healing function, oxidation resistance and water vapor corrosion resistance in combustion environments

of the SiC/YS composites. Furthermore, the increase of SiC dispersoid fraction caused the decrease in sintering ability of SiC/YS composites.

6.4 Diffusivity of ions in yttrium monosilicate ceramic

The diffusion of yttrium cations determined the rate of solid state reaction between $Y_2Si_2O_7$ and Y_2O_3 reactants. The diffusion coefficient of Y ions in Y_2SiO_5 layer formed by the solid state reaction of the reactants at 1300°C was determined to be approximately $4x10^{-17}$ m^2s^{-1}. No direct comparison can be made to assess the validity of this result because there have been no diffusivity data of yttrium in Y_2SiO_5 reported previously. The diffusivity of oxygen in Y_2SiO_5 at 1300°C was estimated to be approximately $2.8x10^{-16}$ m^2s^{-1}, which is in agreement with other data reported previously. In the Y_2SiO_5 matrix, the diffusion of oxygen ions was faster than that of yttrium ions. This indicates that the previous discussion on self-healing function and oxidation behavior of SiC/Y_2SiO_5 in this dissertation is reasonable.

Acknowledgements

First of all, I would like to express my honest thanks to my supervisor, Professor Makoto Nanko. I greatly appreciate all his contributions of time, funding and ideas to my Ph.D. research works. His guidance helped me to learn and develop my knowledge in academic research as well as many necessary skills in life and work that I need in afterward future. His enthusiasm and optimism for research have been motivated me during tough time in my research progress.

I would like to thank all members of Nanko Laboratory, who have helped me in life, and shown me a lot of interest in Japanese life and culture. I am especially grateful for helps of Mai Dung Do, Hai Vu Pham, Hien Huu Nguyen, who always not only help me during my life in Nagaoka, but also give me instructions on conducting research, using equipment. I am also thankful to Mr. Kazuki Takahashi, former student of Nanko Lab and my tutor, for helping me since I first came to Japan.

In regards to the micro Vickers hardness tester, I thank Professor Shigeharu Kamado (Nagaoka University of Technology) and his students. They have allowed me using the instrument and helped me with the operating instructions.

For the dissertation, I would like to thank my reading and oral defense committee members: Prof. Masatoshi Takeda, Prof. Yukio Miyashita, Prof. Tomoyuki Homma, and Prof. Satoshi Yamagishi for their time, interest, and helpful comments.

I gratefully acknowledge the Japan Science and Technology Agency in the frame of the Advanced Low Carbon Technology Research and Development program for supporting partially that made my Ph.D. work possible.

Lastly, I would like to thank my family for their love and encouragement all the times. Especially, for my parents who always support me in all my tournaments.

References

[1] M. P. Boyce, Gas Turbine Engineering Handbook, Fourth Edition. Butterworth-Heinemnn, Oxford, 2012.

[2] N. P. Padture, "advanced structural ceramics in aerospace propulsion", Nature Materials, 15[8] 804-809 (2016).

[3] F. W. Zok, Ceramic matrix composites enable revolutionary gains in turbine engine efficiency, American Ceramic Society Bulletin, 95[5] 22-28 (2016).

[4] D. R. Clarke, M. Oechsner, and N. P. Padture, Thermal barrier coatings for more efficient gas turbine engines, MRS Bull., 37[10] 891-898 (2012).

[5] J. T. Demasi-Marcin and D. K. Gupta, Protective coatings in the gas turbine engines, Surface Coating Technology, 68 1-9 (1994).

[6] J. C. Williams and E. A. S. Jr, Progress in structural materials for aerospace systems1, Acta Materials, 51[19] 5775-5779 (2003).

[7] A. G. Evans, D. Mumm, J. Hutchinson, G. Meier, and F. Pettit, Mechanism controlling the durability of thermal barrier coatings, Progress in materials science, 46[5] 505-553 (2001).

[8] A. Evans and J. Hutchinson, The mechanics of coating delamination in thermal gradients, Surface and Coatings Technology, 201[18] 7905-7916 (2007).

[9] H. Zhao, Z. Yu, and H. N. Wadley, The influence of coating compliance on the delamination of thermal barrier coating, Surface and Coatings Technology, 204[15] 2432-2441 (2010).

[10] M. R. Begley and H. N. Wadley, Delamination of Ceramic Coatings with Embedded Metal Layers, Journal of American Ceramic Society, 94[s1] 96-103 (2011).

[11] A. Davis and A. Evans, Some effects of imperfection geometry on the cyclic distortion of thermally grown oxides, Oxidation of metals, 65[1-2] 1-14 82006).

[12] Z. Yu, H. Zhao, and H. N. Wadley, The vapor deposition and oxidation of platinum- and Yttria-stabilized Zirconia Multilayers, Journal of American Ceramic Society, 94[8] 2671-2679 (2011).

[13] S. Kramer, J. Yang, C. G. Levi, and C. A. Johnson, Thermochemical Interaction of Thermal Barrier Coatings with Molten CaO-MgO-Al_2O_3-SiO_2

(CMAS) Deposits, Journal of American Ceramic Society, 89[10] 3167-3175 (2006).

[14] S. Kramer, J. Yang, and C. G. Levi, Infiltration-Inhibiting Reaction of Gadolinium Zirconate Thermo Barrier Coatings with CMAS Melts, Journal of American Ceramic Society, 91[2] 576-583 (2008).

[15] J. A. Dicarlo, Advances in SiC/SiC Composites for Aero-Propulsion. In: B. P. Narottam, J. Lamon, editors. Ceramic Matrix Composites: Materials, Modeling and Technology. Wiley; 2015. P. 217-235.

[16] N. R. Council, Ceramic Fibers and Coatings: Advanced Materials for the Twenty-First Century, The National Academies Press, Washington, DC, 1998.

[17] R. Naslain and F. Christin, SiC Matrix Composites Materials for Advanced Jet Engines, MRS Bulletin, 28[9] 654-658 (2003).

[18] R. Naslain, Design, preparation and properties of non-oxide CMCs for application in engines and nuclear reactors: an overview, Composites Science Technology, 64[2] 155-170 (2004).

[19] J. A. Dicarlo and H. M. Yun, Non-oxide (Silicon Carbide) Fibers, pp. 33-52 in Handbook Ceramic Composistes Edited by N. P. Bansal. Springer US, Boston, MA, 2005.

[20] A. G. Evans, F. W. Zok, and J. Davis, The role of interfaces in fiber-reinforced brittle matrix composites, Composites Science Technology, 42[1] 3-24 (1991).

[21] J. J. Brennan, Interfacial characterization of a slurry-cast melt-infiltrated SiC/SiC ceramic matrix composite, Acta Materials, 48[18-19] 4619-4628 (2000).

[22] R. Naslain, SiC Matrix Composites: Nonbrittle Ceramic for Thermo-Structural Application, International Journal of Applied Ceramic Technology, 2[2] 75-84 (2005).

[23] L. U. Ogbuji and E. J. Opila, A comparison of the oxidation kinetics of SiC and Si_3N_4, Journal of Electrochemical Society, 142[3] 925-930 (1995).

[24] C. E. Ramberg, G. Cruciani, K. E. Spear, R. E. Tressler, and C. F. Ramberg, Passive oxidation kinetics of high purity silicon carbide from 800°C to 1100°C, Journal of American Ceramic Society, 79[11] 2897-2911 (1996).

[25] E.J. Opila, J. L. Smialek, R. C. Robison, D. S. Fox, and N. S. Jacobson, SiC recession caused by SiO_2 scale volatility under combustion conditions: II,

Thermodynamics and Gaseous Diffusion Model, Journal of American Ceramic Society, 82[7] 1826-1834 (1999).

[26] E. J. Opila and R. E. Hann, Paralinear oxidation of CVD SiC in water vapor, Journal of American Ceramic Society, 80[1] 197-205 (1997).

[27] E. J. Opila, Oxidation kinetics of chemically vapor deposited silicon carbide in wet oxygen, Journal of American Ceramic Society, 77[3] 730-736 (1994).

[28] E. J. Opila, Oxidation and Volatilization of Silica Formers in Water Vapor, Journal of American Ceramic Society, 86[8] 1238-1248 (2003).

[29] E. J. Opila, D. S. Fox, and N. S. Jacobson, Mass Spectrometric Identification of Si-O-H (g) Species from the Reaction of Silica with Water Vapor at Atmospheric Pressure, Journal of American Ceramic Society, 80[4] 1009-1012 (1997).

[30] E. J. Opila, Variation of the Oxidation Rate of Silicon Carbide with Water Vapor Pressure, Journal of American Ceramic Society, 82[3] 625-636 (1999).

[31] K. N. Lee, Current status of environmental barrier coatings for Si-based ceramics, Surface and Coatings Technology, 133-134 1-7 (2000).

[32] K. N. lee, R. A. Miller, and N. S. Jacobson, New generation of plasma sprayed mullite coatings on silicon carbide, Journal of American Ceramic Society, 78[3] 705-710 (1995).

[33] K. N. Lee, Key Durability Issues with Mullite-based Environment Barrier Coating for Si-based Ceramics, Journal of Engineering for Gas Turbine and Power, 122 632-636 (2000).

[34] K. N. Lee and R. A. Miller, Development and environmental durability of mullite and mullite/YSZ dual layer coatings for SiC and Si_3N_4 ceramics, Surface and Coatings Technology, 86-87 142-148 (1996).

[35] M. Y. He, J. W. Hutchinson, and A. G. Evans, Simulation of stresses and delamination in a plasma-sprayed thermal barrier system upon thermal cycling, Materials Science and Engineering: A, 345[1-2] 172-178 (2003).

[36] A. G. Evans and J. W. Hutchinson, The mechanics of coating delamination in thermal gradients, Surface and Coating Technology, 201[18] 7905-7916 (2007).

[37] K. N. Lee, Contamination Effects on Interfacial Porosity during Cyclic Oxidation of Mullite-Coated Silicon Carbide, Journal of American Ceramic

Society, 81 3329-3332 (1998).

[38] H. E. Eaton, G. D. Linsey, E. Y. Sun, K. L. more, J. B. kimmel, J. R. Price et al., EBC protection of SiC/SiC composites in the gas turbine combustion environment continuing evaluation and refurbishment consideration, ASME paper 2001-GT-0513 ASME TURBOEXPO 2001, June 4-7, 2001. New Orleans, Louisiana.

[39] K. N. Lee, D. S. Fox, J. I. Eldridge, D. Zhu, R. C. Robinson, N. P. Bansal and R. A. Miller, Upper Temperature Limit of Environment Barrier Coatings Based on Mullite and BSAS, Journal of American Ceramic Society, 86 1299-1306 (2003).

[40] K. N. Lee, D. S. Fox, and N. P. Bansal, Rare earth silicate environmental barrier coatings for SiC/SiC composites and Si_3N_4 ceramics, Journal of American Ceramic Society, 25 1705-1715 (2005).

[41] N. S. Jacobson, D. S. Fox, J. L. Smialek, E. J. Opila, C. Dellacorte, and K. N. Lee. In: ASM Handbook. S. D. Cramer, B. S. Jr. Covino, editors. ASM International; Materials Park, OH, USA: 2005. pp. 565-578.

[42] C. B. Cater and M. G. Norton, Ceramic Materials Science and Engineering, New York: Springer, 2013.

[43] T. K. Gupta, Crack Healing and Strengthening of Thermally Shocked Alumina, Journal of the American Ceramic Society, 59[5-6] 259-262 (1976).

[44] S. R. Choi and V. Tikare, Crack Healing Behavior of Hot Pressed Silicon Nitride Due to Oxidation, Scripta Metallurgica et Materialia, 26 [8] 1263-1268 (1992).

[45] M. C. Chu, S. Sato, Y. Kobayashi and K. Ando, Damage healing and strengthening behavior in intelligent mullite/SiC ceramics, Fatigue Fracture of Engineering Material Structure, 18[9] 1019-1029 (1995).

[46] K. Ando, B. S. Kim, M. C. Chu, S. Saito, and K. Takahashi, Crack-healing and mechanical behaviour of SiC/Al_2O_3 composites at elevated temperature, Fatigue Fracture Engineering Materials Structure, 27 533-541 (2004).

[47] A. L. Salas-Villasenor, J. Lemus-Ruiz, M. Nanko and D. Maruoka, Crack-disappearance by high-temperature oxidation of alumina toughened by Ni nano-particles, Advanced Materials Research, 68 34-43 (2009).

[48] D. Maruoka, Y. Sato and M. Nanko, Recovery of mechanical properties on

nano-Co particles dispersed Al_2O_3 via high-temperature oxidation, Materials Transactions, 53[10] 1816-1821 (2012).

[49] H. V. Pham, N. Nanko and W. Nakao, Self-healing of Ni/Mullite Hybrid Material via High-Temperature Oxidation, Materials Transactions, 58[7] 1081-1088 (2017).

[50] Y. Chen, Y. Lu, Q. Ye, and Y. Wang, A self-healing environmental barrier coating: $TiSi_2$-doped $Y_2Si_2O_7$/barium strontium aluminumsilicate coating, Surface and Coatings Technology, 37 436-440 (2016).

[51] S. T. Nguyen, T. Nakayama, H. Suematsu et al., Strength improvement and purification of $Yb_2Si_2O_7$-SiC nanocomposites by surface oxidation treatment, Journal of American Ceramic Society, vol. 100[7] 3122-3131 (2017).

[52] S. T. Nguyen, T. Nakayama, H. Suematsuet al., Self-crack healing ability and strength recovery in ytterbium disilicate/silicon carbide nanocomposites, Journal of Applied Ceramic Technology, vol. 16[1] 39-49 (2019).

[53] N. Maier, K. G. Nickel, and G. Rixecker, High temperature water vapor corrosion of rare earth silicates (Y, Yb, Lu)$_2Si_2O_7$ in the presence of $Al(OH)_3$ impurities, Journal of European Ceramic Society, 27[7] 2705-2713 (2007).

[54] J. Liu, L. Zhang, F. Hu, J. Yang, L. Cheng, and Y. Wang, Polymer-derived yttrium silicate coating on 2D C/SiC composites, Journal of European Ceramic Society, 33[2] 433-439 (2013).

[55] E. Courcot, F. Rebillat, and F. Teyssandier, From the Volatility of Simple Oxides to that of Mixed Oxides: Thermodynamic and Experimental Approaches, pp. 235-244 in Des. Dev. Appl. Eng. Ceram. Compos. John Wiley&Sons, Inc. 2010.

[56] D. Cupid and H. Seifert, Thermodynamic Calculations and Phase Stabilities in the Y-Si-C-O System, Journal of Phase Equilibria Diffusion, 28[1] 90-100 (2007).

[57] J. Ito and H. Johnson, Synthesis and Study of Yttrialite, American Mineralogist, 53 1940-1952 (1968).

[58] S. Kumar and C. H. Drummod, Crystallization of various compositions in the Y_2O_3-SiO_2 system, Journal of Materials Research, 7[4] 997-1003 (1992).

[59] M. D. Dolan, B. Harlan, J. S. White, M. Hall, S. T. Misture, S. C. Bancheri, and B. Bewlay, Structure and anisotropic thermal expansion of the α, β, γ, and δ

polymorphs of $Y_2Si_2O_7$, Powder Diffraction, 23[1] 20-25 (2008).

[60] K. Fukuda and H. Matsubara, Anisotropic thermal expansion in yttrium silicate, Journal of Materials Research, 18[7] 1715-1722 (2003).

[61] K. Fukuda and H. Matsubara, Thermal Expansion of δ-Yttrium Disilicate, Journal of American Ceramic Society, 87[1] 89-92 (2004).

[62] J. Felsche, The crystal chemistry of the rare earth silicates, Structure and Bonding, 13 99-199 (1973)

[63] A. I. Becerro, M. Naranjo, M. D. Alba, and J. M. Trillo, Structure-directing effect of phyllosilicates on the synthesis of γ-$Y_2Si_2O_7$. Phase transition in $Y_2Si_2O_7$, Journal of Material Chemistry, 13[7] 1835-1842 (2003).

[64] N. Maier, G. Rixecker, and K. G. Nickel, Formation and stability of Gd, Y, Yb and Lu disilicates and their solid solutions, Journal of Solid State Chemistry, 179[6] 1630-1635 (2006).

[65] J. W. Nowok, J. P. Kay, and R. J. Kulas, Thermal expansion and high-temperature phase transformation of the yttrium silicate Y_2SiO_5, Journal of Materials Research, 16[8] 2251-2255 (2001).

[66] N. A. Toropov, and I. A. Bondar, Silicates of the rare earth elements, Bulletin of Academy of Science of USSR, Division Chemical Science, 10[4] 502-508 (1961).

[67] D. Maruoka and M. Nanko, Crack-healing of Nano-Ni/Al_2O_3 Hybrid Material via High-Temperature Oxidation, Material Science Forum, 696 378-383 (2011).

[68] D. Maruoka and M. Nanko, Recovery of mechanical strength by surface crack disappearance via thermal oxidation for nano-Ni/Al_2O_3 hybrid material, Ceramics International, 39[3] 3221-3229 (2013).

[69] Z. Q. Sun, J. Y. Wang, M. S. Li, and Y. C. Zhou, Mechanical properties and damage tolerance of Y_2SiO_5, Journal of European Ceramic Society, 28 2895-2901 (2008).

[70] Z. Q. Sun, M. S. Li, and Y. C. Zhou, Thermal properties of single-phase Y_2SiO_5, Journal of European Ceramic Society, 29 551-557 (2009).

[71] H. J. Seifert, S. Wagner, O. Fabrichnaya, H. Lukas, F. Aldinger, T. Ullmann, M. Schmuker, and H. Schneider, Yttrium silicate coating on chemical vapor deposition SiC-precoated C/C-SiC: thermodynamic assessment and

high-temperature investigation, Journal of American Ceramic Society, 88 424-430 (2005).

[72] K. Niihara, R. Morena, and D. P. H. Hasselman, Evaluation of K_{IC} of brittle solids by indentation method with low crack-to-indent ratios, Journal of Materials Sicence Letters, 1 13-16 (1982).

[73] K. Ando, M. C. Chu, K. Tsuji, T. Hirasawa, Y. Kobayashi, and S. Sato, Crack healing behaviour and high-temperature strength of mullite/SiC composites ceramics, Journal of European Ceramic Society, 22 1313-1319 (2002).

[74] K. Takahashi, M. Yokouchi, S. K. Lee, and K. Ando, Crack-healing behavior of Al_2O_3 toughened by SiC whiskers, Journal of American Ceramic Society, 86[12] 2143-2147 (2003).

[75] M. Nanko, K. Matsumaru, K. Ishizaki, Role of cation diffusion on high temperature oxidation of metal dispersed ceramic matrix composites, Advances in Technology of Materials and Materials Processing Journal, 7[1] 5-8 (2005).

[76] K. L. Lurtha and H. D. Park, Oxidation of Silicon Carbide-Reinforced Oxide-Matrix Composites at 1375 to 1575°C, Journal of American Ceramic Society, 73[4] 1014-1023 (1990).

[77] Z. Q. Sun, Y. C. Zhou, J. Y. Wang, and M. S. Li, Thermal Properties and Thermal Shock Resistance of γ-$Y_2Si_2O_7$, Journal of American Ceramic Society, 91[8] 2623-2629 (2008).

[78] Z. Q. Sun, Y. C. Zhou, and M. S. Li, Low-Temperature Synthesis and Sintering of γ-$Y_2Si_2O_7$, Journal of Material Research, 21[6] 1443-1450 (2006).

[79] Z. Q. Sun, Y. C. Zhou, J. Y. Wang, and M. S. Li, γ-$Y_2Si_2O_7$, a Machinable Silicate Ceramics: Mechanical Properties and Machinability, Journal of American Ceramic Society, 90[8] 2535-2541 (2007).

[80] Z.Q. Sun, Y. C. Zhou, and M. S. Li, Hot Corrosion of γ-$Y_2Si_2O_7$ in Strongly Basic Na_2CO_3 Molten Salt Environment, Journal of European Ceramic Society, 28 259-265 (2008).

[81] Z. Q. Sun, M. S. Li, and Y. C. Zhou, Kinetic and Mechanism of Hot Corrosion of γ-$Y_2Si_2O_7$ in Thin Film Na_2SO_4 Molten Salt, Journal of American Ceramic Society, 91[7] 2236-2242 (2008).

[82] M. Nanko, M. Yoshimura, and T. Maruyama, High Temperature Oxidation of

Y_2O_3 Partially-Stabilized ZrO_2 Composites Dispersed Ni Particles, Materials Transactions, 44[4] 736-742 (2003).

[83] W. G. Sloof, S. R. Turteltaub, A. L. Carabat, Z. Derelioglu, S. A. Ponnusami, and G. M. Song. Crack healing in yttria stabilized zirconia thermal barrier coatings. In: Zwaag VD, Brinkman E, editors. Self-healing materials. Amsterdam (Netherlands): IOS Press; (2015) 219-227.

[84] M. Aparico and A. Duran, Yttrium Silicate Coating for Oxidation Protection of Carbon-Silicon Carbide Composites, Journal of American Ceramic Society, 83[6] 1351-1355 (2000).

[85] R. A. S. Golden (2017), Matrix Development for Water Vapor Resistant SiC-Based Ceramic Matrix Composites (Doctoral dissertation), University of Virginia, US

[86] M. I. Osendi, Oxidation behaviour of mullite-SiC composites, Journal of materials science, 25 3561-3565 (1990).

[87] K. Kawamura, A. Saiki, T. Maruyama, and K. Nagata, Diffusion coefficient of yttrium ion in $YCrO_3$, Journal of Electrochemical Society, 142[9] 3073-3077 (1995).

[88] T. Akashi, M. Nanko, and T. Maruyama, Solid-State Reaction Kinetics of $LaCrO_3$ from the Oxides and Determination of La^{3+} Diffusion Coefficient, Journal of Electrochemical Society, 145[6] 2090-2094 (1998).

[89] T. Akashi, Y. Mizuno, M. Nanko, T. Maruyama, A. Saiki, K. Tsukui, and J. Tanabe, Determination of Diffusion Coefficient of Nd^{3+} in $NdCrO_3$ Based on Solid State Reation, Material Transactions, 42[7] 1411-1416 (2001).

[90] DR. H. Schmalzried, Solid-State Reaction, Angewandte Chemmie International Edition, 2[5] 251-254 (1963).

[91] O. Fabrichnaya, H. J. Seifert, R. Weiland, T. Ludwig, F. Aldinger, and A. Navrotsky, Phase equilibrium and thermodynamic in the Y_2O_3-Al_2O_3-SiO_2 system, Z. Fur Met., 92[9] 1083-1097 (2001).

[92] C. Argirusis, G. Antonaropoulos, G. Sourkouni, and F. Jomard, Oxygen tracer diffusion in single crystalline yttrium silicate, Solid State Ion., 262 548-550 (2014)

[93] K. N. Lee, Protective Coatings for Gas Turbines. In the Gas Turbine Handbook, R. Dennis, editor. United State Department of Energy (DOE), 2006.

[94] F. J. Norton, Permeation of Gaseous Oxygen through Vitreous Silica, Nature, 191[4789] 701 (1961).

[95] M. F. Berard, C. D. Wirkus, and D. R. Wilder, Diffusion of Oxygen in Selected Monocrystalline Rare Earth Oxides, Journal of American Ceramic Society, 51[11]643-647 (1968).

Research activities

List of Journal papers

1. H. D. Vu and M. Nanko, “Crack-healing behavior and mechanical strength recovery of 5 vol% silicon carbide particle dispersed yttrium monosilicate composites”, Materials Transactions, Vol. 60[1], pp. 149-155.
2. H. D. Vu and M. Nanko, “Crack-healing performance and oxidation behavior of SiC dispersed yttrium silicate composites”, Journal of Asian Ceramic Societies, Vol. 8[2], pp. 298-308.

List of Conference papers

1. H. D. Vu and M. Nanko, “Self-healing behavior of Y_2SiO_5 toughened by SiC particles”, Key Engineering Materials, Vol. 728, pp. 149-154.

List of international conferences

1. Huy Dinh Vu and Makoto Nanko, "Crack healing behavior of 5 vol% SiC particle dispersed Y_2SiO_5 composites", the International symposium on the Science of Engineering Ceramics (EnCera 2016), Niigata, Japan, May 2016.
2. Huy Dinh Vu and Makoto Nanko, "Self-healing behavior of Y_2SiO_5 toughened by SiC particles", International conference on Engineering Innovation (ICEI 2016), Bangkok, Thailand, June 2016.
3. Huy Dinh Vu and Makoto Nanko, "Self-healing of SiC/Y_2SiO_5 hybrid composites via thermal oxidation", 4th International conference on Competitive Materials and Technology Processes (IC-CMTP4), Miskolc, Hungary, Oct. 2016.
4. Huy Dinh Vu and Makoto Nanko, "Self-healing of reinforced SiC-dispersed Y_2SiO_5 composites via high-temperature oxidation", International conference on Metallurgical Engineering and Advanced Materials Technology for Sustainable Development Industry (ICMAMT 2016), Hanoi, Vietnam, Oct. 2016.
5. Huy Dinh Vu and Makoto Nanko, "Self-healing behavior of yttrium silicates-based composites with SiC dispersion via high-temperature oxidation", 6th International conference on Self-healing Materials (ICSHM 2017), Friedrichshafen, Germany, June, 2017.
6. Huy Dinh Vu and Makoto Nanko, "Thermal expansion coefficient of yttrium silicate ceramics and their composites dispersed with SiC particles", International conference on powder and powder metallurgy (JSPMI 2017), Kyoto, Japan, Nov. 2017.

7. Huy Dinh Vu and Makoto Nanko, "Development of self-healing materials applied to EBCs system for SiC/SiC composites", the first International conference on Materials, Machines and Methods for Sustainable Development (MMMS 2018), Da Nang, Vietnam, May 2018.
8. Huy Dinh Vu and Makoto Nanko, "High-temperature oxidation behavior of yttrium silicate composites dispersed with SiC particles in air", International symposium on high-temperature oxidation and corrosion (ISHOC 2018), Shimane, Japan, Oct. 2018.
9. Huy Dinh Vu and Makoto Nanko, "Crack-healing function of yttrium silicate composites dispersed with various volume fraction SiC particles", 7th International conference on Self-healing Materials (ICSHM 2019), Yokohama, June 2019.

List of Domestic conferences

1. Vu Dinh Huy and Nanko Makoto, “Thermal oxidation induced crack-healing of 5 vol% SiC particles dispered Y_2SiO_5 composites”, Spring Meeting of the Ceramic Society of Japan, Tokyo, Japan, Mar. 2016.
2. Huy Dinh Vu and Makoto Nanko, “Crack healing behavior and mechanical property recovery of SiC particle dispersed Y_2SiO_5 composites”, Spring Meeting of the Japan Institute of Metals and Materials, Tokyo, Japan, Mar. 2017.
3. Huy Dinh Vu and Makoto Nanko, “Self-healing behavior of $Y_2Si_2O_7$ ceramic composites dispersed SiC particles”, Fall Meeting of the Japan Institute of Metals and Materials, Sapporo, Hokkaido, Japan, Sep. 2017.
4. Huy Dinh Vu and Makoto Nanko, “Self-healing function of yttrium silicate composites dispersed with various volume fraction of SiC particles”, Spring Meeting of the Japan Institute of Metals and Materials, Chiba, Japan, Mar. 2018.

Honor and Award

1. Huy Dinh Vu and Makoto Nanko, Best Poster Presentation, International Conference on Engineering Innovation, Bangkok, Thailand, 2016.